ISTANBUL TECHNICAL UNIVERSITY ★ GRADUATE SCHOOL OF SCIENCE ENGINEERING AND TECHNOLOGY

PREPARATION AND CHARACTERIZATION OF POLYLACTIDE/POLY (BUTYLENE ADIPATE-CO-TEREPHTHALATE)/CELLULOSE NANOCRYSTAL BLEND NANOCOMPOSITES

M.Sc. THESIS

Deniz Sema SARUL

Graduate School of Science Engineering and Technology
Polymer Science and Technology Graduate Programme

JULY 2020

ISTANBUL TECHNICAL UNIVERSITY ★ GRADUATE SCHOOL OF SCIENCE ENGINEERING AND TECHNOLOGY

PREPARATION AND CHARACTERIZATION OF POLYLACTIDE/POLY (BUTYLENE ADIPATE-CO-TEREPHTHALATE)/CELLULOSE NANOCRYSTAL BLEND NANOCOMPOSITES

M.Sc. THESIS

Deniz Sema SARUL
(515171012)

Graduate School of Science Engineering and Technology

Polymer Science and Technology Graduate Programme

Thesis Advisor: Asst. Prof. M. Reza NOFAR

JULY 2020

ISTANBUL TEKNİK ÜNİVERSİTESİ ★ FEN BİLİMLERİ ENSTİTÜSÜ

SELÜLOZ NANOKRİSTAL İÇEREN POLİLAKTİK/POLİ (BÜTİLENADİPAT-ko-TEREFTALAT) HARMAN NANOKOMPOZİTLERİN HAZIRLANMASI VE KARAKTERİZASYONU

YÜKSEK LİSANS TEZİ

Deniz Sema SARUL
(515171012)

Fen Bilimleri Enstitüsü

Polimer Bilim ve Teknolojisi Programı

Tez Danışmanı: Dr. Öğr. Ü. M. Reza NOFAR

TEMMUZ 2020

Deniz Sema Sarul, a M.Sc. student of ITU Graduate School of Science Engineering and Technology student ID 515171012, successfully defended the thesis entitled "Preparation and Characterization of Polylactide/Poly (butylene adipate-co-terephthalate) containing Cellulose Nanocrystal Blend Nanocomposites", which she prepared after fulfilling the requirements specified in the associated legislations, before the jury whose signatures are below.

Thesis Advisor:	**Assoc. Prof. M. Reza Nofar** İstanbul Technical University	.....
Jury Members:	**Prof. Dr. Oğuz Okay** Istanbul Technical University	.....
	Prof. Dr. Güralp Özkoç Kocaeli University	.....

Date of Submission : 15 June 2020
Date of Defense : 16 July 2020

To my family

FOREWORD

First and foremost, I would like to express my sincere gratitude and thanks to my supervisor, Assoc. Prof. M.Reza NOFAR, for his guidance, encouragements and support during this study. Your advice on research have been priceless. It was a wonderful opportunity to work with him.

I would like to thank Assos. Prof. Ali DURMUŞ at Istanbul University for their great support and provide for melt mixing equipment of this project. I am also grateful to Prof. Seniha GÜLER to give me permission to have access to her Rheology lab. I would also like to thank Prof. Sinan ŞEN and Prof. Metin Hayri ACAR for the providing their laboratories and equipment. A sincere appreciation goes to all the staff and technicians of ITU Faculty of Chemical and Metallurgical Engineering for their help and meaningful contribution to this thesis.

I would also like to thank my friends especially Haluk ALTAY, Doğan ARSLAN, Emre VATANSEVER, Ece GÜLER, Burcu ÖZDEMİR and Merve GÜÇLÜ for their outstanding scientific and spiritual support. Along the last years, I have had the pleasure to meet different people who are truly generous and helpful.

My heartfelt thank goes to my mom and dad for their invaluable love and support. My dear sister Derya, thank you for being there for me.

I am also grateful of the financial supports and scholarships from The Scientific and Technological Research Council of Turkey-TUBITAK 1001 project (Project No: 117M238).

July 2020

Deniz Sema SARUL
(Chemical Engineer)

TABLE OF CONTENTS

Page

ABBREVIATIONS

CB	**:** Carbon black
CNC	**:** Cellulose nanocrystals
CNT	**:** Carbon nanotube
C18-g-CNC	**:** Alkyl chain grafted CNC
DMA	**:** Dynamic mechanical analysis
DMF	**:** Dimethylformamide
DSC	**:** Differential scanning calorimetry analysis
EFG	**:** Epoxy functionalized graphene
GNPs	**:** Graphene nanoplatelets
HDT	**:** Heat deflection temperature
IM	**:** Internal mixer
MMT	**:** Montmorillonite clay
MWNT	**:** Multi-walled carbon nanotube
PA	**:** Polyamide
PBAT	**:** Poly(butylene adipate-co-terephyhalate)
PBSA	**:** Poly[(butylene succinate)-co-adipate]
PCL	**:** Polycaprolactone
PE	**:** Polyethylene
PET	**:** Polyethylene terephthalate
PEO	**:** Poly (ethylene oxide)
PHB	**:** Poly(hydroxybutirate)
PLA	**:** Polylactide
PDLA	**:** Poly(D-lactide)
PLLA	**:** poly(L-lactide)
PLA-g-CNC	**:** Polylactide grafted CNC
PMMA	**:** Poly(methyl methacrylate)
PP	**:** Polypropylene
PPD	**:** Poly(para-dioxanone)
PS	**:** Polystyrene
SEM	**:** Scanning electron microscope
TSE	**:** Twin screw extruder

SYMBOLS

Ca	**:** capillary number
Ca_{crit}	**:** critical capillary number
E	**:** elastic modulus
G'	**:** storage modulus
t	**:** time
η_o	**:** zero shear viscosity
η*	**:** complex viscosity
p	**:** dispersed phase/matrix viscosity ratio
tan δ	**:** loss tangent
Tc	**:** crystallization temperature
Tcc	**:** cold crystallization temperature
Tg	**:** glass transition temperature
Tm	**:** melting temperature
ω	**:** frequency of oscillation
Xc	**:** crystallinity percentage
ΔGm	**:** Gibbs free energy of mixing
ΔHm	**:** enthalpy of crystal melting
ΔHcc	**:** enthalpy of cold crystallization
γ_{ij}	**:** interfacial tension between component i and j
γi	**:** surface tension of component i
γ_i^d	**:** non-polar (dispersive) component of surface energy of component I
γ_i^p	**:** polar component of surface energy of component I
ω_{AB}	**:** wetting coefficient
W_{PLA}	**:** weight fraction of the PLA
$\dot{\gamma}$	**:** shear rate

LIST OF TABLES

Page

LIST OF FIGURES

Page

PREPARATION AND CHARACTERIZATION OF POLYLACTIDE/POLY (BUTYLENE ADIPATE-CO-TEREPHTHALATE) CONTAINING CELLULOSE NANOCRYSTAL BLEND NANOCOMPOSITES

SUMMARY

Biopolymers have been developed to replace petroleum-based polymers due to their environmental damage. Poly (lactic acid) or polylactide (PLA) is one of the most common biopolymers derived from sustainable sources such as corn starch and sugar cane with attractive properties such as renewability, high strength, modulus and transparency. Therefore, it stands out in the industry and is an alternative to petroleum-based polymers. PLA also suffers from a series of disadvantages, such as high brittleness, low toughness, low service temperature, slow crystallization and low melt strength, which limits its processability, formability and foamability. Many approaches have been reported in the literature to overcome these disadvantages, such as copolymerization, blending and composition with nanoparticles. Blending PLA with biodegradable polymers such as poly (butylene adipate-co-terephthalate) (PBAT), polycaprolactone (PCL) and poly [(butylene succinate)-co-adipate] (PBSA) is the most economical way to increase its toughness without compromising its biodegradability. In this thesis context, the second selected polymer is PBAT, which is 100% biodegradable synthetic random copolymer. Despite PLA, PBAT has remarkable properties such as ductility and flexibility, and it shows a very low tensile modulus and strength. The PLA/PBAT blend is an immiscible blend. Morphology of the immiscible blend varies depending on intrinsic properties of each polymer and blend ratio. The morphology greatly influences final blend performance; therefore, it must be checked to obtain the desired properties. According to literature, blending PLA with PBAT has been observed to significantly reduce the modulus and mechanical strength of PLA. A solid nanoparticle is added to the blend to increase compatibility between components and provide the stiffness/toughness balance. The selective localization of the nanoparticle is very important for the morphology design and for the blend to show the desired properties. The selective localization of nanoparticles depends on thermodynamic and kinetic parameters. While surface energy is a thermodynamic effect, viscosity is a kinetic effect. If the nanoparticle is localized in a low-viscous phase, it can reduce the viscoelastic difference between the two components or if it is found at the interface, it can prevent the coalescence of discrete domains. In this dissertation, cellulose nanocrystal (CNC) nanoparticles have been used to act as a filler. CNCs are rod-like particles that can be obtained by acid hydrolysis of cellulose, which has unique properties such as low cost, abundance in nature, renewability, biodegradability, high aspect ratio and high surface area. On the other hand, it is difficult to obtain a well dispersion of the CNC due to the presence of hydroxyl groups on the surface and strong interactions between the particles.

In this thesis, the dispersion and selective localization of CNC in PLA/PBAT/CNC blend nanocomposites prepared by different ways are investigated. First, the thermodynamic equilibrium localization of the CNC was found in the PBAT phase with the Young's module, utilizing the surface energy values of PLA, PBAT and CNC given in the literature. In the literature, it is stated that the CNC is not well dispersed in the hydrophobic polymer when prepared directly by the melt mixing method. Therefore, samples were prepared using a combination of solution casting and melt mixing for a good dispersion of CNC. Firstly, blend nanocomposites containing 1, 3, 5, 7 and 10 wt.% CNCs were prepared by directly solution casting method using dimethylformamide (DMF) as the solvent. From scanning electron microscopy (SEM) images, the droplet size of PBAT increased in blend nanocomposites containing 1 wt.% CNC compared to neat blend indicating that the CNC is localized in PBAT. It was assumed that the CNC is migrated to the interface or PLA due to the decrease in PBAT droplet size with increasing CNC content. Rheological analysis showed that the CNC formed a strong network in the PLA phase, since the percolation threshold was formed above 1 wt.% CNC. The preference of CNC to be localized in low viscosity PLA indicates that kinetic factors could become more dominant than thermodynamic factors. The masterbatch containing 7 wt.% CNC prepared through solution casting was used and diluted by twin-screw extruder to produce PLA/PBAT/CNC blend nanocomposites with 1, 3, and 5 wt.% of CNC contents. In addition, the selective localization of CNC in PLA/PBAT/CNC blend nanocomposites was investigated using different processing method (twin-screw extruder and internal mixer) with three mixing strategies. It was observed that CNC migrated to PLA phase in each strategy since the internal mixer method took place over a long period of time. However, finer droplets of PBAT were obtained in PLA/PBAT/CNC blend nanocomposites prepared through twin-screw extruder due to higher shear force. In general, it was concluded that the viscoelastic properties of PLA/PBAT/CNC blend nanocomposites prepared with the combination of solution casting and melt mixing increased, but the desired results in mechanical properties could not be achieved.

SELÜLOZ NANOKRİSTAL İÇEREN POLİLAKTİK/POLİ (BÜTİLENADİPAT-ko-TEREFTALAT) HARMAN NANOKOMPOZİTLERİN HAZIRLANMASI VE KARAKTERİZASYONU

ÖZET

Çevreye verdikleri hasarlar nedeniyle petrol bazlı polimerlerin yerini almak için biyopolimerler geliştirilmeye başlanmıştır. Poli (laktik asit) (PLA), mısır nişastası ve şeker kamışı gibi sürdürülebilir kaynaklardan elde edilen, yenilenebilirlik, yüksek mukavemet, modül ve şeffaflık gibi çekici özelliklere sahip en yaygın biyopolimerlerden biridir. Bu nedenle, endüstride öne çıkar ve petrol bazlı polimerlere bir alternatif olarak görülmektedir. PLA ayrıca işlenebilirliğini, şekillendirilebilirliğini ve köpürebilirliğini sınırlayan yüksek kırılganlık, düşük tokluk, düşük servis sıcaklığı, yavaş kristalleşme ve düşük eriyik mukavemeti gibi bir dizi dezavantaja sahiptir. Literatürde, kopolimerizasyon, harmanlama ve nanoparçacıklarla kompozisyon gibi bu dezavantajların üstesinden gelmek için birçok yaklaşım bildirilmiştir. PLA'nın poli (bütilen adipat-ko-tereftalat) (PBAT), polikaprolakton (PCL) ve poli [(butilen süksinat) -ko-adipat] (PBSA) gibi biyolojik olarak bozunabilir polimerler ile harmanlanması, biyolojik olarak bozunabilirliğinden ödün vermeden tokluğunu arttırmanın en ekonomik yoludur. Bu bağlamda, seçilen ikinci polimer, petrol bazlı polimere dayanan %100 biyolojik olarak bozunabilir sentetik rastgele kopolimer olan PBAT'dir. PBAT, süneklik ve esneklik gibi dikkate değer özelliklere sahip olmasına rağmen, çok düşük bir gerilme modülü gösterir. PLA ve PBAT birbiriyle karışmaz. Karışmayan bir harmanın morfolojisi, her polimerin kendine özgü özelliklerine ve karışım oranına bağlı olarak değişir. Morfoloji nihai karışım performansını büyük ölçüde etkiler; bu nedenle istenen özellikleri elde etmek için kontrol edilmelidir. Literatürde, PLA'nın PBAT ile harmanlanmasının PLA'nın modülünü ve mekanik mukavemetini önemli ölçüde azalttığı raporlanmıştır. Bileşenler arasındaki uyumluluğu artırmak ve sertlik/tokluk dengesini sağlamak için harmana bir uyumlaştırıcı veya katı nanoparçacık eklenir. Uyumlaştırıcılar pahalı oldukları için genellikle uyumlaştırıcı görevi gören nanoparçacıklar kullanılır. Nanoparçacığın seçici lokalizasyonu morfoloji tasarımı ve numunenin istenen özellikleri göstermesi için çok önemlidir. Nanopartiküllerin seçici lokalizasyonu termodinamik ve kinetik parametrelere bağlıdır. Yüzey enerjisi termodinamik bir etki iken, viskozite kinetik bir etkidir. Eğer nanoparçacık düşük viskoz bir fazda lokalize olmuş ise, iki bileşen arasındaki viskoelastik fark azaltılabilir veya arayüzeyde lokalize olmayı terci ederse, dağılmış fazın birleşmesini engeller. Bu tezde uyumlulaştırıcı olarak kullanılan CNC, düşük maliyetli, doğada bol bulunan, yenilenebilirlik, biyobozunurluk, yüksek en boy oranı ve yüksek yüzey alanı gibi benzersiz özelliklere sahip selülozun asit hidrolizi ile elde edilebilen çubuk benzeri parçacıklardır. Bu üstün özelliklerinin yanında CNC'nin

ayrıca ciddi dezavantajları vardır. Yüzeyindeki hidroksil gruplarının varlığı ve parçacıklar arasındaki güçlü etkileşimler nedeniyle CNC'nin iyi bir dispersiyonu elde etmesi zordur.

Bu tezde, CNC'nin PLA/PBAT/CNC harman nanokompozitlerinde dağılımı ve seçici lokalizasyonu araştırılmıştır. İlk olarak, CNC'nin termodinamik denge lokalizasyonu, literatürde verilen PLA, PBAT ve CNC'nin yüzey enerji değerlerinden yararlanarak Young modülü ile PBAT aşamasında olduğu bulunmuştur. Literatürde, doğrudan eriyik karıştırma yöntemi ile CNC'nin hidrofobik polimer içinde iyi bir şekilde dağılamadığı belirtilmektedir. Bu nedenle numuneler, iyi bir CNC dağılımı için çözelti dökümü ve eriyik karıştırma kombinasyonu kullanılarak hazırlandı. Çözelti dökümü yöntemiyle hazırlanan anakarışım, çift vidalı ekstrüder ile seyreltilerek ağırlıkça % 1, 3 ve 5 CNC'i içeren harman nanokompozitleri elde edilmiştir. Bu sebeple, anakarışımın ağırlıkça yüzde kaç CNC'i içermesi gerektiğini bulmak için dimetilformamid (DMF) çözücüsü kullanarak direkt çözelti dökümü yöntemiyle ağırlıkça %1, 3 ,5, 7 ve 10 CNC'i içeren harman nanokompozitleri hazırlanmıştır. Çözelti dökümü ile hazırlanan harman nanokompozitlerde çözücüyü uçurabilmek için ilk olarak bir vakumlu fırında 36 saat 85 °C'de kurutuldu ve daha sonra toz haline getirildi. Muhtemel çözücü kalıntılarını gidermek için, toz haline getirilen harman nanokompozit tekrardan 85 °C'de vakumlu bir fırında 48 saat daha kurutuldu. Seyreltme işlemi sıcaklık aralığı 120, 150, 170, 170 ve 170 °C'lik olan çift vidalı bir ekstrüder kullanılarak yapılmıştır. Ayrıca, CNC'nin seçici lokalizasyonu daha iyi anlayabilmek için üç farklı karıştırma stratejisiyle birlikte çift vidalı ekstrüder veya dahili karıştırıcı yöntemleri kullanılarak PLA/PBAT/CNC harman nanokompozitleri hazırlanmıştır. Dahili karıştırıcıda numuneler 170 °C sıcaklıkta 10 dakika boyunca karıştırılmıştır. Üç farklı karıştırma stratejileri ise şu şekildedir; (m1) PLA, PBAT ve CNC'nin aynı anda karıştırılmasıyla elde edilen anakarışım, (m2) PLA ve CNC'nin karıştırılmasıyla elde edilen anakarışım ve (m3) PBAT ve CNC'nin karıştırılmasıyla elde edilen anakarışımdır. Daha sonra bu anakarışımlar saf PLA ve PBAT polimerleri ile birlikte eriyik karıştırma yöntemi ile seyreltilmiştir.

Sonuçlara baktığımızda, direkt olarak çözelti döküm yöntemiyle hazırlanan ağırlıkça %1 CNC'i içeren harman nanokompozitlerin SEM görüntülerinde, dağılmış faz olan PBAT'in damlacık boyutu saf harmana kıyasla büyüdüğü gözlemlenmiştir. Bu nedenle, CNC'nin PBAT fazında lokalize olduğu varsayılmıştır ve bu sonuç termodinamik denge lokalizasyon sonucunu doğrular niteliktedir. Ancak artan CNC içeriği ile PBAT damlacık boyutunda azalma gözlemlenmiştir. Çözücüyü uçurma esnasında yani 85 °C'de PBAT fazı kristallenmeye başladığı için viskozitesi artar. Viskozitesindeki bu artış sebebiyle CNC'i PBAT fazına giremez ve CNC'i arayüzeyde veya PLA fazında lokalize olur. Reoloji grafiklerinden CNC'nin perkolasyon eşiği konsantrasyonu ağırlıkça %1 üzeri olarak gözlemlenmiştir. Sonuç olarak, bu konsantrasyonda CNC'nin PLA matrisi içerisinde güçlü bir ağ yapısı oluşturduğu düşünülmüştür. CNC'nin düşük viskoziteye sahip PLA'da lokalize olmayı tercih etmesi ile kinetik faktörlerin lokalizasyon üzerinde termodinamik faktörlerden daha baskın olduğu raporlanmıştır. Ayrıca ağırlıkça %7 ve 10 CNC'i içeren harman nanokompozitlerin kompleks viskoziteleri düşük frekansta çakıştığı gözlemlenmiştir. Bu yüzden, anakarışım ağırlıkça %7 CNC'i içerir çünkü en yüksek CNC'i içeren harman nanokompozitte CNC'lerin topaklanmaya başladığı varsayılmıştır. Anakarışımdan elde edilen ağırlıkça %1, 3 ve 5 CNC'i içeren harman nanokompozitlerin kompleks viskoziteleri çözelti dökümü yöntemi ile hazırlananlara kıyasla düşük çıkmıştır. Bunun sebebi olarak da ağırlıkça %7 CNC'i içeren harman

nanokompozitlerde CNC'nin PLA matrisinde lokalize olduğu için seyreltiği esnada topaklanmaya başlamasına atfedilmiştir. Mekanik özelliklerde ise ağırlıkça %5 CNC'i içeren harman nanokompozit haricinde istenilen bir gelişme gözlemlenmemiştir. Bu harman nanokompozitte izod darbe dayanımındaki artış ile birlikte çekme dayanımı ve modül değerleri düşmemiştir. Literatürde, nanopartiküllerin matris fazında seçici lokalizasyonu, dağılmış faz boyutunu azalttığı ve sadece modül ve mukavemeti değil, aynı zamanda darbe özelliklerini de artırdığını raporlamıştır. Sonuç olarak morfoloji, reoloji ve mekanik analizleri birbirlerini doğrulamaktadır. Farklı yöntemler ile hazırlanan harman nanokompozitleri karşılaştırdığımızda, dahili karıştırıcıya kıyasla çift vidalı ekstrüderde daha yüksek kesme kuvveti olması nedeniyle bu yöntem ile hazırlanan PLA/PBAT/CNC harman nanokompozitlerinde daha ince PBAT damlacıkları elde edilmiştir. Dahili karıştırıcı yönteminde ise uzun bir süre boyunca gerçekleştiği için CNC'nin her stratejide PLA fazına göç ettiği gözlemlenmiştir.

Bu tez içeriğinde genel olarak, çözelti dökümü ve eriyik karıştırma kombinasyonu ile hazırlanan PLA/PBAT/CNC harman nanokompozitlerinin viskoelastik özelliklerinde bir artış olduğu, ancak mekanik özelliklerde istenilen sonuçların elde edilemediği sonucuna varılmıştır.

1. INTRODUCTION

Biopolymers obtained from renewable resources have been started to be used instead of petroleum-based polymers in recent years [1-3]. Poly (lactic acid) or polylactide (PLA) stands out among biopolymers as it has satisfactory physical and mechanical properties such as high modulus and strength that can replace petroleum-based polymers such as polyethylene (PE), polypropylene (PP), polystyrene (PS) and polyethylene terephthalate (PET), which are widely used in commodity and engineering applications [4, 5]. Therefore, there are many approaches to overcome the PLA's disadvantages such as low melt strength, slow crystallization, brittleness, low toughness, and poor processability. This approach could be using nanoparticles, blending with other biopolymers, and copolymerization. In this context, the approach to blending PLA with poly(butylene adipate-co-terephthalate) (PBAT) has been chosen to improve PLA properties without sacrificing biodegradability [6]. PBAT is a 100% biodegradable synthetic random copolymer and shows attractive properties such as high ductility and flexibility, although it possesses low tensile modulus and strength. According to the literature, PLA and PBAT show immiscible morphology. Although PBAT could enhance the elongation of PLA, it has been reported to reduce tensile strength and modulus [7-9]. For this reason, cellulose nanocrystals (CNC) have been used to improve the compatibility of PLA and PBAT by affecting interfacial properties. CNCs are rod-like particles that can be obtained by acid hydrolysis of cellulose, with unique properties such as high aspect ratio, high surface area and high crystallinity. On the other hand, CNC is difficult to well dispersion due to the presence of hydroxyl groups on the surface and the strong interactions between the particles [10-12]. Also, the selective localization of the CNC is important for the properties of the blend nanocomposites. The purpose of selective localization of nanoparticles is to improve the compatibility between the two phases and bring the viscosities closer together, thereby preventing the coalescence of the domains [13]. In this context, PLA/PBAT/CNC blend nanocomposites were prepared with two different approaches; (i) solution casting (SC) and (ii) the dilution of solution casted masterbatch by melt mixing using a twin-screw extruder (mTSE) or internal mixer (mIM). In addition, three

different mixing strategies have been used to better understand the selective localization of the CNC.

2. LITERATURE REVIEW

2.1. BIOPOLYMERS

The use of petroleum-based polymers has become a global concern because they remain as non-degradable wastes in the environment while the oil resources are diminishing and its price is fluctuating. For these reasons, there is a tendency to produce biopolymers that are either derived from renewable resources such as agricultural, animal, and microbial sources or are biodegradable or are bio-based and biodegradable. Figure 2.1 shows classification and examples of these three biopolymers categories [1-3].

Biodegradable polymers are being developed to be used in various commodity applications where petroleum-based polymers are currently being used. Furthermore, due to their biocompatible and biodegradable features, biopolymers are also promising candidates to be used in biomedical applications such as tissue engineering and drug delivery. Besides all these advantages, most of the biopolymers could have series of limitations. These limitations could originate from their intrinsic features that could be revealed during the processing or in the properties of the final products. Another limitation could be considered as the thermal stability of most of these biopolymers [1, 14].

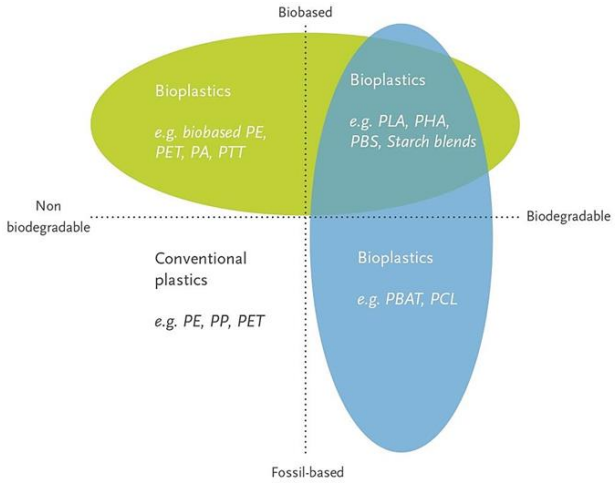

Figure 2.1 : Classification and examples of polymers.

2.2. POLYLACTIDE (PLA)

Poly (lactic acid) or polylactide (PLA) is highly versatile, aliphatic polyester biopolymer obtained from renewable resources such as cornstarch, sugarcane and other renewable biomass products and wastes. PLA is the most remarkable and researched polymer among biopolymers. As an environmentally friendly biopolymer, PLA could stand out as a promising candidate in a wide range of industries and applications. There are two polymerizations routes to synthesize PLA as shown in figure 2.2. These are either direct polycondensation of lactic acid monomers or ring-opening polymerization of the cyclic lactide dimer. In direct polycondensation polymerization, water is produced as a by-product and only a low molecular weight PLA could be obtained. In this regard, ring opening polymerization, which is the commercialized method, is more preferred than direct polycondensation polymerization because in this route high molecular weight PLA with better molecular entanglement could be obtained [7, 15, 16]. PLA production offers numerous advantages such as: (a) being derived from 100% renewable agricultural resources; (b) consumption of large amounts of carbon dioxide during its production; (c) saving a significant amount of energy; (d) being recyclable and compostable; (e) assisting the improvement of farm economies; and (f) the physical and mechanical properties can be manipulated by means of polymer architecture [17].

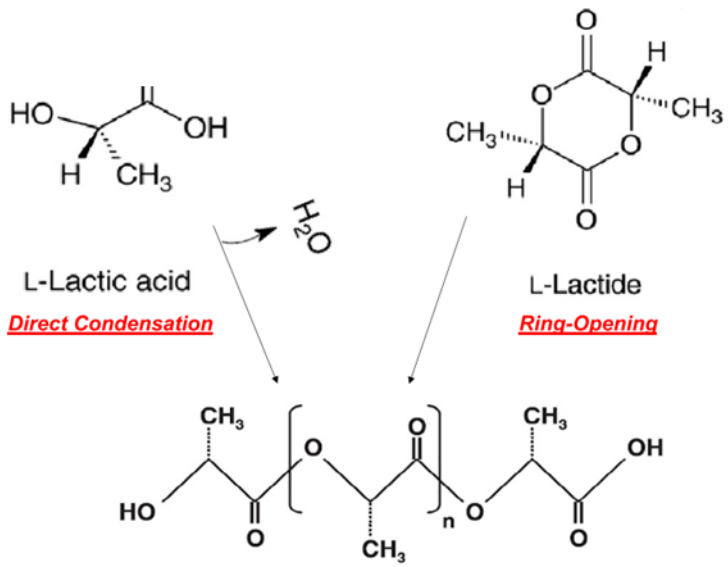

Figure 2.2 : Polymerization routes to produce PLA through direct condensation and ring opening polymerizations [7].

Lactic acid and lactide molecules are described by different stereochemistry that are illustrated in figure 2.3. There are two types of monomers of lactic acid that are L-lactic acid or D-lactic acid. The lactide molecule that has three types of DD-lactide, LL-lactide or LD-lactide (meso-lactide) is a cyclic dimer and is formed by condensation of lactic acid. Poly (L-lactic acid) (PLLA) or poly (D-lactic acid) (PDLA) are homopolymers which are made up from only L- or D- lactic acid by direct condensation polymerization and also is formed by ring opening polymerization from LL- or DD- lactide dimers, respectively [16, 18]. The glass transition temperature (T_g) and the melting temperature (T_m) of PLA are reported around 50-60 °C and up to 180 °C, respectively [19, 20].

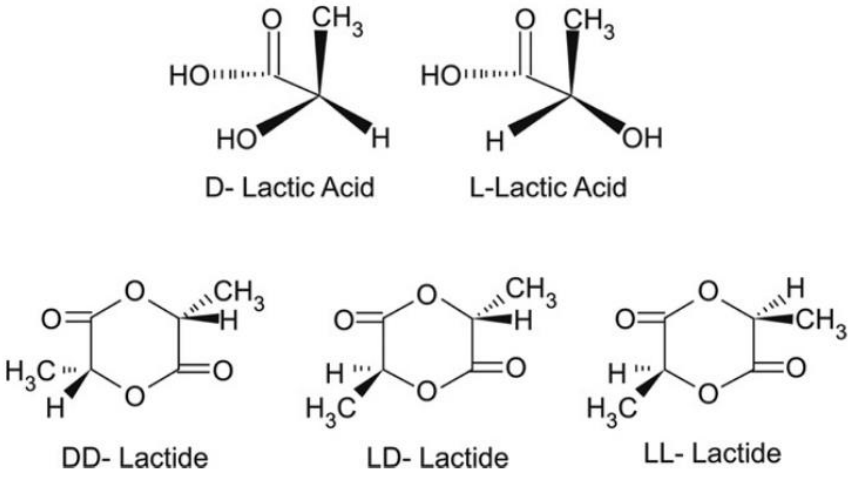

Figure 2.3 : Stereochemistry forms of lactic acid and lactide molecules [18].

The production of homopolymer PLAs is very expensive. In this context, the commercial PLAs are often copolymers with various L/D ratios. The ratio of L and D isomers in the PLA structure affects the workability, degradation and crystallization behavior of PLA. If the D-lactic acid content is greater than 8-10%, PLA could not crystallize at all and hence would possess only an amorphous structure. The decrease in D-lactic acid, on the other hand, increases the chance of crystallization and thereby the degree of closed packness of crystallites resulting in increase in T_m of PLA [6, 15, 18].

PLA has a great potential to be used in various products related to commodity applications such as industrial packaging field [6, 17, 21] or in biomedical applications [22, 23]. This is due to its excellent properties such as biodegradable, biocompatible, non-toxic, transparency, good clarity, high barrier features, high strength and high

modulus. Figure 2.4 shows the comparison of mechanical properties PLA and some petroleum-based polymers like high density polyethylene (HDPE), polypropylene (PP) and polystyrene (PS). PLA and PS shows similar mechanical properties therefore PLA can be used in a wide range of daily products where PS is being used. PLA could even have a higher performance than PS if the chain structure of the PLA is oriented and crystal structures could be formed [4, 5]. On the other hand, PLA has a higher tensile and flexural modulus than HDPE and PP, but has a lower notched izod impact and elongation at break than the noted polymers. Therefore, PLA's brittleness, low toughness and low impact strength are considered as its drawbacks from mechanical properties perspective [19].

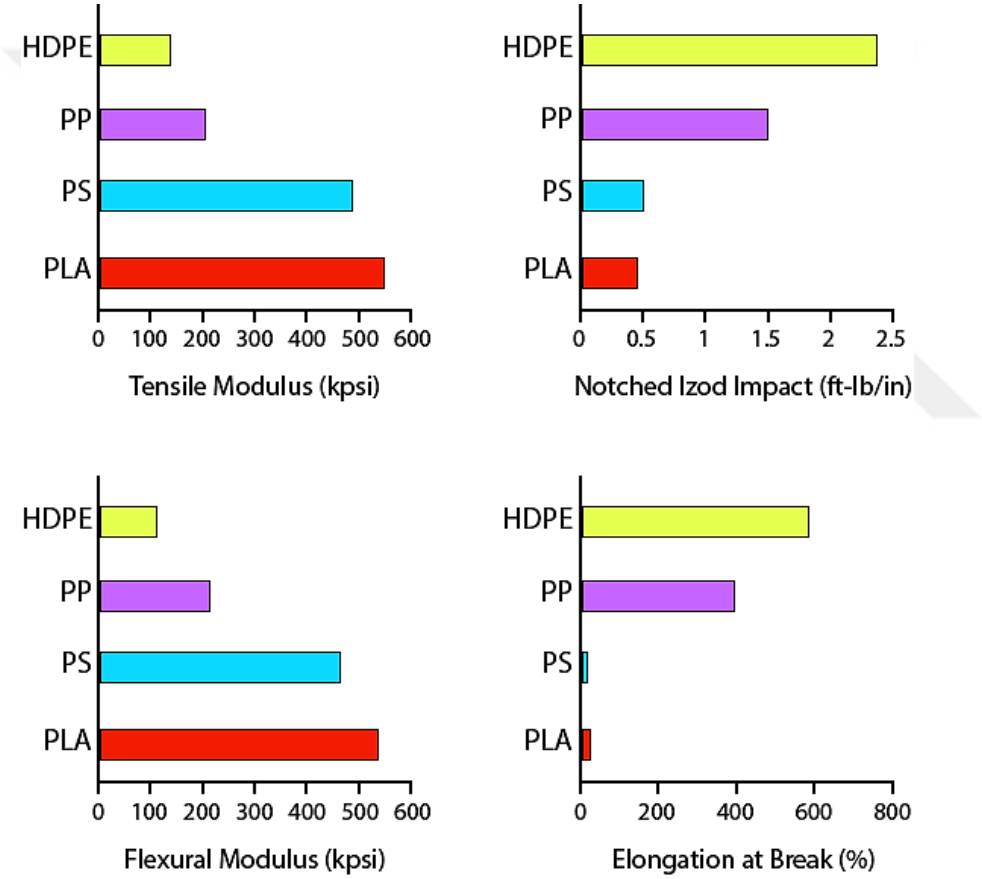

Figure 2.4 : Comparison of the mechanical properties of PLA with some common plastic packaging materials [5].

PLA could also suffer from some other series of drawbacks. PLA has low melt strength and slow crystallization kinetics regardless of its D-content [18, 24]. These two drawbacks would consequently hamper PLA's processability, formability and foamability. For instant, during the foaming process, the low melt strength could cause cell coalescence and cell-wall rupture and hence a severe non-homogenous foam

morphology with very low expansion [19]. In this context, there are strategies to overcome these drawbacks such as using modifiers, blending with other biopolymers, copolymerization, development of their composites, or physical treatments [6].

As mentioned, the slow crystallization kinetics of PLA is one of the disadvantages that limits its processability and service temperature. Due to this disadvantage, PLA will deteriorate beyond its T_g, thereby the service temperature is relatively limited to temperatures below T_g which is about 50-60 °C. In addition, due to the very slow crystallization kinetics, PLA shows another crystallization phenomenon upon heating. Similar to what exists in polyethylene terephthalate (PET), this phenomenon is called cold crystallization with T_{cc} as the cold crystallization peak. This crystallization indeed occurs when the melt crystallization during the cooling is not completed and hence upon heating the molecules that had the potential to crystallize, would indeed crystallize upon heating. This also happens above the T_g of PLA because the molecular mobility above the T_g could provide the required activation energy for a new crystallization (i.e., cold crystallization) which is also shown in Figure 2.5 [18, 19, 24, 25]. It should be reminded that the crystallization behavior of PLA depends on the D-Lactide content, molecular weight and chain branching [17, 18]. The effect D-content on the PLA crystallization was disclosed earlier. As the molecular weight of PLA decreases, melt crystallization and cold crystallization occurs at low temperatures due to the PLA's higher molecular mobility, so that crystals can form at a lower temperature with the reduce in perfection of the formed crystals. Chain branching has also been shown to cause induction of crystallization by providing chain extended sites as crystal nucleation locations for PLA. However, the further increase in the degree of branching will prevent molecular mobility and hence the branching would hinder the crystallization [18, 19, 24].

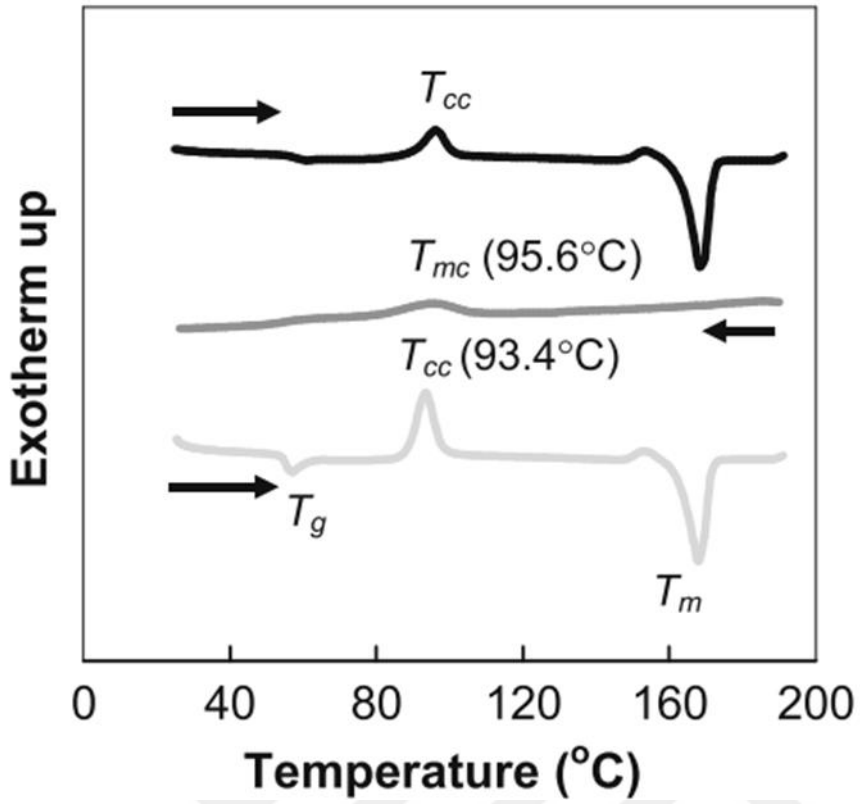

Figure 2.5 : DSC thermograms of PLA (3051D) at the same heating and cooling rates of 5 °C/min in three scans [25].

The rheological and viscoelastic properties of PLA also depend on the PLA molecular weight and its molecular architecture (i.e., linear or branched structures).

If PLA has a high molecular weight, it shows shear thinning (non-Newtonian fluid) behavior. In contrast, if it has a low molecular weight, it shows non-Newtonian behavior. The rheological and viscoelastic properties of polymer melts can mathematically be obtained with the zero-shear viscosity parameter (η_0) which is a function of the molecular weight by Carreau-Yasuda model (equation 2.1) [18].

$$\frac{\eta - \eta_\infty}{\eta_0 - \eta_\infty} = \frac{1}{(1+\lambda\gamma^m)} \qquad (2.1)$$

where η, γ, λ, m, and η_∞ determine viscosity, shear rate, relaxation time, shear thinning behavior, and viscosity at infinite shear rate, respectively. Figure 2.6 shows the viscosity dependence of the molecular weight of linear PLA as a function of shear rate with Carreau-Yasuda fitted model. This figure shows that the increase in the molecular weight of the linear structure of PLA increases the η_0 of PLA [18].

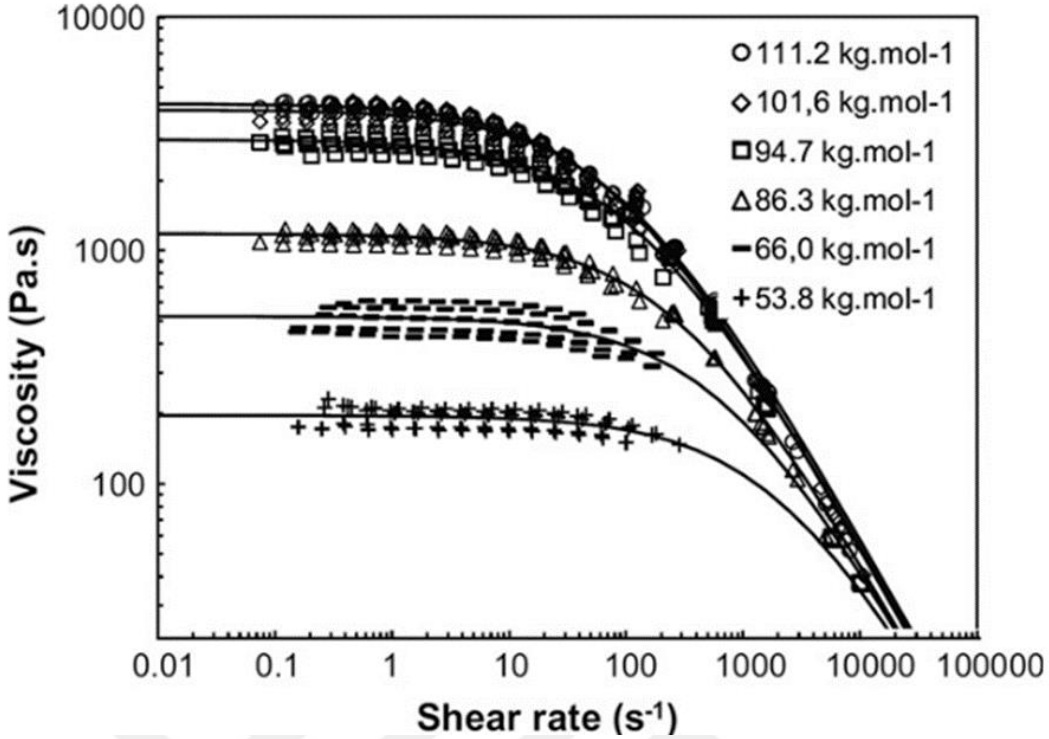

Figure 2.6 : Viscosity of PLA at different molecular weights [18].

The rheological properties of PLA can be significantly changed by branching. When linear PLA shows low melt strength, it is desirable to increase melt strength by adding long chain branching. Figure 2.7 shows the graph of complex viscosity versus frequency for branched and linear PLA [5].

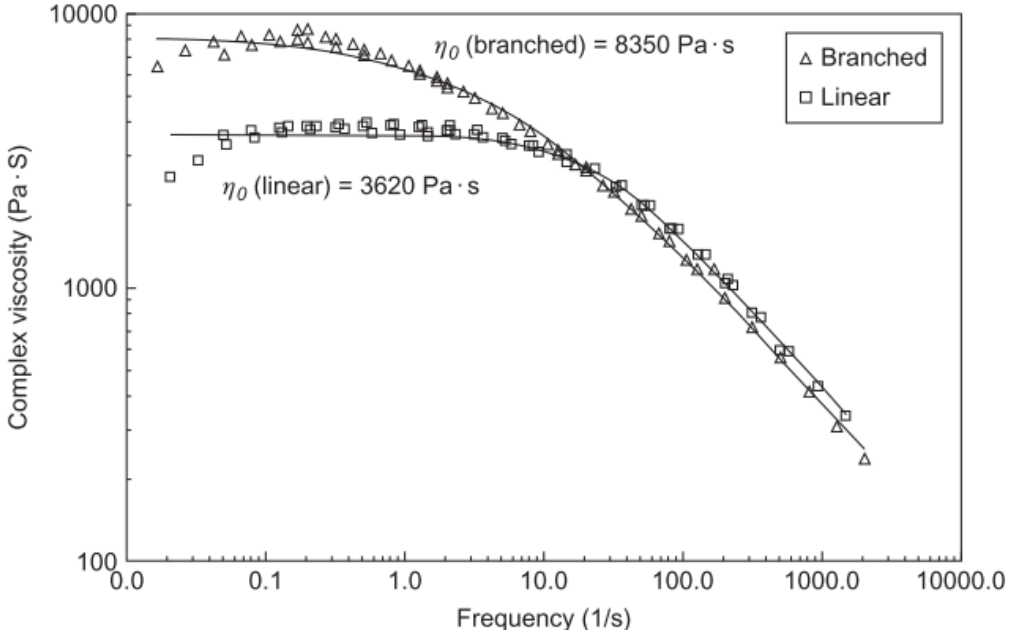

Figure 2.7 : Comparative flow curves for commercial-grade branched and linear materials [5].

2.3. POLY (BUTYLENE ADIPATE-CO-TEREPHTHALATE) (PBAT)

PBAT is synthetic random copolymers based on petroleum-based polymers, but 100% biodegradable. PBAT is synthesized by the transterification reaction between adipic acid and dimethyl terephthalate polyesters as shown in Figure 2.8 [26, 27].

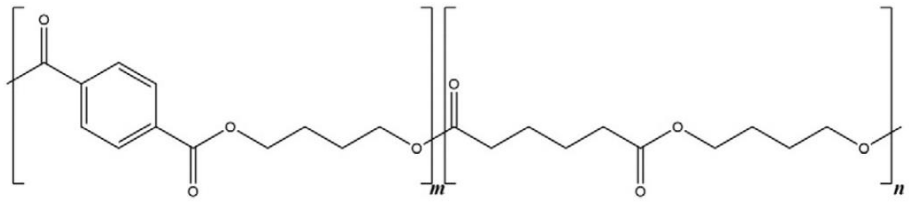

butylene terephthalate butylene adipate

Figure 2.8 : Chemical structure of PBAT [26].

Polyesters containing aliphatic groups in their structures exhibit biodegradable properties. In contrast, aliphatic homopolyesters are insufficient in their mechanical and thermal properties, which are important for application. Aromatic homopolyesters have sufficient mechanical and thermal properties, but are not biodegradable. Therefore, aliphatic-aromatic copolyesters have been developed. This copolyesters provides both the biodegradability of the aliphatic polyester and the good mechanical and thermal strength of the aromatic polyester. As a result of the studies, it is concluded that the aliphatic-aromatic copolyester which has the most suitable properties especially in biodegradability behavior is PBAT [28].

PBAT is flexible polymer, with higher elongation at break (close to 700%), Young modulus of 20–35 MPa, and tensile strength of 32–36 MPa. It also has low density. These properties make PBAT an alternative to polyethylene (PE) [27, 29]. On the other hand, PBAT is an interesting material for industrial packaging applications due to its elongation at break, low water vapor permeability and good processing properties [30].

2.4. POLYMER BLENDS

Polymer blend is a physical mixture of at least two macromolecular substances, polymers or copolymers with different advantages in a single system. Interface is zone across which matrix and reinforcing phases interact. There are two types of polymer blend: miscible blends, and immiscible blends. Gibbs free energy of mixing (equation 2.2) is used to describe thermodynamics of the mixing of the binary polymer-polymer mixture [31].

$$\Delta G_m = RT\ \chi_{AB}\varphi_A\varphi_B + RT\left[\frac{\rho_A\varphi_A ln\varphi_A}{Mw_A} + \frac{\rho_B\varphi_B ln\varphi_B}{Mw_B}\right] \qquad (2.2)$$

where ΔG_m is the Gibbs free energy of blend, R and T are gas constant and the absolute temperature, respectively, χ_{AB} is the Flory-Huggins interaction parameter, φ_i is the volume fraction of the components, ρ_i is the density of components, and Mw_i is the molecular weight of the polymers.

$$\Delta G_m = \Delta H_m - T\Delta S_m \qquad (2.3)$$

where ΔH_m is heat of mixing and ΔS_m is entropy of mixing. Miscible polymer blend shows a single-phase system with has the negative value of the free energy and heat of mixing (equation 2.3), $\Delta G_m \approx \Delta H_m \leq 0$, and $\partial^2 \Delta G_m / \partial \phi^2 > 0$. Further, miscible polymer blend shows only one T_g value, which is between the T_g of the polymers consisting of the blend and depend on the amounts of components of polymer blend. In immiscible polymer blends two separate phases are formed, which system is characterized by a poor adhesion between the phases, coarse and easy to replace morphology. Immiscible polymer blends have $\Delta G_m \approx \Delta H_m > 0$ [31].

2.4.1. Morphology development in immiscible polymer blends

The morphology of the immiscible polymer blends varies depending on the intrinsic properties of each base polymer and blend ratio, generally existed into two general morphology types: matrix/dispersed phase morphology and co-continuous phase morphology. Matrix/dispersed phase morphology is observed when the minor phase has a low concentration. By increasing the concentration of the minor phase, the dispersed/matrix phase morphology becomes continuous morphology as droplets begin to coalescence and reach the percolation threshold. Morphology greatly influences the final blend performance therefore, it must be checked to obtain the desired properties. For instance, the drop morphology improves the toughness and has matrix/dispersed phase morphology. Figure 2.9 shows that different morphologies of polymer blends and their properties [4, 32].

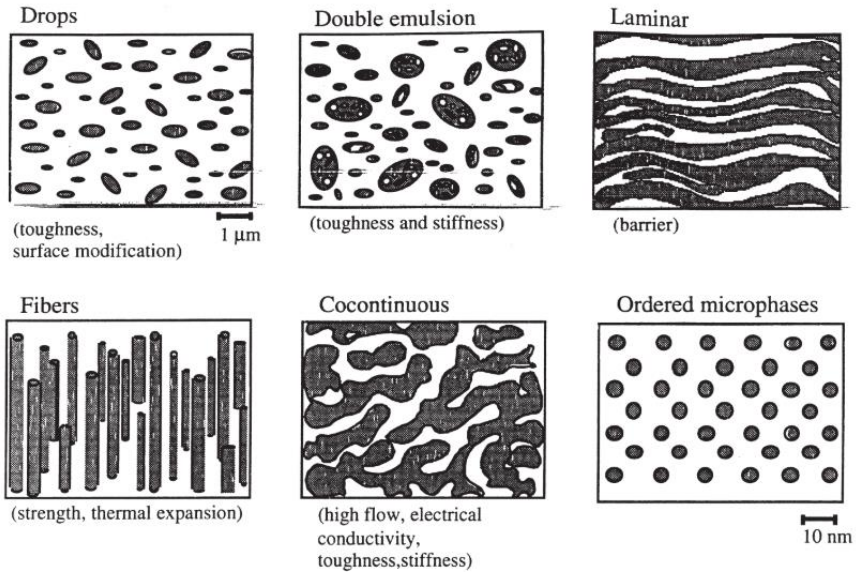

Figure 2.9 : Different morphologies of polymer blend and their properties [32].

In this thesis, the PLA is chosen as the matrix and by using PBAT as the droplet phase, the toughness and ductility is also aimed to be improved. The components that make up the drop morphology of the polymer blends are the matrix phase and the dispersed phase. Matrix phase holds the dispersed phase and have the most amount phase in the blend. Dispersed phase is embedded in the matrix and is usually stronger than the matrix. The distribution and homogeneity of the droplets can be adapted by controlling the viscosity ratio, the interfacial tension, processing conditions, and phase compositions. Finer dispersed phase could be obtained when the viscosity ratio of the blend components is closer to one. If greater than 1, the blend morphology is coarse. The interfacial tension, should be low for a better dispersed phase [33].

2.4.2. Interfacial tension

Interfacial tension is important of immiscible polymer blends because of these polymers have multiple-phase structures containing one or more interfaces. The interfacial tension are the adhesive forces between the phases. The structure and strength of interfaces significantly affect the physical and mechanical properties of immiscible polymer blends due to change of morphology [34]. Good and Girifalco was found that interface tension can be calculated based on work of adhesion concept (equation 2.4) [35].

$$\gamma_{12} = \gamma_1 + \gamma_2 - W_A \qquad (2.4)$$

In which *W*a is the work of adhesion and γ_{12} is the interfacial tension between the two components. γ_1 and γ_2 stand for the surface tension of the component 1 and component 2, respectively. When an interface is formed from two individual surfaces which is work of adhesion, the Gibbs free energy per unit area is reduced. The greater the interfacial attraction, the greater the work of adhesion (as shown in figure 2.10) will be and consequently the smaller the interface tension will be.

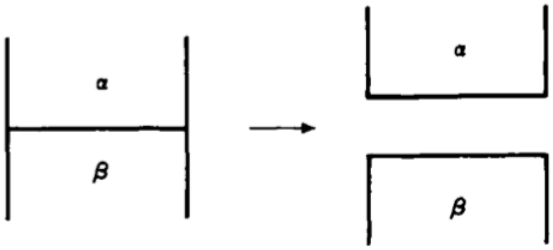

Figure 2.10 : Work of adhesion [34].

Wu offers two approaches for a system with low surface tension. These approaches considered the concept of energy additivity and the contribution of polar (γ^p) and dispersive (γ^d) components in the work of adhesion. The harmonic-mean approach is used between low energy phase interactions (equation 2.5). The geometric-mean approach is preferred for interactions between the low energy phase and the high energy phase, or between the high energy phases (equation 2.6) [34].

Harmonic mean equations;

$$\gamma_{12} = \gamma_1 + \gamma_2 - 4\left[\frac{\gamma_1^d \gamma_2^d}{\gamma_1^d + \gamma_2^d} + \frac{\gamma_1^p \gamma_2^p}{\gamma_1^p + \gamma_2^p}\right] \quad (2.5)$$

Geometric mean equations;

$$\gamma_{12} = \gamma_1 + \gamma_2 - 2\left[\left(\gamma_1^d \gamma_2^d\right)^{1/2} + \left(\gamma_1^p \gamma_2^p\right)^{1/2}\right] \quad (2.6)$$

2.4.3. Palierne model

Morphology development in immiscible polymer blends is greatly influenced by the interfacial tension between the two components from small amplitude oscillatory shear (SAOS) which can be calculated with the Palierne Model (equation 2.7) [36].

$$G_b^*(\omega) = G_m^*(\omega)\,\frac{1+3\phi H^*(\omega)}{1-2\phi H^*(\omega)} \qquad (2.7)$$

where, $G_b^*(\omega)$ is a function of the complex modulus of blend. $G_m^*(\omega)$ and $G_d^*(\omega)$ are the norms of the complex modulus of the matrix and dispersed phase, respectively. ϕ is function of volume fractions, R_v is function of volume fractions of droplets of radius, γ is interfacial tension and ω is frequency.

with $H^*(\omega)$ given through;

$$H^*(\omega) = \frac{4\frac{\gamma}{R_v}\left[2G_m^*+5G_d^*(\omega)\right]+\left[G_d^*(\omega)-G_m^*(\omega)\right]\left[16G_m^*(\omega)+19G_d^*(\omega)\right]}{40\frac{\gamma}{R_v}\left[G_m^*+G_d^*(\omega)\right]+\left[2G_d^*(\omega)+3G_m^*(\omega)\right]\left[16G_m^*(\omega)+19G_d^*(\omega)\right]} \qquad (2.8)$$

Morphological changes during flow such as breakup or coalescence cannot be predicted by equation 2.8, because of this model is limited to linear viscoelasticity. The Palierne model has been shown to predict well the linear behavior of immiscible blends under the SAOS flow, when the polydispersity of the droplet size dv/dn (ratio of the volume and number average diameter, respectively) is less than 2 [33, 36-38].

2.4.4. Droplet breakup

The viscosity ratio (ρ), capillary number (*C*a) and shear field control the droplet breakup. ρ is described as the viscosity of the droplet phase (η_d) over the viscosity of the matrix phase (η_m). Ca is defined as the ratio between the hydrodynamic stresses and the interfacial stresses (Taylor theory). As can be understood from equation 2.9 and 2.10, there is an inverse relationship between Ca and ρ. It is explained that deformation increases with increasing Ca or with decreasing *p* [39, 40].

$$\rho = \eta_d/\eta_m \qquad (2.9)$$

$$Ca = \frac{\eta_{matrix}\dot{\gamma}R}{\gamma_{12}} \qquad (2.10)$$

in which, $\dot{\gamma}$ is the shear rate, R is the droplet radius, γ_{12} is the interfacial tension.

Viscous forces exceed the interfacial ones at a certain critical shear rate and therefore, the droplet breakup occurs. The capillary number corresponding to the critical shear rate is called the critical capillary number (Ca_{crit}). In cases where the Ca_{crit} is lower

than Ca, droplet breakup does not occur, consequently droplet coalescence could exist [41, 42].

Grace et al. developed the Taylor theory and gives the relation between the Ca_{crit} and ρ under elongation and simple shear flow as shown in Figure 2.11. Elongational forces are more effective than shear forces to obtain breakup and dispersion of dispersed phases. Ca_{crit} for the elongational flow is always lower than that of the shear flow. Ca_{crit} in the pure elongational flow is minimum when the viscosity ratio is between $0.25<\rho<1$, therewith breakup occurs. Moreover, under simple shear flow, the droplet breakup happens when $\rho<4$ [43].

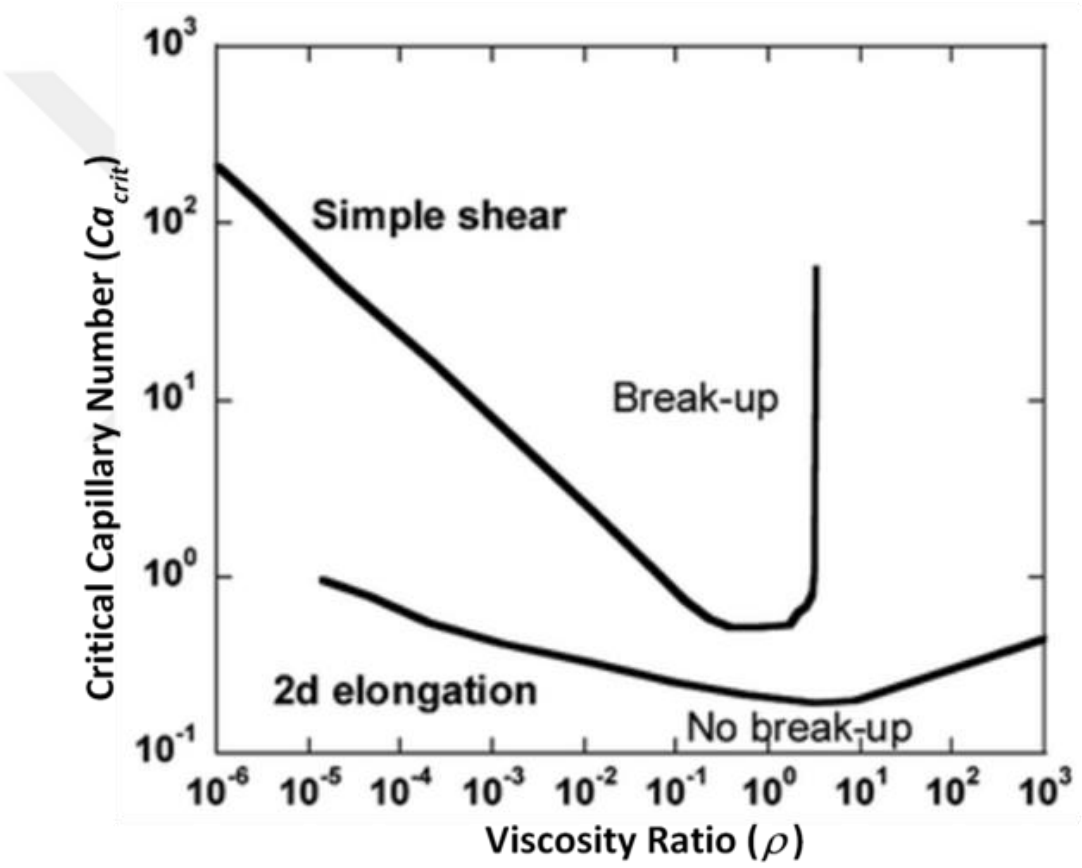

Figure 2.11 : The Grace curve gives the relation between the Ca_{crit} and ρ under elongation and simple shear flow [44].

2.5. PLA/PBAT BLENDS

PBAT has been known to be a promising alternative to produce PLA based blends with improved ductility, toughness, melt strength, and processability that could be used in various commodity applications like packaging [7-9].

2.5.1. Processing

PLA/PBAT blends are generally made in two ways. First way is solution casting (SC) which is dissolving two polymers in the same solvent such as chloroform [45], and dichloromethane [46], followed by evaporation of the solvent. The second way is the melt-mixing process such as twin-screw extruder (TSE) and internal mixer (IM) in which the two polymers are heated together above the glass transition temperatures with shear. Most PLA / PBAT blends were prepared using a melt mixing with extruder due to the most preferred method in the industry. Table 2.1 compares processing of PLA blended with different biopolymers.

Table 2.1 : Summarized studies reported on the solution casting and melt mixing of PLA blend.

References	Type of Processing	Processing condition
Signori et al., (2009) [9]	IM	T=150-200 °C; blade rate= 50 rpm; and mixing time=10 min
Wang et al., (2016) [45]	SC	dissolved into 100 mL of chloroform with a magnetic stirrer at 23 °C for 6 h
Nofar et al., (2017) [47]	TSE and IM	TSE with an L/D ratio of 40: at 160 °C for all the heating zones and 100 rpm IM: under a nitrogen atmosphere for 10 min at 160 °C and 100 rpm.
Kang et al., (2018) [46]	SC	dissolved in dichloromethane solvent (40 mL) at room temperature with a magnetic stirrer for 5 h

2.5.2. Morphological analysis

PLA/PBAT blend is immiscible blend. Nofar et al. [47] investigated the effect of high molecular weight PLA (HPLA) and low molecular weight PLA (LPLA) on PLA/PBAT blend with different processing methods (TSE and IM) as shown in Figure 2.12. For HPLA-PBAT (TSE), HPLA-PBAT (BB) and LPLA-PBAT (BB), they calculated the mean volume-mean diameter (D_v) of the dispersion phase as 0.5, 1.2 and 0.7 μm, respectively. The smaller dispersion phase size in HPLA-PBAT (TSE) is achieved due to shear and elongation deformation applied more than BB during the TSE processing. Figure 2.12 shows SEM images showing the droplets of PBAT dispersed phases in the PLA matrices. As mentioned earlier, the viscosity ratio and interfacial tension affected by different process temperatures and methods are important for the morphology of the blends. The viscosity ratios for HPLA-PBAT and LPLA-PBAT are 0.38 and 0.57, respectively. Thus, LPLA-PBAT is expected to have

finer droplets than HPLA-PBAT because the viscosity ratio is slightly closer to 1. When the processing temperature increases, the interfacial tension between PLA and PBAT drops from 1.3 to 1.0 $mJ.m^{-2}$ and hence finer morphology was obtained.

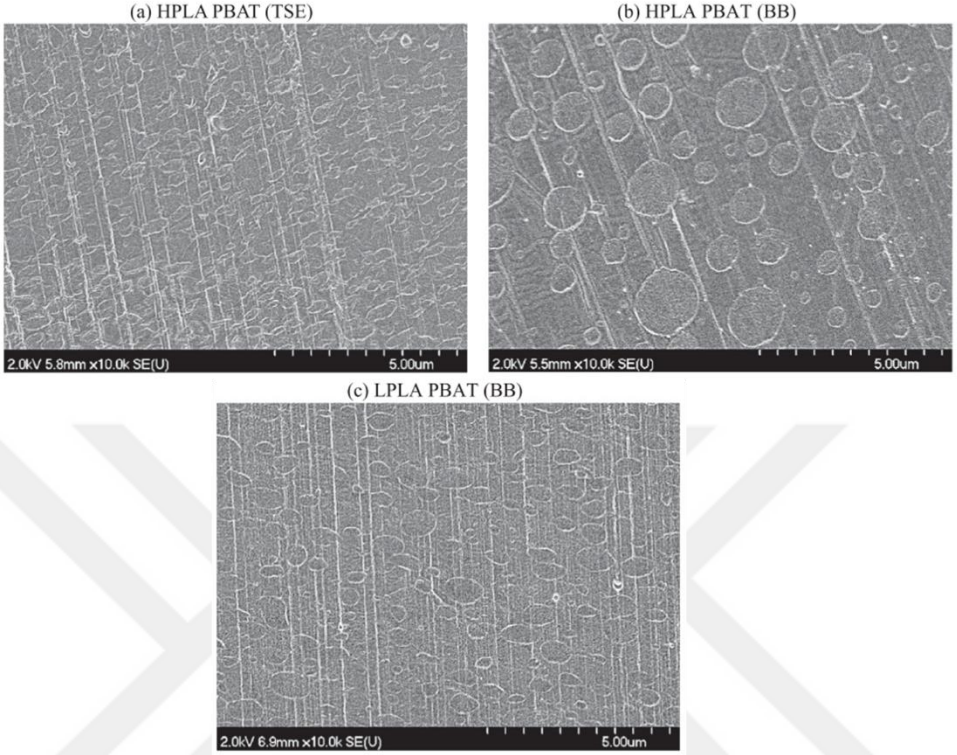

Figure 2.12 : SEM images showing the droplets of PBAT dispersed phases in the PLA matrices [47].

2.5.3. Rheological analysis

The complex viscosity of PBAT is higher than PLA, as shown in Figure 2.13. PLA has a longer Newtonian region than PBAT, and when PBAT was added, the Newtonian region of the blends decreased [48, 49]. The blends have a higher complex viscosity than neat polymers, except for the blend containing 5 wt.% PBAT. This indicates that the melt viscosity and flexibility of PLA increased due to the presence of soft PBAT. The blend with a 20 wt.% PBAT content shows a higher viscosity at all frequencies. However, the blend containing 30 wt.% PBAT exhibits a lower viscosity than the blend with 20 wt.% PBAT, indicating a possible change in morphology. In the blend containing 50 wt.% PBAT, the viscosity continues to decrease, suggesting the formation of a continuous morphology. With the further increase of the PBAT content, a sharp increase in viscosity occurs, indicating a change again in morphology [49]. Nofar et al. [10] reported that PLA exhibits Newtonian behavior at low shear rates, while shear thinning behavior at high shear rates and PBAT exhibits shear thinning

behavior at all shear rates. Also, they reported that the storage module of PLA blending systems is higher than that of neat PLA at low frequencies [50].

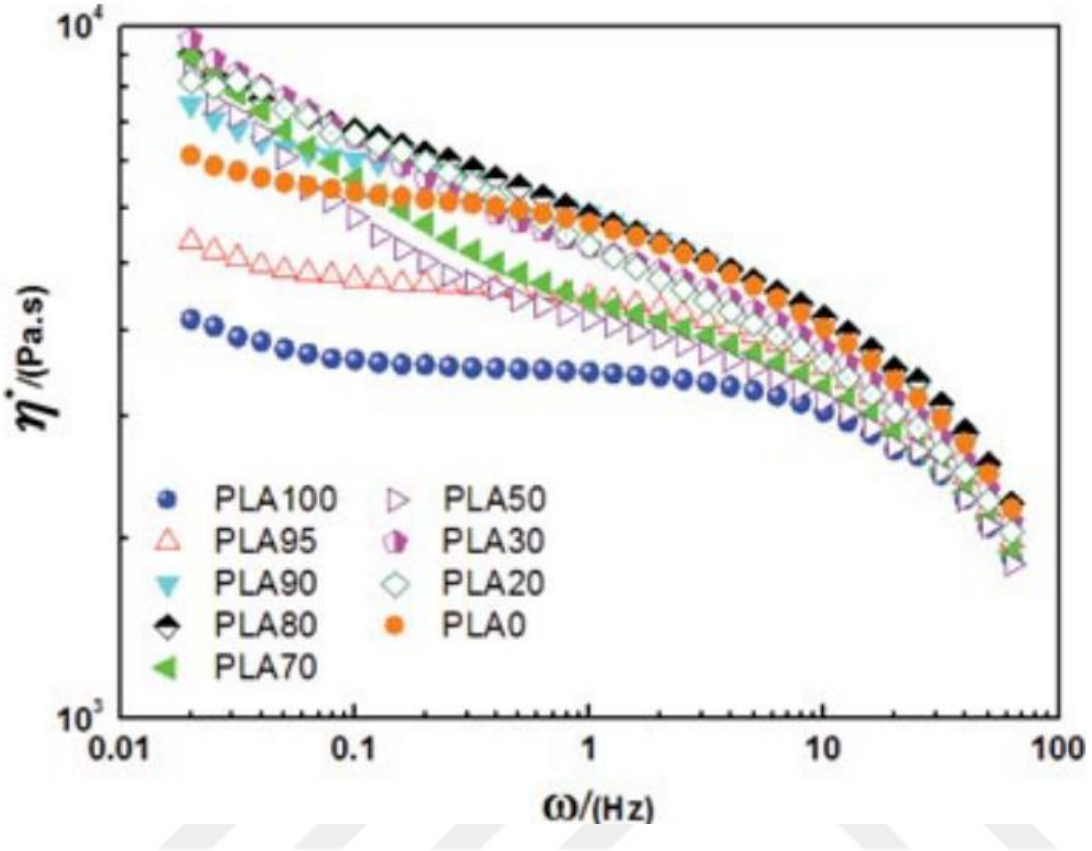

Figure 2.13 : Complex viscosity versus frequency for different PLA/PBAT compositions obtained at 190 °C [49].

2.5.4. Thermomechanical analysis

According to DMA, each neat polymer showed one peak, but the blends showed two glass transitions, one for PBAT and the other for PLA. Therefore, there is no significant molecular interaction between PLA and PBAT as glass transition temperatures remain unchanged with PBAT loading. Figure 2.14 shows DSC thermogram of the neat PLA, neat PBAT and PLA / PBAT blends. With the inclusion of PBAT, the cold crystallization temperature of PLA decreased by about 10 ° C and the peak width narrowed. Jiang showed that enthalpy of crystallization (ΔHc) and enthalpy of fusion (ΔHm) of PLA at a heating rate of 10 ° C/min were much smaller than at 5 ° C/min. When enough time is given, the neat PLA and PLA in the blend will crystallize equally. Although the addition of PBAT increased the crystallization rate and crystalline ability of PLA, it did not change the final crystallinity of PLA in the blend [50].

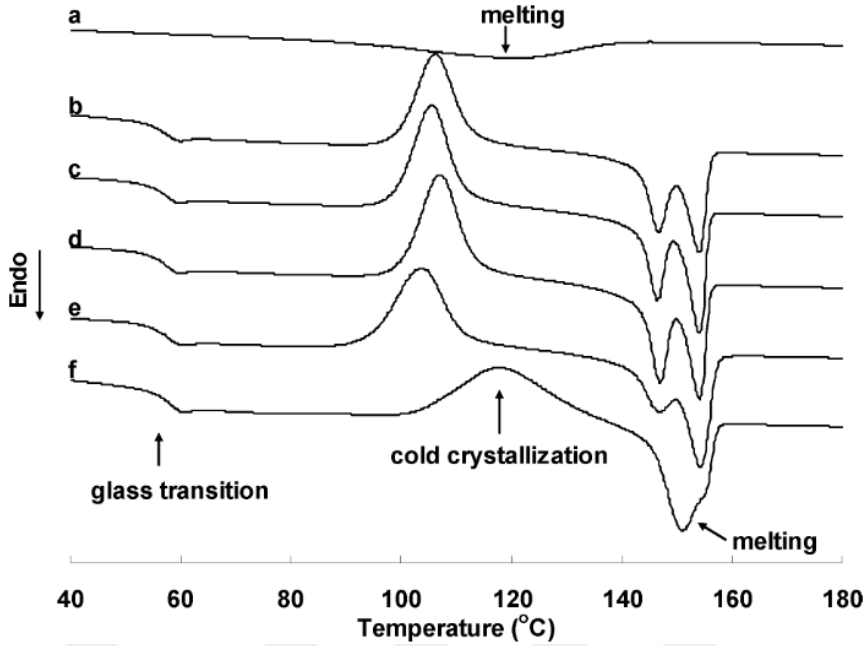

Figure 2.14 : Second heating of PLA/PBAT blends at 5 °C/ min.; (a) PBAT; (b) 20% PBAT; (c) 15% PBAT; (d) 10% PBAT; (e) 5% PBAT; (f) PLA [50].

2.5.5. Mechanical analysis

Table 2.2 compares mechanical properties of PLA blended with different biopolymers. The mechanical properties of PLA are improved by blending with other biopolymers. The PLA/PBAT blend has the best results considering the average of all its mechanical properties [51].

Table 2.2 : Mechanical properties of PLA blended with different biopolymers [51].

Material	Elongation at break (%)		Tensile Modulus (GPa)		Impact strength	
	Neat PLA	Blend	Neat PLA	Blend	Neat PLA	Blend
PLA/PCL (30%)	10	20	2.8	1.6	2 kJ/m^2	3.6 kJ/m^2
PLLA/PCL (20%)	5	175	1.3	1.1	-	-
PLLA/PPD* (20%)	15	55	1.4	1.6	-	-
PLLA/PBS (50%)	7.6	56	3.3	1.7	23.2 J/m	34.5 J/m
PLLA/PBSL** (10%)	3	160	3	2.5	-	-
PLLA/PBSA (25%)	-	150	-	1.2	-	-
PLLA/PHBV*** (40%)	5	7	2.4	1.5	-	-
PLLA/PHB**** (50%)	-	4.4	-	2.7	-	-
PLA/PBAT (25%)	4.2	120	2.1	1.7	22 J/m	31 J/m

*Poly(para-dioxanone) **Poly(butylene succinate-L-lactate) ***Poly(3-hydroxybutyrate-co-hydroxyvalerate) ****Poly(hydroxybutyrate]

Jiang et al. [48] revealed that although the tensile strength and modulus decreased, with the addition of PBAT, the toughness and elongation of the blend increased. They reported that the elongation of the blend was enormously increased (>200%) even when of 5 wt.% PBAT was added. With the addition of 20 wt.% PBAT, the modulus decreased from 3.4 to 2.6 GPa, and while tensile strength from 63 to 47 MPa.

2.6. CELLULOSE NANOCRYSTALS (CNC)

Cellulose is the most abundant biomass material obtained from renewable and sustainable resources such as a number of living organisms ranging from higher to lower plants, some amoebae, sea animals, bacteria and fungi. CNC is one of most favorite reinforcing agents that is general obtained from cellulose microfibrils by acid hydrolysis. Amorphous or non-crystalline regions of cellulose are susceptible to acid hydrolysis (hydrochloric and sulfuric), whereas crystalline regions have a higher resistance to hydrolysis remain intact as shown in Figure 2.15. Also, CNC has different names; "rod-like cellulose microcrystals", "nanocrystalline cellulose", "cellulose nano whiskers" and "cellulose nanocrystals" [10-12].

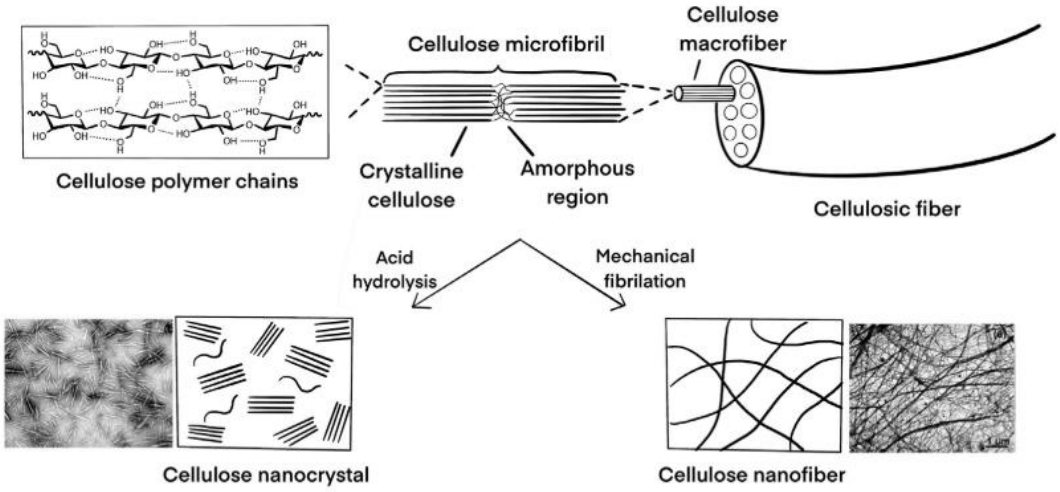

Figure 2.15 : Extraction differences of CNC and CNF from cellulosic fiber and their structural characteristics [12]

CNCs are rod-like particles that has the unique properties of high aspect ratio, high surface area, and containing a high crystallinity depend on the nature of the cellulose source [10]. Table 2.3 shows the crystallinity and dimensions of CNC from different sources [11, 52].

Table 2.3 : The crystallinity and dimensions of CNC from different sources [10, 12].

Cellulose Type	Length (nm)	Cross Section	Crystallinity (%)
Tunicate	100 nm-several μm	10-20 nm	83-90
Bacteria	100 nm-several μm	5-10 nm by 30-50 nm	72-74
Algae (Valonia)	>1000 nm	10 to 20nm	-
Cotton	200-350 nm	5 nm	70-90
Wood	100-300 nm	3-5 nm	70-85

In this paragraph, mechanical and thermal stability of CNC will be briefly mentioned. There is a limited information about the mechanical properties of CNC, because it is not possible to directly measure Young's modulus and strength due to its small size. Mechanical properties of CNC can vary depending on its sources, morphology, geometric dimensions, crystal structures, degrees of crystallinity and synthesis processes. CNCs have low density, high potential for surface modification, renewable and biodegradable structure, so they are distinguished from other nano fillers. For instance; CNC has a greater axial elastic modulus than Kevlar which is a super-strong plastic. The elastic modulus in axial direction of CNC is in the range of 110-220 GPa while Kevlar ranges from 124-130 GPa. Table 2.4 shows properties of CNC compare to other stiff materials. Carbon nanotubes (CNTs) have superior properties than CNC, but CNC is preferred in applications due to its low cost. On the other hand, the onset of thermal chemical degradation of CNCs was reported in literature between 200-300 °C using thermogravimetric analysis (TGA). Many parameters affect the thermal stability of the CNC, for example; the increase in the number of sulfate groups on the CNC surface reduces the degradation temperature [53].

Table 2.4 : Properties of CNC and several reinforcement materials [51, 53].

Material	Density ($g.cm^{-3}$)	Tensile strength (GPa)	Modulus (longtitudinal) (GPa)	Modulus (transverse) (GPa)
Kevlar-49 fiber	1.4	3.5	124-130	2.5
Carbon fiber	1.8	1.5-5.5.	150-500	-
Steel wire	1.8	4.1	210	-
Clay nanoplatelets	-	-	170	-
Carbon nanotubes	-	11-63	270-950	0.8-30
Boron nanowhiskers	-	2-8	250-360	-
CNC	1.6	7.5-7.7	110-220	10-50

Due to its superior properties, CNC is used as an additive in polymer nanocomposites and mixed nanocomposites. However, the CNC has strong inter-particle hydrogen

bonds, hydroxyl groups on the surface and hydrophilic structure, which prevents good dispersion in the polymer matrix [10]. There are different approaches to enhancement of CNC in PLA: surface modification [54], solution casting [55], using surfactants [56] and compatibilizer [57].

2.7. BLEND NANOCOMPOSITES

Immiscible polymer blend can improve the properties of self-forming polymers. For example, the polymer elastomer can improve the brittle material by means of the blend due to its ductile properties. The dispersed phase in the blend must have finer droplet to increase final properties. The final droplet depends on the thermodynamic effect and the kinetic effect of the polymers. Surface tension is a thermodynamic effect. On the other hand, the compound sequence, the viscosity ratio of the polymers and the melt composition time are kinetic effects. If viscosity ratio is not close to 1 or the interfacial tension is higher, coalescence occurs. The compatibilizer or nanoparticles are used to increase the compatibility of the immiscible polymer blends; they reduce the interfacial tension between the polymer blend or bring the viscosity ratio of the polymers closer to each other.

2.7.1. Selective localization of nanoparticles in a polymer blend

The selective localization of the nanoparticle in the blend is crucial to obtain final materials with improved properties. Therefore, it is very important to choose a suitable nanoparticle. In immiscible blends, the nanoparticle may tend to be selectively localized in one of the polymers or at the interface between the polymers. These behaviors depend on thermodynamic and kinetic parameters [58, 59].

2.7.1.1. Thermodynamic effect

The thermodynamically selective localization of the nanoparticle in the blend can be found by the wetting coefficient or another name Young's equation (equation 2.11) [60].

$$\omega_{AB} = \frac{\gamma_{filler-B} - \gamma_{filler-A}}{\gamma_{A-B}} \qquad (2.11)$$

in which, ω_{AB} is wetting coefficient. $\gamma_{filler\text{-}B}$ is interfacial tension between the nanoparticle and the polymer B. $\gamma_{filler\text{-}A}$ is interfacial tension between the nanoparticle

and the polymer A. $\gamma_{A\text{-}B}$ is interfacial tension between the two polymers [60]. Sumita et al. [60] and afterwards Fenouillot et al. [61] described that selective localization as shown in figure 2.16. If $-1<\omega_{AB}<1$, the filler (A) is located at the interface of the two polymers; if $\omega_{AB}>1$, the filler is present only in polymer B and if $\omega_{AB}<1$, the filler is present only in polymer A.

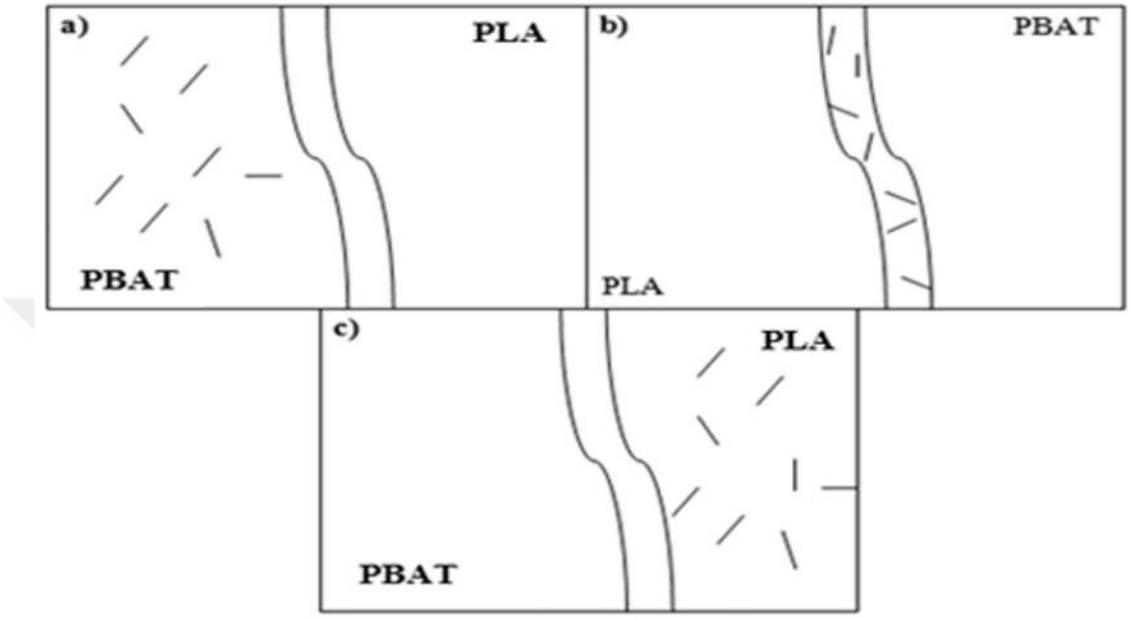

Figure 2.16 : Equilibrium morphologies for a blend nanocomposite system with PLA and PBAT matrices and nanoparticles [62].

2.7.1.2. Kinetic effect

The localization of the nanoparticles depends on the viscosity of the polymers, which is a strong kinetic barrier for the migration of nanoparticles [63-65]. The nanoparticle localized in the low viscosity component can reduce the viscoelastic difference between the polymers and support to the breakup of the droplets. In addition, nanoparticles localized at the interface have a barrier effect in the coalescence of droplets. Feng et al. [63] observed that as the viscosity of poly(methyl methacrylate) (PMMA) increased, the carbon black (CB) was migrated from the PMMA phase to the interface between the PMMA and PP phases. and then, as the viscosity of PMMA continued to increase, CB migrated to the PP phase, as shown figure 2.17.

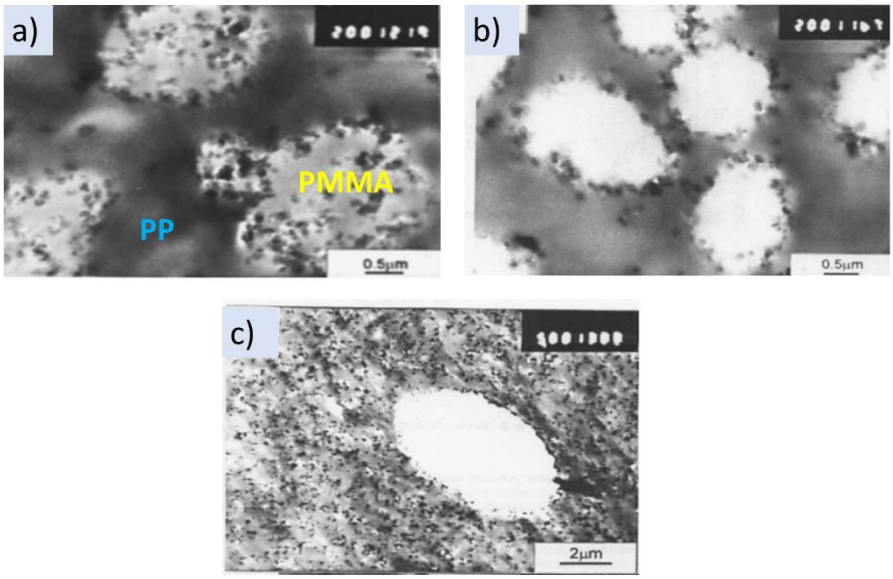

Figure 2.17 : TEM micrographs; a)CB is localized in PMMA, b)CB is localized at interface, and c) CB is localized in PP phase [63].

2.8. PLA/PBAT BLEND NANOCOMPOSITE

2.8.1. PLA/PBAT/CNT

In PLA/PBAT containing CNT prepared using twin screw extruder, CNTs are mainly located in the PBAT phase for any type of blend morphology (Figure 2.18) because they prefer aromatic molecules, low interface tension, and polymer chain flexibility [66, 67]. It was shown that when the addition of CNTs in PLA/PBAT blend, Young's modulus did not increase significantly and the yield strength decreased. This was because PLA has become almost completely amorphous with the addition of the highest CNT, since the presence of CNTs may in some way be said to inhibit the nucleation ability of PBAT on crystallization of PLA. The impact strength of 80/20 and 60/40 PLA/PBAT blends containing 4 and 3 wt.% CNT increased from 23.4 to 65.8 J/m and from 106.7 to 270 J/m, respectively. In addition, the electrical conductivity properties of the blend nanocomposites have increased, which proves the presence of the CNT percolated networks [67]. Ko et al. [66] showed that PLA/PBAT/multi-walled carbon nanotube (MWNT) blend nanocomposite has two-step thermal degradation. In addition, they found that the CNT enhanced thermal property of the blend nanocomposites.

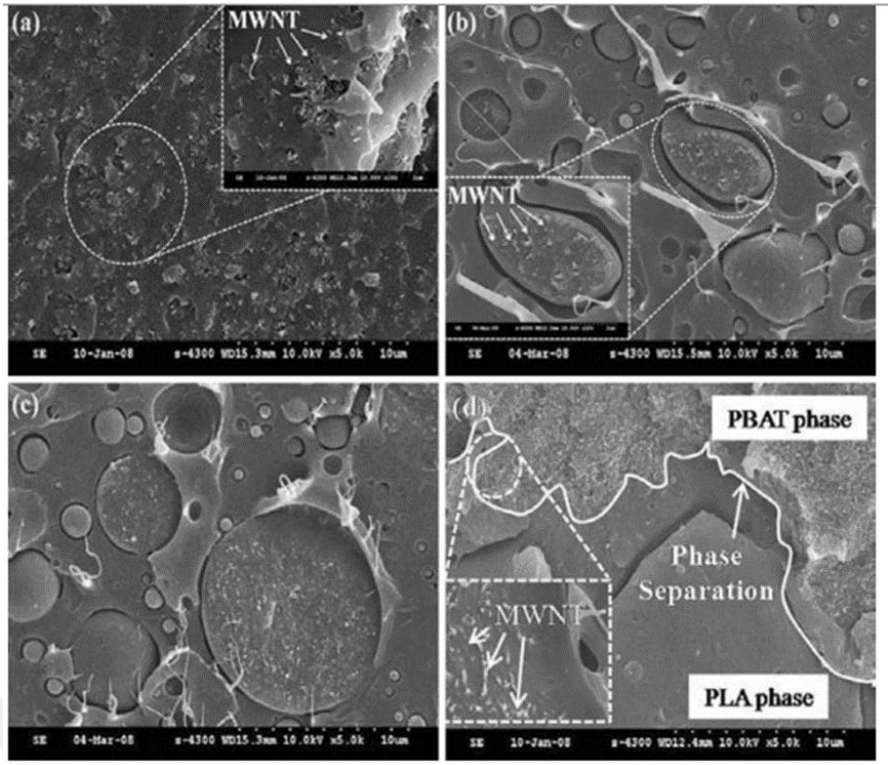

Figure 2.18 : SEM images of various PLA/PBAT compositions with a fixed MWNT ratio of 2 wt.%: a)Neat PLA, b)PLA/PBAT (80/20), c)PLA/PBAT (60/40), and d)PLA/PBAT (50/50) [66].

2.8.2. PLA/PBAT/Clay

Kumar et al. [68] investigated how glycidyl methacrylate (GMA) and nanoclay (C20A) influenced the development of the interface between PLA and PBAT. They show that interface adhesion between PLA/PBAT blend was improved in the presence of GMA and nanoclay. Also, in the DMA test, it was confirmed that there was a strong interface adhesion between PLA and PBAT due to the increased damping factor in the presence of GMA and nanoclay. Although the tensile strength and elongation of the blend nanocomposite decreased with the addition of GMA and clay, an increase in Young modulus and impact strength was observed.

Mohapatra et al. [69] investigated the compatibility between PLA/PBAT/clay using maleic anhydride and benzoyl peroxide as a compatibilizer and as an accelerator respectively. They also prepared blend nanocomposites by melt blending using two nanoclay cloisite 93A (C93A) and cloisite 30B (C30B). It was observed from the TEM micrographs (Figure 2.19) that the blend nanocomposites showed better compatibility and miscibility in the presence of C30B compared to C93A.

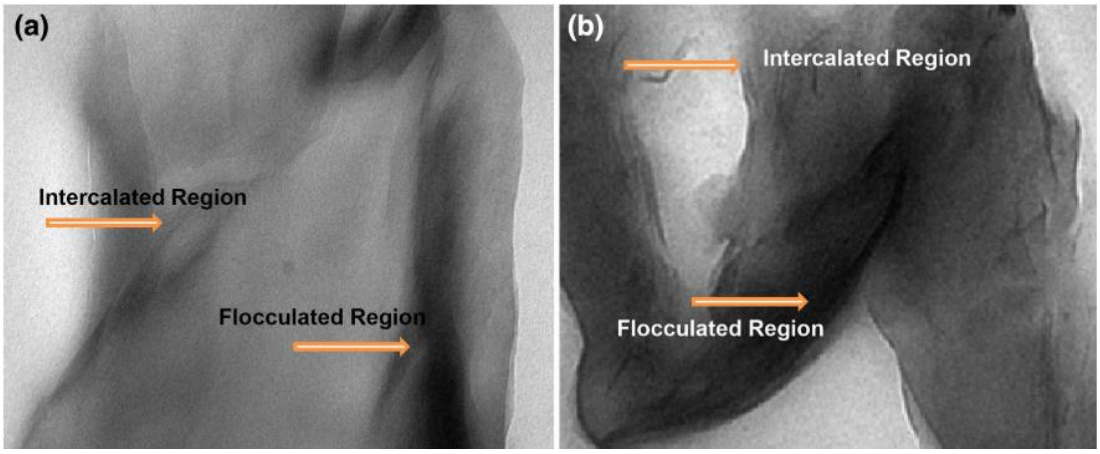

Figure 2.19 : TEM images of a) PLA/PBAT/C30B and b) PLA/PBAT/C93A blend nanocomposites [69].

In addition, the PLA/PBAT blends containing montmorillonite clay (MMT) have been reported to exhibit higher tensile strength and modulus but lower elongation compared to the PLA/PBAT blends containing calcium carbonate (NPCC) due to MMT's much larger surface area and stronger interaction with the polymer matrix compared to NPCC [50].

2.8.3. PLA/PBAT/Nano-silica

Dil et al. [64, 70] investigated the localization of nano-silica particles with different mixing strategies and, accordingly, the effect on the properties of the blends. When nano-silica was added to the PLA/PBAT blend, one of the mixing strategies (Pr1), it was observed that nano-silica dispersed in the PBAT phase. While the pre-mixing of the particles with the PLA phase, using Pr2, it was exhibited that the nano-silica particles were localized at the interface. As shown in Figure 2.20, due to the presence of nano-silica at the interface, the droplet size of PBAT has decreased from 1.3 ± 0.2 μm to 0.8 ± 0.1 μm and narrowed compared to that prepared with Pr1. This result indicates that the interfacial tension between the phases decreases and the nanoparticles around the dispersed phases form a solid shell, and therefore a reduction in coalescence occurs. However, it was observed that morphology changed into a co-continuous structure with the increase of nano-silica content found at the interface assembly.

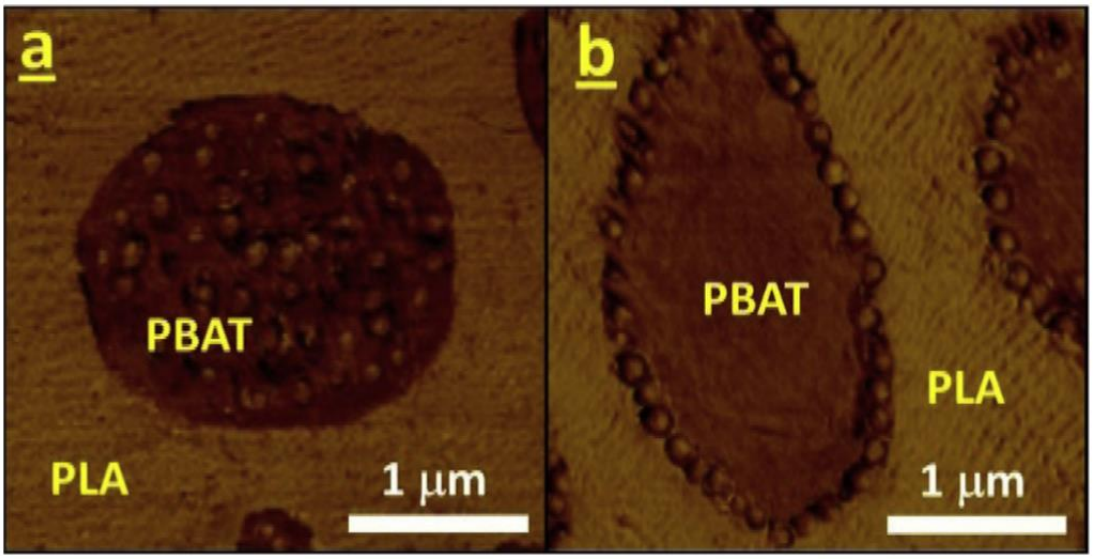

Figure 2.20 : AFM images of the blends containing 3 wt.% of nano-silica prepared using Pr1 (a) and Pr2 (b) [70].

2.8.4. PLA/PBAT/Graphene

Graphene nanoplatelets (GNPs) are used to improve the barrier property of PLA because it has a highly active surface area due to its plate-like morphology at the nanoscale [71]. Girdthep et al. [72] prepared PLA / PBAT containing GNPs blend nanocomposite by solution casting using chloroform solvent. They observed that due to the efficient alignment of large amounts of polymer chains around the GNPs, new polymer crystals formed, leading to high barrier properties for water vapor and light transmittance. In addition, the blend nanocomposite containing GNPs coated electrode cell displays an increased electrical current of 66.7% compared to the polymer blend without GNPs coated electrode system because the GNPs allow electron transport.

Adrar et al. [62] investigated that how the properties of PLA / PBAT blend changed with epoxy functionalized graphene (EFG). They reported that the EFG should be present at the interface between the PLA and PBAT phases according to the Young's model. However, TEM images showed that EFG was completely in the PBAT phase. Based on this result, it was stated that EFG could not reach the thermodynamic equilibrium state. In addition, the mechanical properties of blend with EFG have been observed to increase due to the interactions between the epoxy function of graphene and the carbonyl groups of PBAT. In another study, poly (ethylene oxide) (PEO) was added to improve the GNP distribution in PLA/PBAT blend [73]. They found that very

low PEO loading promotes GNP dispersion in the PBAT phase and improves the toughness and thermal stability of the blend nanocomposites.

2.9. CNC INCORPORATED PLA BASED BLEND NANOCOMPOSITES

2.9.1. PLA/PCL/CNC

Motloung et al.[74] investigated the effect of CNC loading on the properties of PLA/PCL (70/30) blend prepared by twin screw extruder (TSE). They found that the thermodynamically predicted location of the CNC was at the PLA phase, because the Young model was higher than one. However, SEM images showed that the CNC preferred to be localized in the low viscosity PCL phase compared to PLA due to the increase in the droplet size of PCL. This result indicates that kinetic factors control the localization of CNC particles rather than thermodynamic factors. Figure 2.21 shows that the complex viscosity of the blend nanocomposites decreases with an increase in the CNC content. The authors note that a transesterification reaction may have occurred between PLA and PBAT at processing temperature and this reaction may have been inhibited in the presence of CNC. On the other hand, the impact strength of PLA/PCL with 2 wt.% CNC increased by about 111% compared to the neat blend.

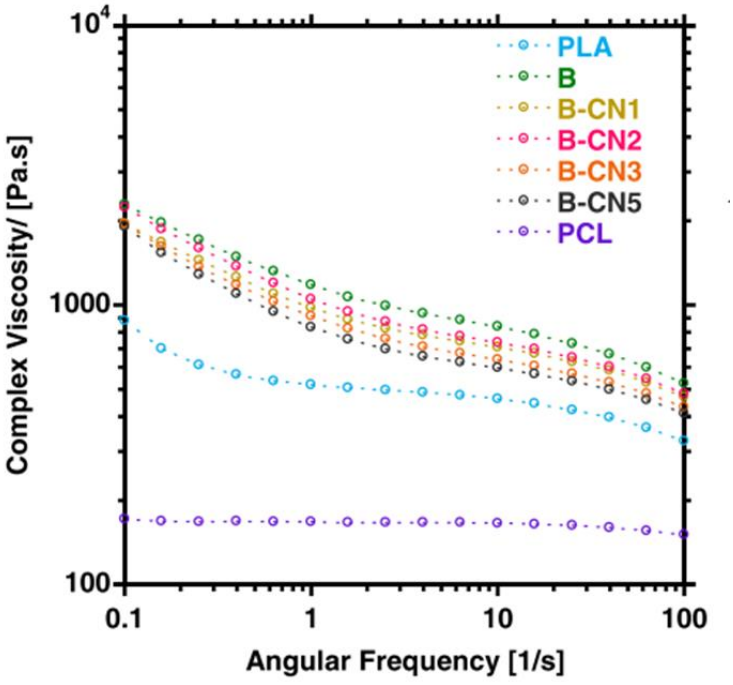

Figure 2.21 : Complex viscosity curve as a function of frequency. (B: PLA/PBAT blend, B-CN: PLA/PBAT with 1,2,3 and 5wt.% CNC) [74].

2.9.2. PLA/Polyamide (PA11)/CNC

Heshmati et al. [75] prepared PLA/PA11/CNC using a combination of solution casting and melt mixing. Due to the strong affinity of CNC particles for the PA11 phase, CNC was found in the PA11 phase for any type of blend morphology as shown in Figure 2.22. It also matched the prediction of the Young's model. In another study [76], a versatile approach was presented to control the localization of the CNC in the blend. This approach was as follows; CNC with PEO is prepared in an aqueous medium and then freeze-dried to prevent CNC agglomeration as water is removed. The authors showed that although the CNC prefers to be localized in the PA11 phase, PEO-coated CNC prefers to be selectively localized in the PLA phase due to the high affinity of PEO to PLA.

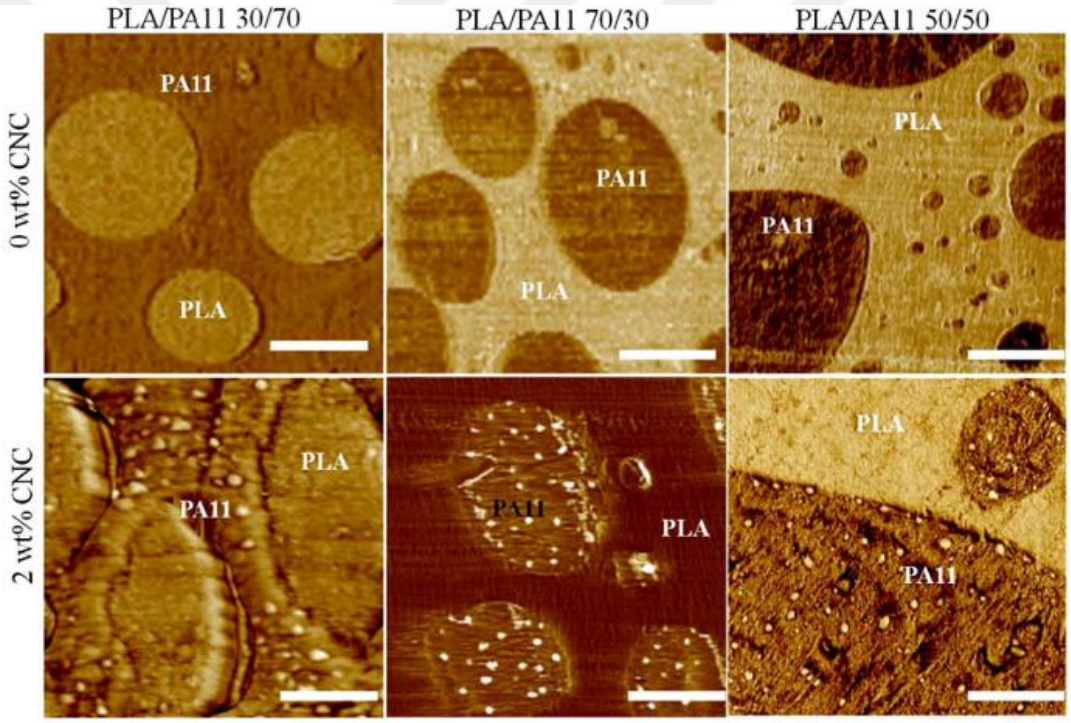

Figure 2.22 : AFM phase micrographs of the PLA/PA11 blends with and without CNC particles [75].

2.9.3. PLA/PHB/CNC

Many studies have focused on increasing PLA crystallinity because the presence of the crystal phase plays an important role on mechanical and permeation properties. In the case of the addition of PHB, PHB crystals acted as nucleating agents, resulting in increased PLA crystallinity with water resistance, oxygen barrier and slight UV blocking effect. CNC and surfactant modified CNC (CNCs) were added to the blend

to improve the interaction between phases and also increase crystallinity, processability and thermal stability. It was observed that the initial degradation temperature of the systems shifts to 10 ˚C higher temperatures. According to the DSC analysis, the degree of crystallinity raised up 18.5 and 21.3% for PLA/PHB/CNC and PLA/PHB/CNCs, respectively. As showed in Figure 2.23, there are two peaks in the blend during melting process, while the blend nanocomposites containing CNC and CNC have a single peak. This result is associated with a well-dispersed CNC that can improve interface adhesion and consequently increase compatibility between phases. On the other hand, the elongation at break of the PLA matrix with the PHB and CNCs increased 175% compared to the neat PLA, which means that the PLA/PHB/CNCs are stretchable and rigid with high strength and this is important for food packaging applications [77, 78]. In addition, acetyl (tributyl citrate) (ATBC), a plasticizing agent, has been used to improve the processability of PLA/PHB/CNC blend nanocomposites and to obtain flexible films [79, 80].

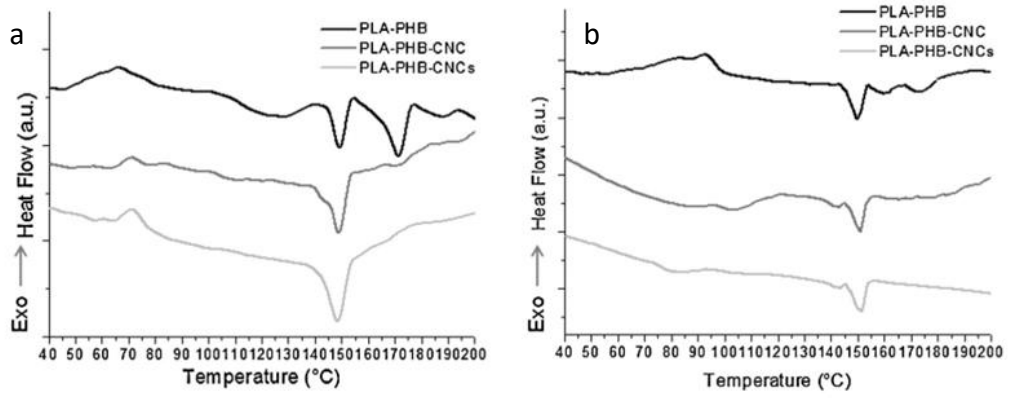

Figure 2.23 : DSC curves of blend and blend nanocomposite films during first (a) and second (b) heating scans [78].

2.9.4. PLA/Natural rubber (NR)/CNC

Bitinis et al. [81, 82] used three types of CNCs in the PLA/NR blend prepared by two method (i.e., direct extrusion or solvent casting combined with extrusion) and showed that each type has different morphologies that strongly influence the final properties. As shown in Figure 2.24, unmodified CNC and PLA grafted CNC (PLA-g-CNC) nanoparticles are localized in PLA, while the alkyl chain grafted CNC (C18-g-CNC) prefers to be localized in NR phase. According to rheological analysis, when using a combination of solvent casting and extrusion method, CNC was added in PLA/NR blend, while the viscosity and storage module increased at low frequencies. As a result,

a network structure has been obtained. In the case of direct extrusion, there have been no changes indicating that a nanoscale level dispersion was obtained. In the PLA/NR/C18-g-CNC, the percolation threshold occurred beyond 3 wt.% modified CNC, indicating the formation of a network structure at low frequency. In the case of PLA/NR/PLA-g-CNC, the storage modulus and complex viscosity have slightly increased and show that it has not attained solid-like behavior. DSC thermograms showed that PLA-g-CNC has a nucleation effect on the blend, but the presence of CNC negatively affects PLA crystallization. This behavior indicated that the PLA-g-CNC is better compatible with the PLA matrix. On the other hand, the addition of C18-g-CNC reduced the nucleation effect of NR droplets.

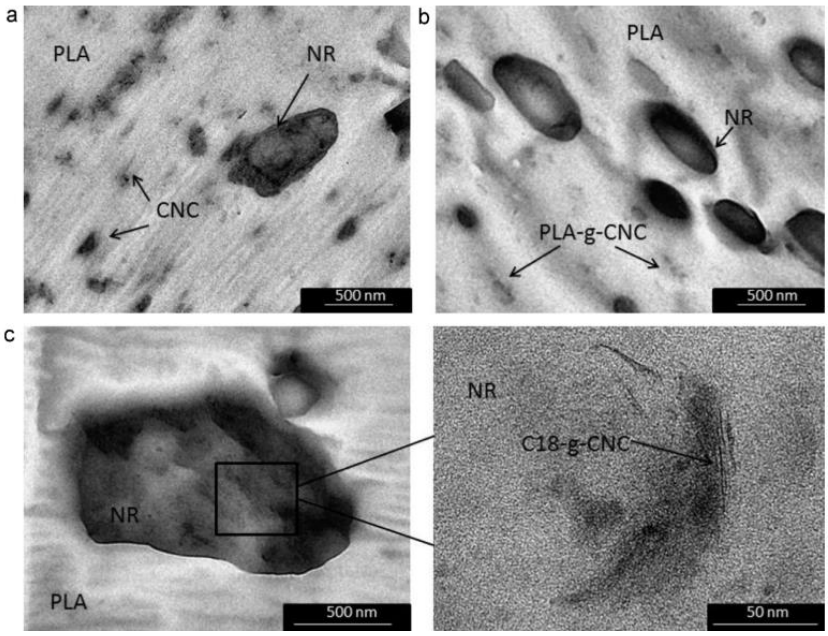

Figure 2.24 : TEM images of blend nanocomposites containing (a) CNC, (b) PLA-g-CNC and (c) C18-g-CNC at two magnifications [81].

2.9.5. PLA/PBAT/CNC

Ma et al. [83] prepared PLA/PBAT containing CNC−silver (Ag) nanohybrids by solution casting using chloroform. The compatibility between PLA and PBAT has increased with the addition of NCC - Ag nanohybrids. The crystallization rate, thermal stability and the storage module (E ') of the blend nanocomposites was enhanced by the addition of CNC− Ag nanohybrids, their tensile properties dropped very little. In the presence of CNC−Ag nanohybrids, The Kirby−Bauer disc diffusion test showed that antibacterial activity of the blend nanocomposites against both of the Gram-positive Staphylococcus aureus and the Gram-negative Escherichia coli increased.

3. EXPERIMENTAL PROCEDURE

3.1. MATERIALS

A commercial semi-crystalline PLA (Ingeo 3001D) was supplied from NatureWorks LLC. The PBAT (Ecoflex® F Blend C1200) was provided by BASF. Spray-dried CNCs obtained from sulfuric acid hydrolysis of wood pulp were provided by CelluForce (Montreal, Canada). N, N-dimethylformamide (DMF) as solvent with 99% purity was purchased from Sigma-Aldrich.

3.2. PREPARATION OF PLA/PBAT/CNC BLEND NANOCOMPOSITES

PLA/PBAT/CNC blend nanocomposites were prepared with two different approaches; (i) solution casting (SC) and (ii) the dilution of solution casted masterbatch by melt mixing using a twin-screw extruder (mTSE) or internal mixer (mIM). The preparation details of all samples are given in Table 3.1.

Figure 3.1 shows the experimental setup of PLA/PBAT/CNC blend nanocomposites prepared by solution casting method. First, the desired amount of CNC was dispersed in 100 ml DMF with a water bath sonicate for 2 h to obtain a CNC/DMF suspension. Then, the PLA and PBAT pellets added to the CNC/DMF suspension were mixed with the magnetic stirrer at 70 °C for approximately 2.5 h until completely dissolved. The prepared PLA/PBAT/CNC solution was poured into petri dishes and dried under vacuum oven at 85 °C for 36 h and then powdered using a coffee grinder and kept in the vacuum oven at 85 °C for a further 48 h to completely remove the solvent.

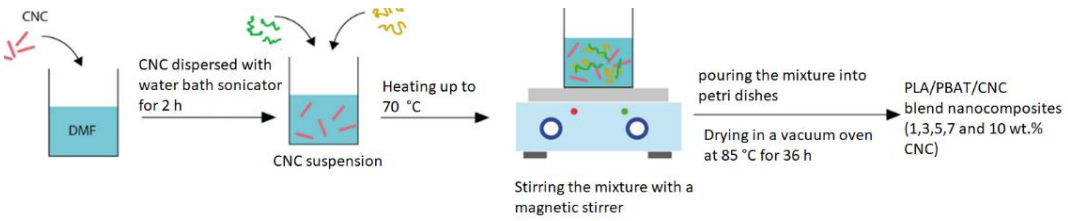

Figure 3.1 : Schematic of the experimental setup of samples prepared through SC.

The PLA/PBAT/CNC masterbatch containing 7 wt.% CNC was prepared through the SC method. The masterbatch was diluted into 1, 3 and 5 wt.% CNC with the addition of PLA and PBAT using a twin-screw extruder (TSE), as shown in Figure 3.2. The extruder used is a co-rotating TSE (Micro lab Twin Screw-Rondol) (figure 3.3) with a screw diameter of 10 mm and a length of 200 mm (20 L/D). The melt compounding temperature profiles of 120, 150, 170, 170 and 170 ^{o}C, with the screw speed of 50 rpm.

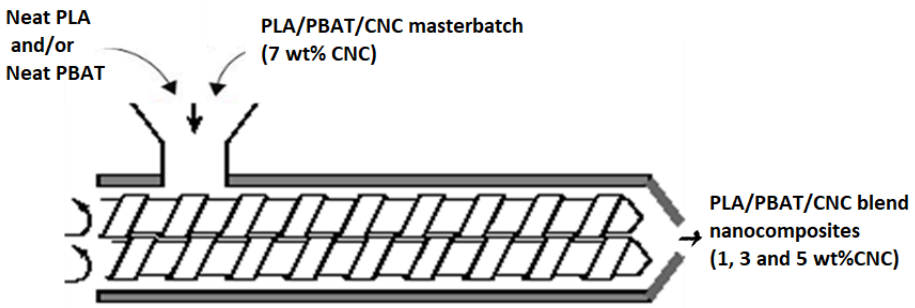

Figure 3.2 : Schematic of the experimental setup of samples prepared through TSE.

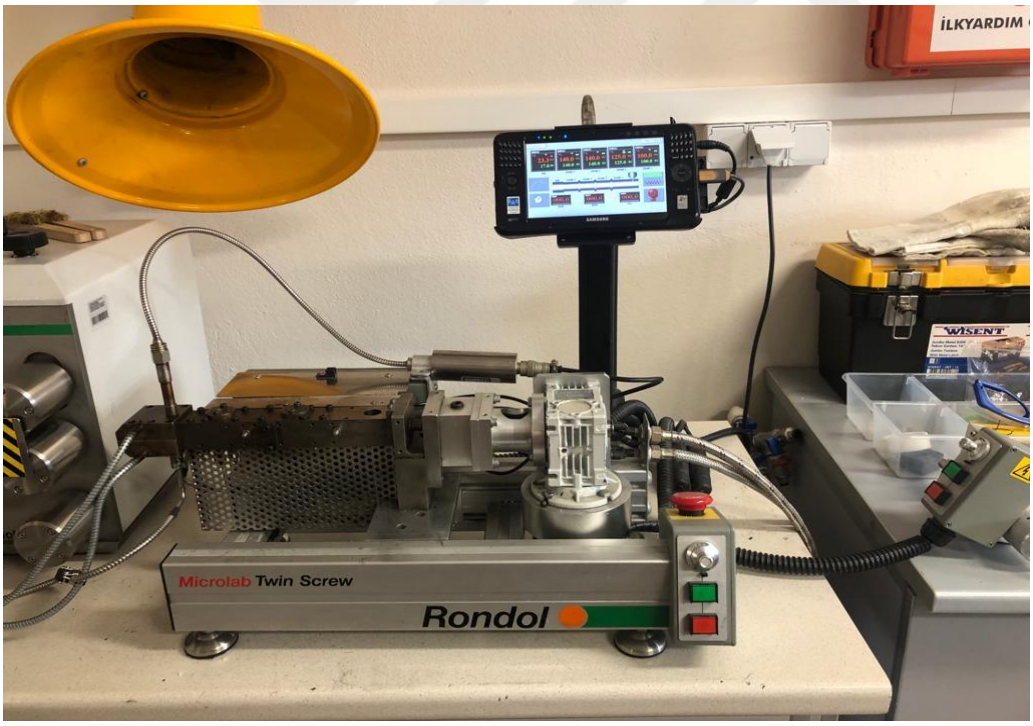

Figure 3.3 : Twin-screw extruder (TSE) (Micro lab Twin Screw-Rondol).

PLA/PBAT/CNC with a fixed 3 wt.% CNC and 10, 25 and 50 wt.% of PBAT blend nanocomposites were prepared with combination of SC and melt mixing methods (mTSE). Also, PLA/PBAT blends with 10, 25 and 50 wt.% PBAT were prepared by direct melt mixing methods using TSE.

The masterbatches containing 7 wt.% CNC prepared by SC was diluted with internal mixer (IM) (RTX-M40 Melt Mixer) (figure 3.4) at 50 rpm for 10 min at a temperature of 170 °C.

Figure 3.4 : Internal mixer (IM) (RTX-M40 Melt Mixer).

PLA/PBAT/CNC blend nanocomposites with a fixed 3 wt.% CNC were prepared with the combination of SC and melt mixing methods (mTSE and mIM) with three mixing strategies. Figures 3.5 and 3.6 show the scheme of the experimental setup of the samples prepared with mTSE and mIM, respectively. These strategies are followed;

- M1: Masterbatch prepared by direct mixing of all three components through SC method and then diluted using mTSE or mIM with the addition of PLA and PBAT,
- M2: PLA/CNC masterbatch prepared through SC method and then diluted using mTSE or mIM with the addition of PLA and PBAT,
- M3: PBAT/CNC masterbatch prepared through SC method and then diluted using mTSE or mIM with the addition of PLA and PBAT.

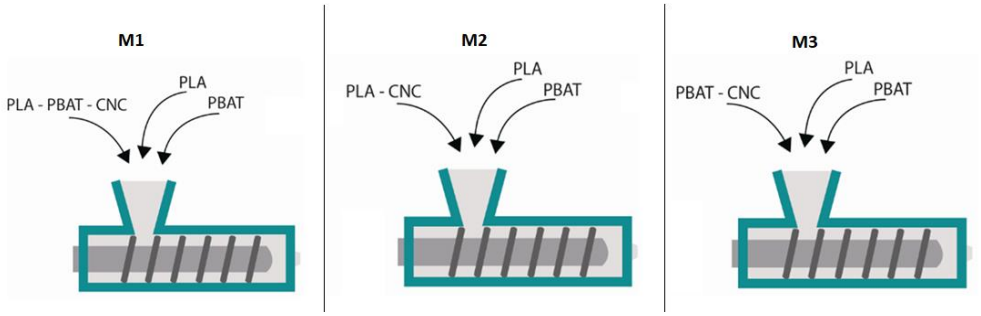

Figure 3.5 : Schematic of the experimental setup of samples prepared with three strategies through mTSE.

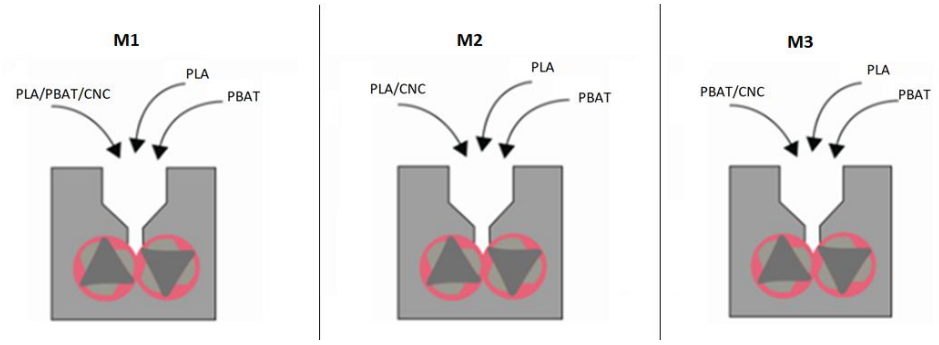

Figure 3.6 : Schematic of the experimental setup of samples prepared with three strategies through mIM.

All blend nanocomposites were compression moulded with a hydraulic press for 5 min at 180 ^{o}C to prepare the characterization test samples. Before molding, each sample was dried in a vacuum oven for overnight at 50 °C.

Table 3.1 : The composition details of all samples.

No	Samples	CNC content (wt.%)	Method
1	PLA/PBAT (75/25)	0	SC
2	PLA/PBAT (74/25)	1	
3	PLA/PBAT (72/25)	3	
4	PLA/PBAT (70/25)	5	
5	PLA/PBAT (68/25)	7	
6	PLA/PBAT (65/25)	10	
7	PLA/PBAT (90/10)	0	TSE
8	PLA/PBAT (75/25)	0	
9	PLA/PBAT (50/50)	0	
10	PLA/PBAT (74/25)	1	SC + mTSE
11	M1 - PLA/PBAT (72/25)	3	
12	PLA/PBAT (70/25)	5	
13	M2 - PLA/PBAT (72/25)	3	
14	M3 - PLA/PBAT (72/25)	3	
15	PLA/PBAT (87/10)	3	
16	PLA/PBAT (48/48)	3	
17	PLA/PBAT (75/25)	0	IM
18	PLA/PBAT (74/25)	1	SC + mIM
19	PLA/PBAT (72/25)	3	
20	PLA/PBAT (70/25)	5	

3.3. MORPHOLOGICAL ANALYSIS

To investigate the selective localization of the CNC, the morphology of blend nanocomposites was characterized using a field emission gun scanning electron microscope (SEM JEOL 7600F FEG, Japan).

3.4. RHEOLOGICAL ANALYSIS

Rheological analysis was carried out using an MCR-301 rotational rheometer (Anton Paar, Austria) (figure 3.7) with 1 mm gap and 25 mm parallel plate geometry at 170 °C under a nitrogen atmosphere. Small amplitude oscillatory shear (SAOS) experiments were performed from high to low frequencies (ω) scans from 665 to 0.1 rad/s using a strain amplitude of 0.01, which was found to be in the linear viscoelastic regime. Stress-growth experiments were conducted at 0.01 s^{-1} shear rate.

Figure 3.7 : MCR-301 rotational rheometer (Anton Paar, Austria).

3.5. THERMAL ANALYSIS

3.5.1. Differential scanning calorimetry (DSC)

Differential scanning calorimetry (DSC) analysis was done under nitrogen atmosphere using a TA Instruments Q1000 DSC apparatus (Figure 3.8) with a sample weight of ~10 mg. Each sample was heated from 25 to 200°C with heating rate of 10°C/min and then cooled to -40 at the cooling rate of 2°C/min and then reheated under the same conditions. Glass transition temperature (T_g), cold crystallization temperature (T_{cc}), crystallization temperature (T_c), the melting

temperature (T_m), and heat enthalpy of crystal melting (ΔH_m) and cold crystallization (ΔH_{cc}) were determined. The degree of crystallinity, X_c, was calculated from DSC curves according to the following Equation (2.12):

$$X_c = \frac{(\Delta H_m - \Delta H_{cc}) \times 100}{w_{PLA} \Delta H_m^0} \quad (2.12)$$

where ΔH^o_m is the melting enthalpy for a 100% crystalline PLA (i.e., 93 J/g) and W_{PLA} is the weight fraction of the PLA [84].

Figure 3.8 : Differential scanning calorimetry (TA Instruments Q1000 DSC).

3.5.2. Dynamic mechanical analyzer (DMA)

The viscoelastic properties of the blend nanocomposites were determined through using a Perkin Elmer – DMA 8000 (Figure 3.9). The DMA was done in a single cantilever mode at an oscillation amplitude of 30 μm and frequency of 1 Hz. The prepared samples are rectangular shaped with thickness of 2 mm, length of 50 mm and width of 10 mm and heated from 25 to 120 °C with a heating rate of 3 °C/min.

Figure 3.9 : Dynamic mechanical analyzer (Perkin Elmer – DMA 8000).

3.6. MECHANICAL ANALYSIS

According to ISO 527 standard, the tensile test was measured at room temperature using Instron 8801 (Figure 3.10), with a drawing speed of 5 mm/min and a load cell of 25 kN. The samples are dog bone shaped with gage length of 20 mm, width of 4 mm and thickness of 3 mm. At least three samples were tested for each sample and their averages reported as the test result.

According to ASTM D256, the izod impact strength test was carried out using the Zwick Roell impact device, and the device has a 1J pendulum that was dropped at an angle of 160°. The samples are rectangular with length of 80mm, width of 10 mm and thickness of 4 mm. Before the test, all samples were made 2 mm notch at 45^{o} angle. The test was repeated 6 times for each sample and their averages reported as the test result.

According to ASTM D 790-03, the flexure tests were performed at rate of 3 mm/min using an Instron 8801, a three-point loading system utilizing center loading, with 25 kN load cells and support span of 2 mm. The samples are rectangular with length of 80 mm, width of 10 mm and thickness of 4 mm. The test was repeated 3 times for each sample, and their averages reported as the test result.

Figure 3.10 : Static tensile and compression device (Instron 8801).

4. RESULTS AND DISCUSSION

4.1. THERMODYNAMICS THE SELECTIVE LOCALIZATION OF CNC IN PLA/PBAT BLENDS

The surface tension parameters of PLA, PBAT and CNC as well as the interface tensions are given in Table 4.1. The total surface tension values, including polar and dispersive components of PLA, PBAT and CNC particles measured at room temperature obtained from the literature [75, 85]. The surface tensions of polymers and nanoparticles were taken from 25 °C and extrapolated to 170 °C using their reported thermal coefficient of -0.06 and -0.2 mN/(mK), respectively [65, 86]. The harmonic-mean approach (equation 2.5) is used between low energy phase interactions. The interfacial tension between PLA/PBAT, PLA/CNC and PBAT/CNC were estimated using the harmonic-mean approach:

$$\gamma_{12} = \gamma_1 + \gamma_2 - 4\left[\frac{\gamma_1^d \gamma_2^d}{\gamma_1^d + \gamma_2^d} + \frac{\gamma_1^p \gamma_2^p}{\gamma_1^p + \gamma_2^p}\right] \quad (2.5)$$

in which, γ_i is the surface energy, γ_i^d and γ_i^p , respectively, dispersive component and polar component of surface energy and γ_{12} is the interfacial tension between phases 1 and 2.

The thermodynamic equilibrium localization of solid particles in a multiphase polymer blend can be predicted by the Young's model (equation 2.11):

$$\omega_{AB} = \frac{\gamma_{filler-B} - \gamma_{filler-A}}{\gamma_{A-B}} \quad (2.11)$$

where $\gamma_{\text{filler}-i}$ is the interfacial tensions between polymer i and filler and ω is the wetting coefficient. When ω < -1, the filler is present only in polymer 1. For values of ω > 1, filler found in polymer 2. For -1 < ω < 1, filler will preferentially be located at the interface between the two polymer phases. By taking PLA as phase 1 and PBAT as phase 2, ω in PLA/PBAT/CNC blends nanocomposites can be estimated as 16.67

which indicates that, at the thermodynamic equilibrium condition, CNC should be localized in the PBAT phase.

Table 4.1 : Surface tension parameters of the PLA, PBAT and CNC at 25 and 170 °C as well as the calculated interfacial tensions at 170 °C.

	Surface energies (mN/m) at 25°C			Surface energies (mN/m) at 170°C			Thermal coefficient of surface tension	Interfacial Tension (mN/m) at 170°C	
	γ	γ^d	γ^p	γ	γ^d	γ^p	$\frac{d_\gamma}{d_T}$	$\gamma_{1,2}$	
PLA [85]	39.4	33.6	5.8	30.7	26.2	4.5	-0.06	PLA/PBAT	0.06
PBAT [85]	38.4	32.1	6.3	29.7	24.8	4.9	-0.06	PLA/CNC	5.3
CNC [75]	55	32.5	22.5	26	15.4	10.6	-0.2	PBAT/CNC	4.3

4.2. PLA/PBAT/CNC BLEND NANOCOMPOSITES PREPARED THROUGH SC

4.2.1. Morphology analysis

Figure 4.1 represents the SEM images of PLA/PBAT blends with different CNC contents prepared through solution casting. As reported in the literature, the PLA/PBAT blend shows a phase-separated morphology due to low interface adhesion between the two polymers. The PLA/PBAT blend showed matrix-dispersed phase morphology where PLA and PBAT are matrix and dispersed phase, respectively. With the addition of 1 wt.% CNC to the PLA/PBAT blend nanocomposite, it was observed that the droplet size of the PBAT phase increased compared to neat blend. As a result, it can be seen that the CNC is located in the PBAT phases. On the other hand, the droplet size of PBAT is reduced in blend nanocomposites containing up to 7 wt.% CNC. The excessive amount of CNC cannot enter the PBAT droplets and therefore CNC may be located at the interface or PLA matrix. The CNC located in the PLA can decrease the viscoelastic difference between the PLA and PBAT, which leads to droplet breakup. CNC located at the interface can prevent coalescence of PBAT droplets. It can be concluded that the kinetic parameter is more dominant than the thermodynamic effect, because the CNC prefers to be localized in the low viscosity

polymer. In addition, when addition of 10 wt.% CNC, it is assumed that the CNC starts to agglomerate in the PLA phase due to changes in morphology.

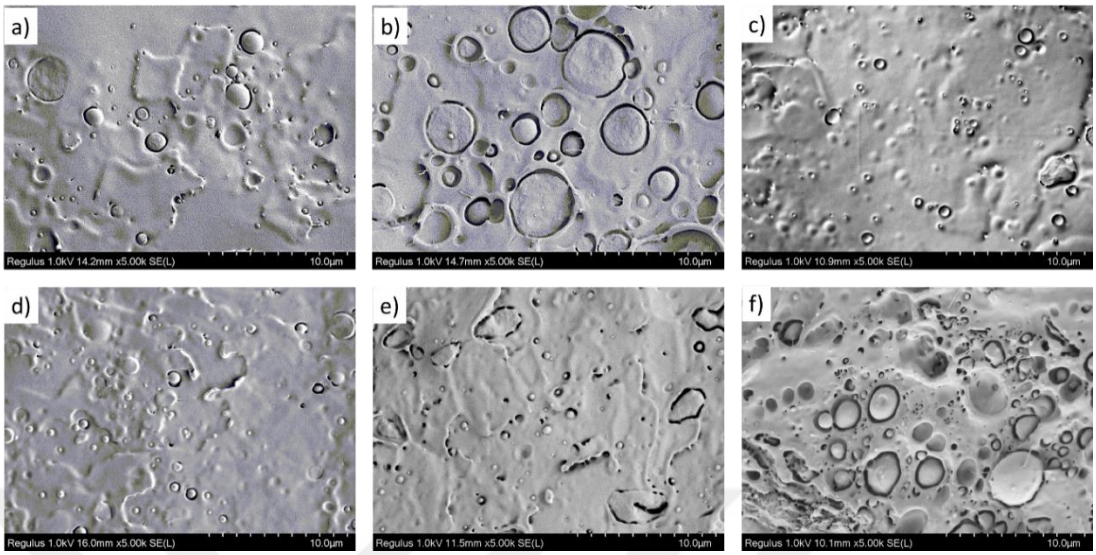

Figure 4.1 : SEM images of blend and blend nanocomposites prepared by SC; a)PLA/PBAT (75/25), b)PLA/PBAT/CNC1, c)PLA/PBAT/CNC3, d)PLA/PBAT/CNC5, e)PLA/PBAT/CNC7 and f)PLA/PBAT/CNC10.

4.2.2. Rheology analysis

Figure 4.2 shows the complex viscosity, η∗, and storage modulus, G′, versus frequency, ω, of the neat polymers, neat blend and blend nanocomposites with different CNC contents prepared through SC method. Neat polymers and neat blend exhibited Newtonian plateau at low frequency region with a slight shear-thinning behavior at high frequencies. G′ of neat polymers is typical of molten polymers with a terminal zone of slope equal to 2 on the log–log plot of G′ versus ω. Compared to neat PLA, PBAT shows higher modulus and viscosity because of greater chain entanglement. Also, the neat blend has slightly higher viscosity and storage modulus shows a plateau region at low frequency compare to its neat component because, PBAT dispersed phase has droplet morphology in PLA matrix as confirmed from morphological results and the surface area between PLA and PBAT hinder the molecular mobility and gives additional elasticity as a result the viscosity and storage modulus increased. It was clearly observed that η∗ and G′ increased with increasing CNC contents over the entire frequency range, as a result of the melt reinforcement effect of the nanofiller and morphological change of dispersed phase. It can be seen from morphological results that the inclusion of more than 1 wt.% CNC clearly affects the blend morphology when the droplet size is significantly decrease. We assumed that

CNC nanoparticles thermodynamically tent to localize in PBAT matrix which was estimated using the harmonic-mean approach. However, the rheological data suggested that the CNC localized in PLA matrix and the solid-like behavior (plateau at the terminal flow zone) was observed at 3 wt.% CNC as a result of the formation of percolation CNC network within PLA. Moreover, localization of CNC nanoparticles in PLA matrix increased the matrix viscosity and reduce the viscosity ratio between PLA matrix and PBAT dispersed phase which is resulted in finer PBAT morphology. It was observed that SAOS data of the blends containing 7 and 10 wt.% overlapped at low frequency. This can be explained by a significant formation of agglomerates at this high CNC content. These results confirm the morphology results. Also, as mentioned in the literature, nanoparticles in the matrix phase are expected to increase viscosity, and consequently rheology results and morphology results confirm each other. It could be seen from Figure 4.2.b, incorporation of CNC and increasing of interface enhanced the storage modulus of blend system in which storage modulus shows a plateau region at low frequency confirming more elastic structure. Moreover, for 1 wt.% of CNC incorporation a shoulder appeared because of shape relaxation of dispersed droplets. We couldn't see this shoulder like behavior by further incorporation of CNC because addition of nanoparticles could shift the shoulder lower frequency indicating longer relaxation time. The longer interfacial relaxation means a large decrease of interfacial tension due to a reduction in droplet size [87]. Figure 4.2.c shows transient shear viscosity of blend and blend nanocomposites in stress growth experiments at a rate of 0.05 s^{-1}. When low shear is applied to the blends or blend nanocomposites, it is understood whether there is any coalescence. In the rheology section to be shown later (section 4.3.2), no coalescence was observed at 0.01 s^{-1}. Thus, the decrease in viscosity over time in the neat PLA/PBAT blend is an indication of the thermal degradation of PLA. In the PLA/PBAT blend containing 1 wt.% CNC, no viscosity drop was observed. The blend nanocomposite containing 5 wt.% CNC, the viscosity decreased more rapidly compared to that of the neat blend and the blend containing 3 wt.% CNC. The reasons for this decrease can either the rapid degradation of PLA during shearing in presence of a larger content of CNC nanoparticles or partial destruction of the network created by the CNC. It is not possible to conclude to droplet coalescence for the blend nanocomposites.

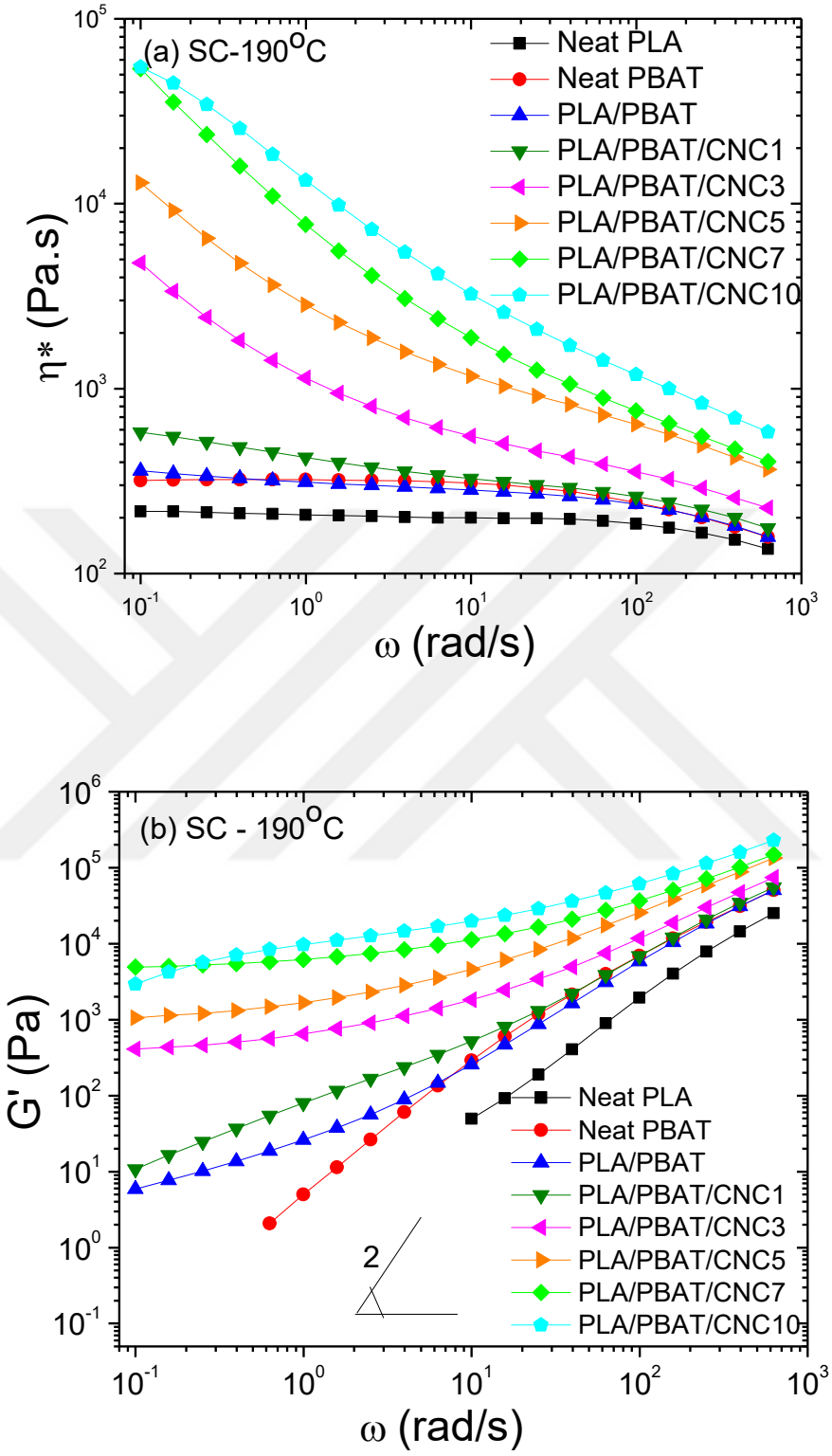

Figure 4.2 : Rheological properties of the neat polymers, neat blend and blend nanocomposites with various CNC contents at 190 °C: (a) complex viscosity, η∗, (b) storage modulus, G′, and (c) transient shear viscosity, η^{+}.

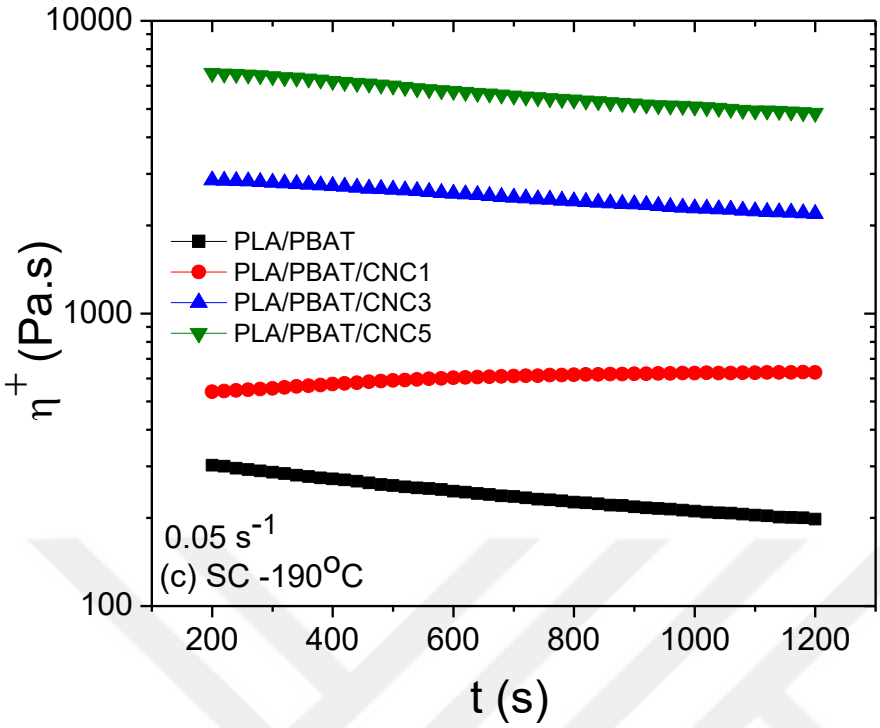

Figure 4.2 (continued): Rheological properties of the neat polymers, neat blend and blend nanocomposites with various CNC contents at 190 °C: (a) complex viscosity, η∗, (b) storage modulus, G′, and (c) transient shear viscosity, η^+.

4.2.3. DSC analysis

Figure 4.3 shows the DSC thermograms of neat blend and blend nanocomposites with different CNC contents prepared through SC route. The glass transition (T_g), cold crystallization (T_{cc}), melt crystallization (T_c), and melting (T_m) temperatures as well as the degree of crystallinity (X_c) of the samples are also reported in Table 4.2. Since the samples had different thermal backgrounds, the first heating results were not interpreted. During the cooling cycle, it was observed that the T_c of PLA/PBAT blends decreased with incorporation of 1 wt.% CNC. However, the increase in CNC content caused an increase in T_c of blend nanocomposites. This result indicates that the low CNC content (1 wt.%) is localized in the PBAT and, at higher contents, the CNC migrates to the interface or PLA, thereby triggering the crystallization of the PLA. Also, the reduction in T_{cc} in the second heating supports the conclusion that CNC accelerates the crystallization of PLA. However, it was observed that CNC had no effect on the T_g and had a negative effect on the degree of crystallinity.

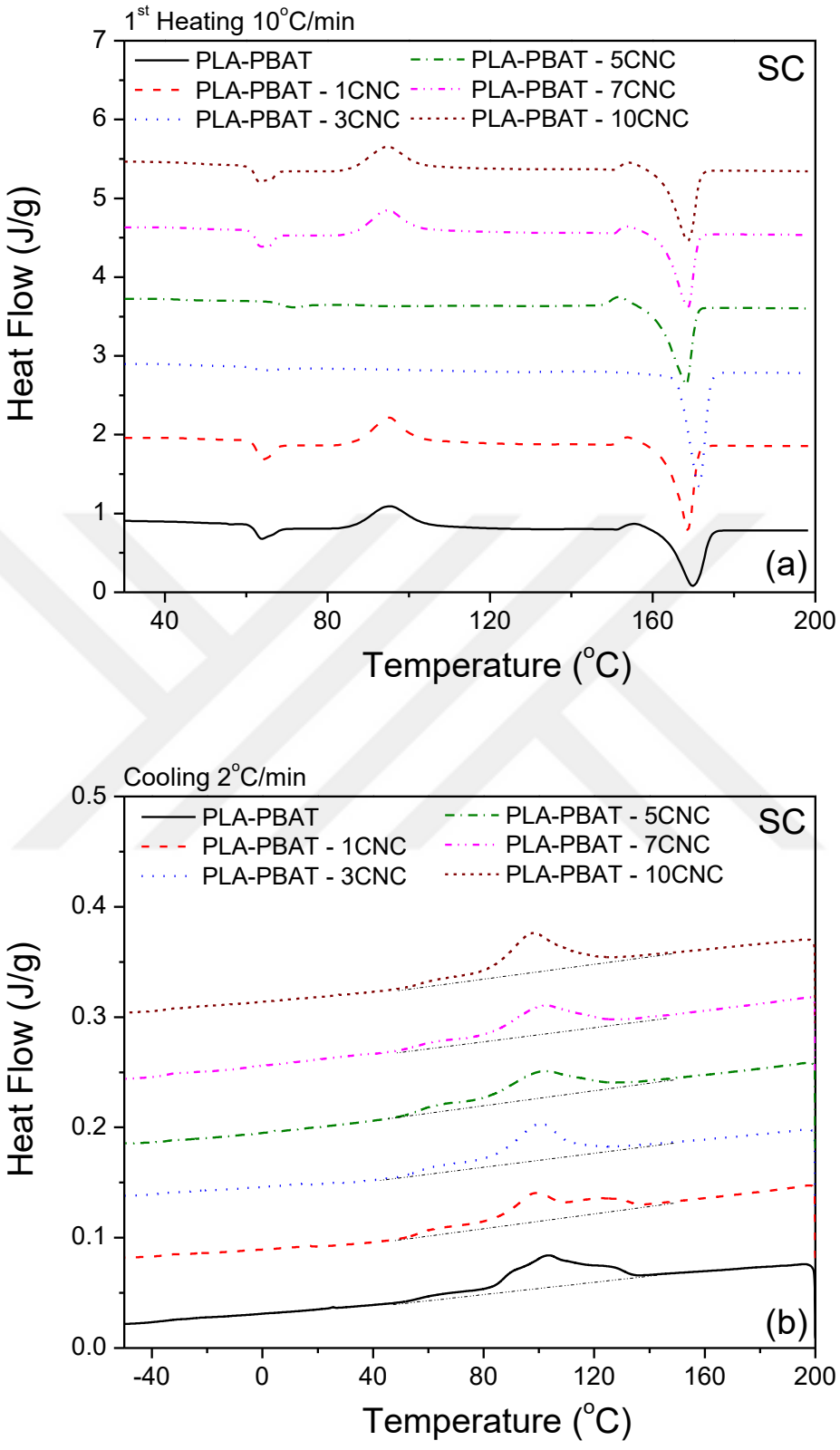

Figure 4.3 : DSC curves of samples prepared through SC; a) first heating, b) cooling and c) second heating scans.

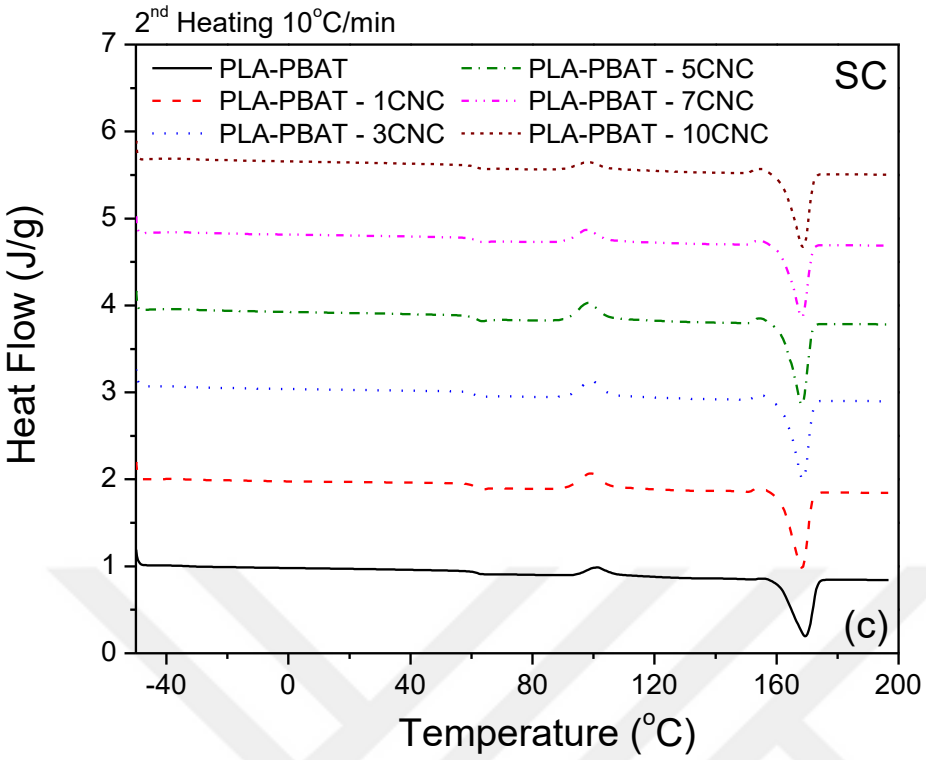

Figure 4.3 (continued): DSC curves of samples prepared through SC; a) first heating, b) cooling and c) second heating scans.

Table 4.2 : DSC data of samples prepared through SC obtained from first heating, cooling and second heating scans.

	1st Heating				Cooling			2nd Heating			
	T_g	T_{cc}	T_m	Xm	T_g	T_c	Xc	T_g	T_{cc}	T_m	Xm
PLA/PBAT 75/25	62	95	170	19	55	103	33	61	101	169	43
PLA/PBAT/CNC 74/25/1	62	95	169	19	55	99	25	61	99	168	33
PLA/PBAT/CNC 72/25/3	62	-	171	64	55	100	24	61	100	169	34
PLA/PBAT/CNC 70/25/5	62	-	168	64	55	101	23	61	99	168	37
PLA/PBAT/CNC 68/25/7	62	95	169	16	55	101	24	61	98	168	38
PLA/PBAT/CNC 65/25/10	62	95	168	21	55	98	33	61	99	169	44

4.2.4. DMA

Figure 4.4 shows the storage modulus (E′) and tan delta (tanδ) as a function of temperature of the samples prepared through SC. Figure 4.5 compare the E′ of the samples at two different temperatures which are 45 and 85 °C, below and beyond T_g,

respectively. All storage module curves first hold the plateau and then begin to decrease rapidly after 60 °C due to glass transition, after 100 °C, there is an increase again due to cold crystallization [88]. The blend and blend nanocomposites have a relatively lower modulus compare to neat PLA below T_g due to flexible PBAT phase in PLA matrix. Also, with the inclusion of the CNC, there is no trend in the E′ of the blend, because in the glassy state, molecular mobility is already hindered. However, as the temperature increased, the effect of CNC nanoparticles became more dominant. It was observed that the E′ tends to increase with increasing CNC content in rubbery region. The cold crystallization began at a relatively lower temperature for the PLA/PBAT blend compared to neat PLA, which may be due to the presence of more free volume created by more mobile PBAT molecules. The tan delta peak shifted to a higher temperature with the presence of CNC content as shown in Figure 4.4.b, which is attributed to the increased stiffness of the blend. Moreover, the intensity of the tan delta peak decreased with PBAT and CNC content compared to neat PLA, and this is attributed to the less polymer chains involved in this transition. It can be considered that the increase in E′ and T_{cc}, and the positive shift in tan delta peak position are due to the limited mobility of the polymer molecular chains by nanoparticles [89].

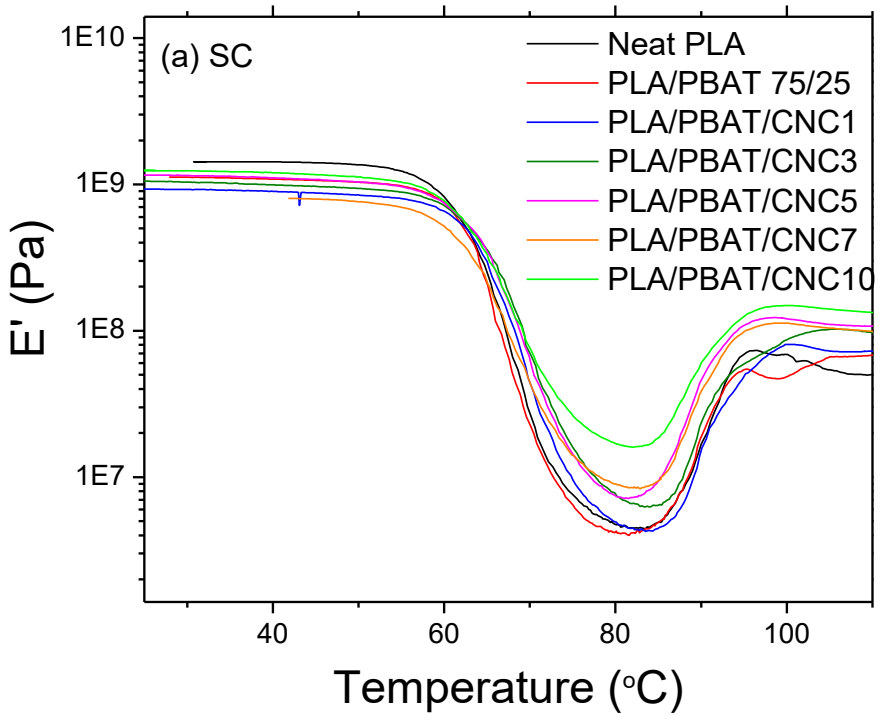

Figure 4.4 : DMA of samples prepared by SC; a) E′ and b) tanδ curves.

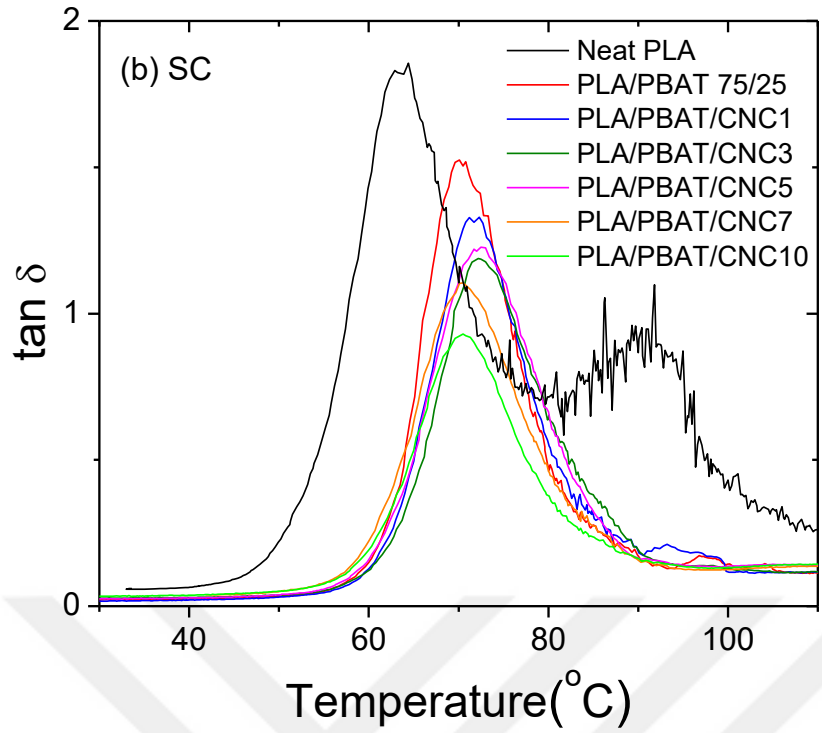

Figure 4.4 (continued) : DMA of samples prepared by SC; a) E′ and b) tanδ curves.

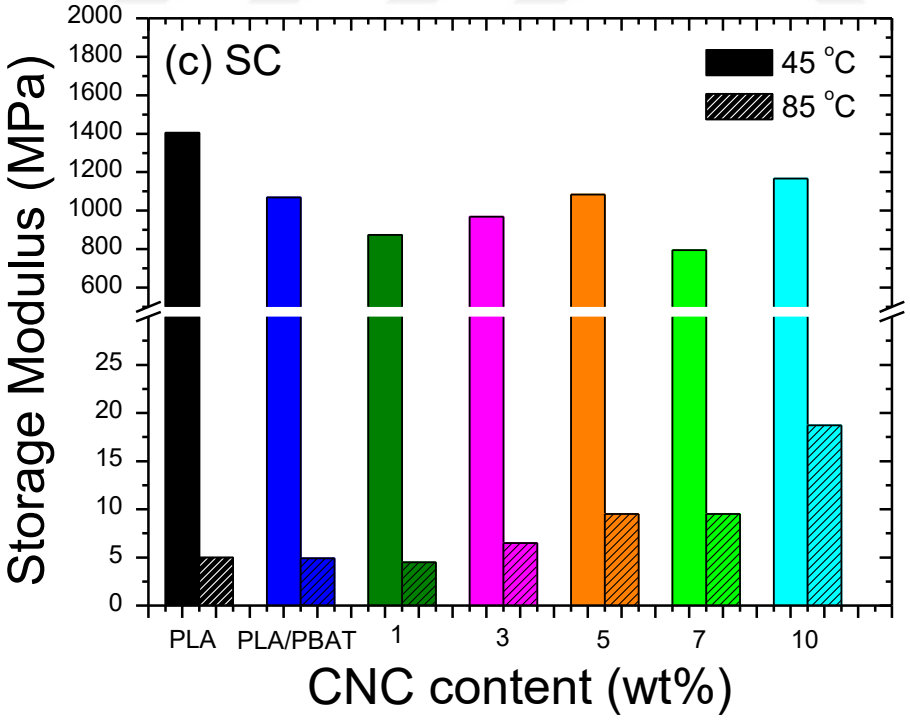

Figure 4.5 : Comparison of the E′ of PLA and PLA/PBAT/CNC blend nanocomposites with different CNC loadings at two different temperatures.

4.3. PLA/PBAT/CNC BLEND NANOCOMPOSITES PREPARED THROUGH COMBINATION OF SC AND MTSE

4.3.1. Morphology analysis

Figure 4.6 shows SEM images of blend and blend nanocomposites containing different CNC contents prepared by two different methods, which are solution casting (SC) and the combination of solvent casting and melt mixing (mTSE). Regardless of processing routes, with the addition of 1 wt.% CNC, the droplet size of the PBAT phase increased. This may be due to the localization of the CNC in the PBAT phase, which leads to increased viscosity, consequently increased droplet size. This can conclude that thermodynamic factors controlled the localization of CNC particles. Then, with the increase of CNC content, the droplet size of PBAT decreased. This may be associated with the excessive amount of CNC being unable to enter the PBAT droplets. Therefore, the CNC may be located at the interface or PLA matrix. The CNC located in the PLA can decrease the viscoelastic difference between the PLA and PBAT, which leads to droplet breakup. CNC located at the interface can prevent coalescence of PBAT droplets. It can be concluded that the kinetic parameter is more dominant than the thermodynamic effect, because the CNC prefers to be localized in the low viscosity polymer.

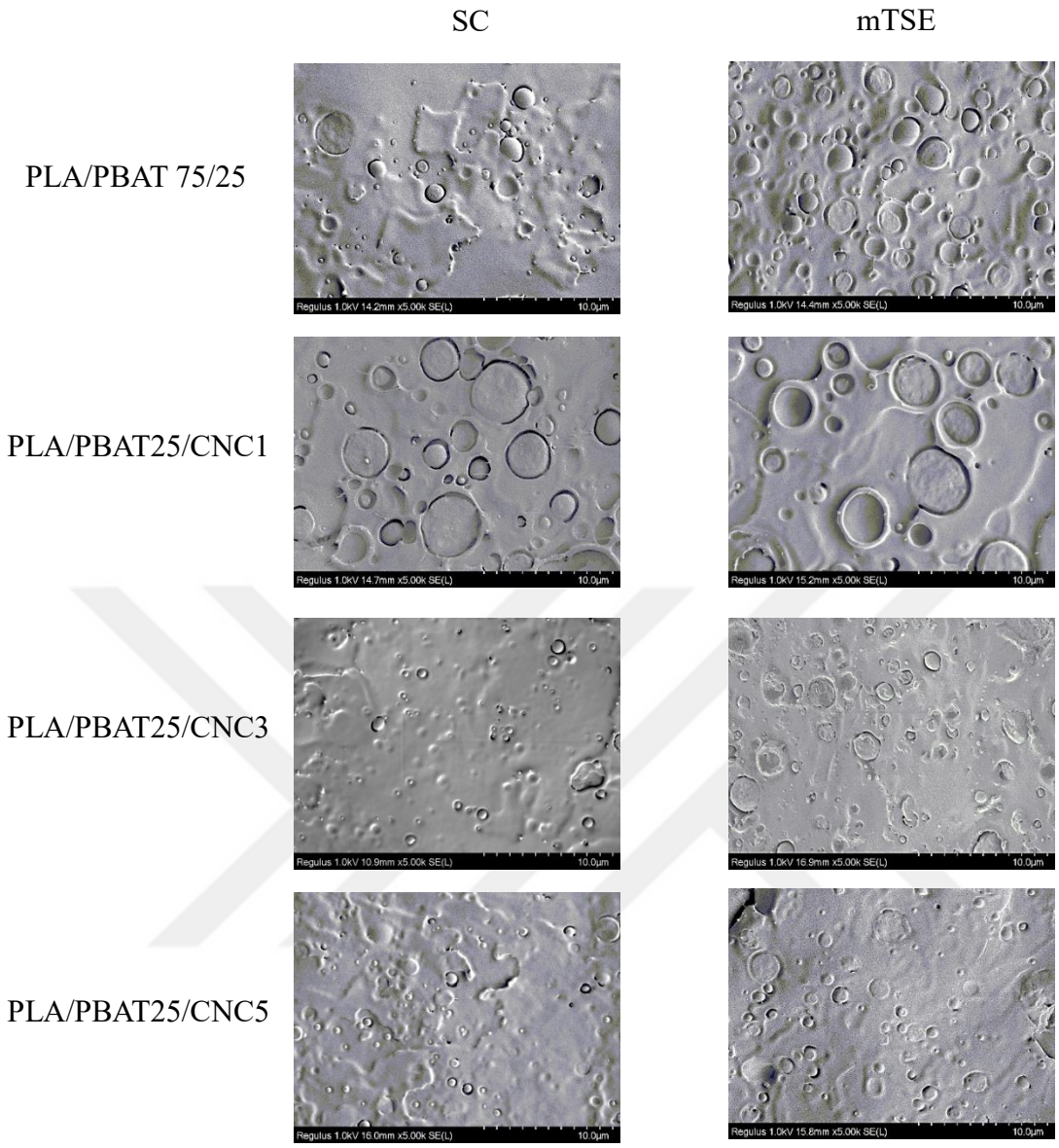

Figure 4.6 : SEM images of blend and blend nanocomposites with 1,3 and 5 wt.% CNC contents prepared by SC and mTSE.

4.3.2. Rheology analysis

Figure 4.7 shows the comparison of the rheological properties of blend and blend nanocomposites containing 1, 3 and 5 wt.% CNC prepared through SC and mTSE. According to SEM images, the blend prepared through SC gives a non-uniform morphology, while the blend prepared with directly with the extruder gives a uniform morphology. In addition, although the solvent is dried to evaporate in the blend prepared by the SC method, this blend contains a small amount of solvent. Therefore, the $\eta*$ and G' of the blend prepared with SC is lower than that prepared with directly TSE. Compared to the blend nanocomposites prepared with mTSE, large differences

are observed between the η∗ and G′ values of the blend nanocomposites prepared with SC. There is a trend in the η∗ of blend nanocomposites containing above 1wt.% CNC prepared with SC, suggesting that CNC is localized in the PLA matrix and forms a solid network. However, no trend was observed among the blend nanocomposites prepared with mTSE and their η∗ values were low compared to the neat blend. This may be due to the re-agglomeration of CNC in the PLA matrix or presence of residual solvent in the blend nanocomposites during dilution of masterbatch, which prevents the effect of CNC. When we look at Figure 4.7.c, although the blend nanocomposite containing 3 wt.% CNC prepared with mTSE showed low η∗ compared to neat blend, stress growth test indicated that there is no PBAT coalescence. As a result, the viscosity reduction indicates that CNC dispersion at the nanoscale level is not achieved.

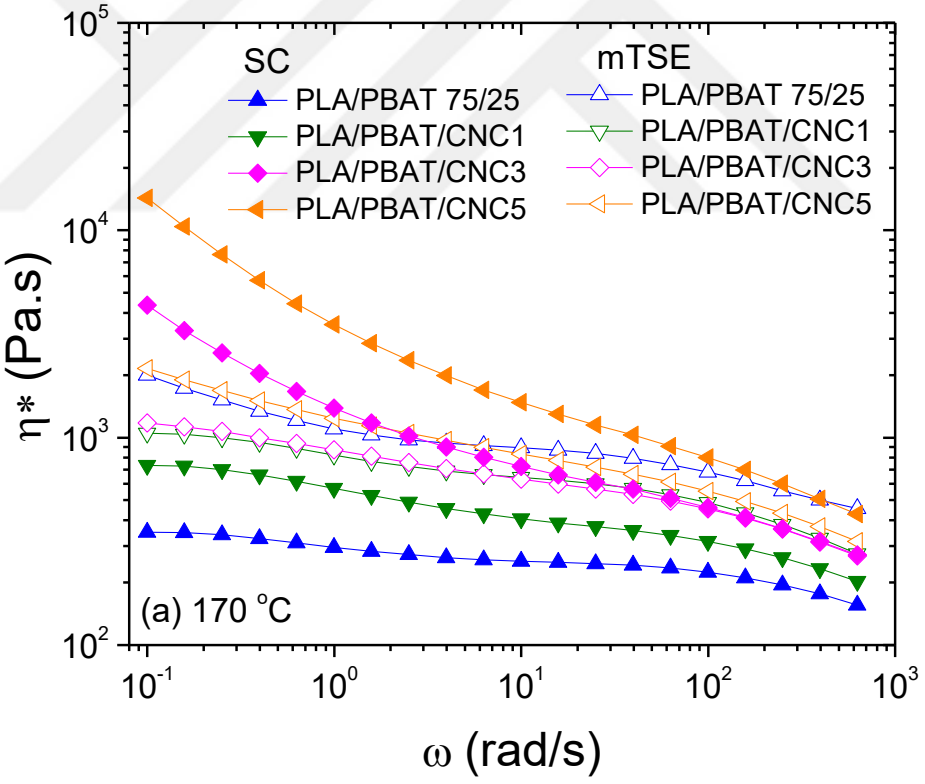

Figure 4.7 : Rheological properties of the blend nanocomposites with various CNC contents at 170 °C prepared with different processing route: (a) complex viscosity, η∗, (b) storage modulus, G′, and (c) transient shear viscosity, η^+.

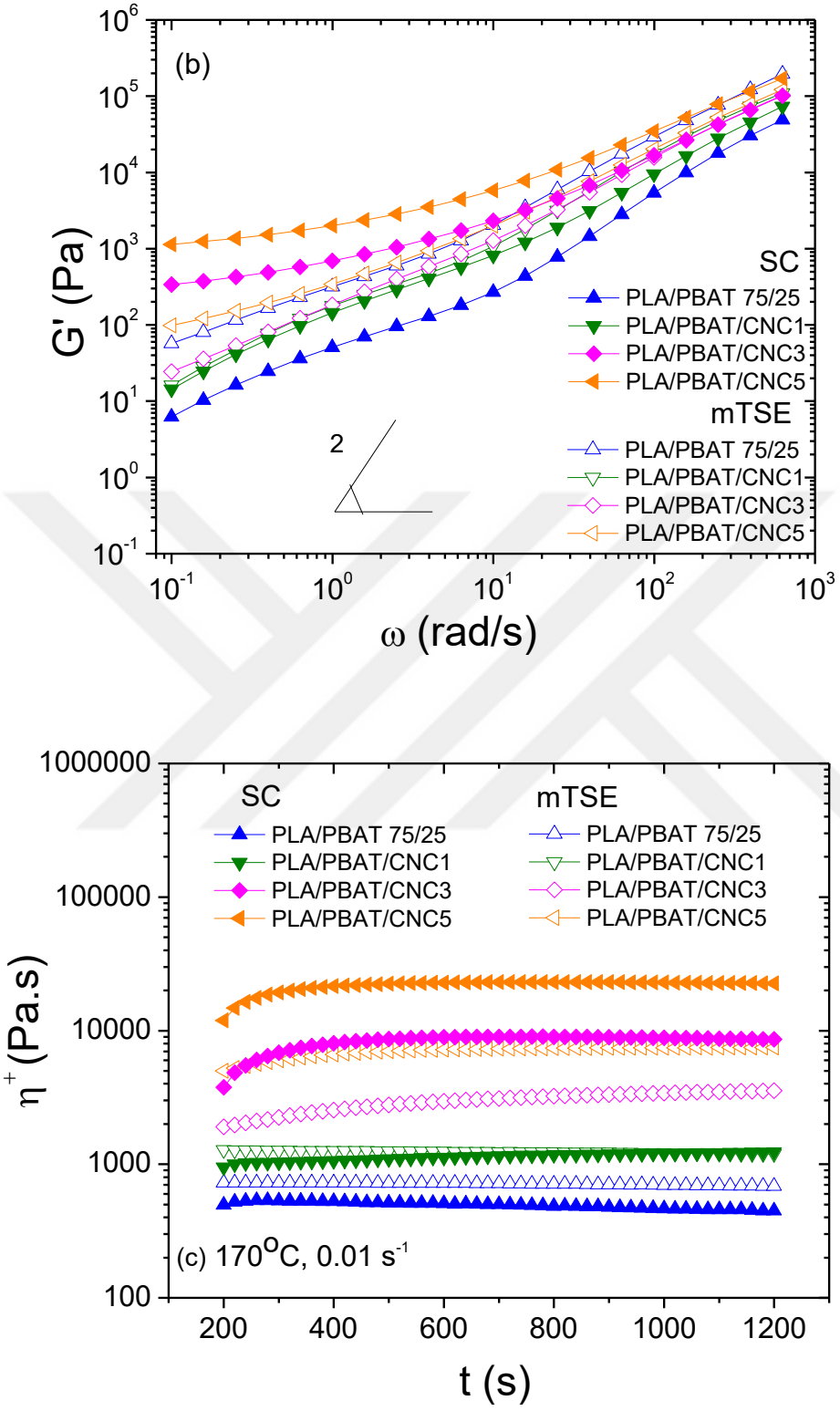

Figure 4.7 (continued) : Rheological properties of the blend nanocomposites with various CNC contents at 170 °C prepared with different processing route: (a) complex viscosity, η∗, (b) storage modulus, G′, and (c) transient shear viscosity, η^+.

4.3.3. DSC analysis

Figure 4.8 shows the comparison of DSC thermograms of neat blend and blend nanocomposites prepared with SC and mTSE. The glass transition (T_g), cold crystallization (T_{cc}), melt crystallization (T_c), and melting (T_m) temperatures as well as the degree of crystallinity (X_c) of the samples are also reported in Table 4.3. The first heating was not interpreted due to the thermal backgrounds of the samples. In cooling, with the addition of CNC, the T_g of blend nanocomposites prepared by SC did not change, but the T_g of blend nanocomposites prepared with mTSE increased. Also, T_c of blend nanocomposites prepared with SC decreased, but T_c increased in blend nanocomposites prepared with mTSE. This shows that different crystallization mechanisms are occurred in two different preparation methods. While CNC acts as nucleation agent when using the mTSE method, this behavior is not seen when using the SC method. In addition, it has been shown in the literature that depending on the localization of nanoparticles in the blend, the crystallization behavior of the system can be affected differently [90]. In the blend nanocomposites prepared by mTSE preparation method, it was observed that the increase of CNC content caused an increase in the crystallization temperature of the system. This is considered to be an indication of the CNC migrating to the interface or PLA. In the second heating, the T_{cc} was not observed in the blend nanocomposite prepared by the mTSE. This is because PLA crystallization accelerated with the addition of CNC, and therefore PLA crystallization occurred completely during cooling.

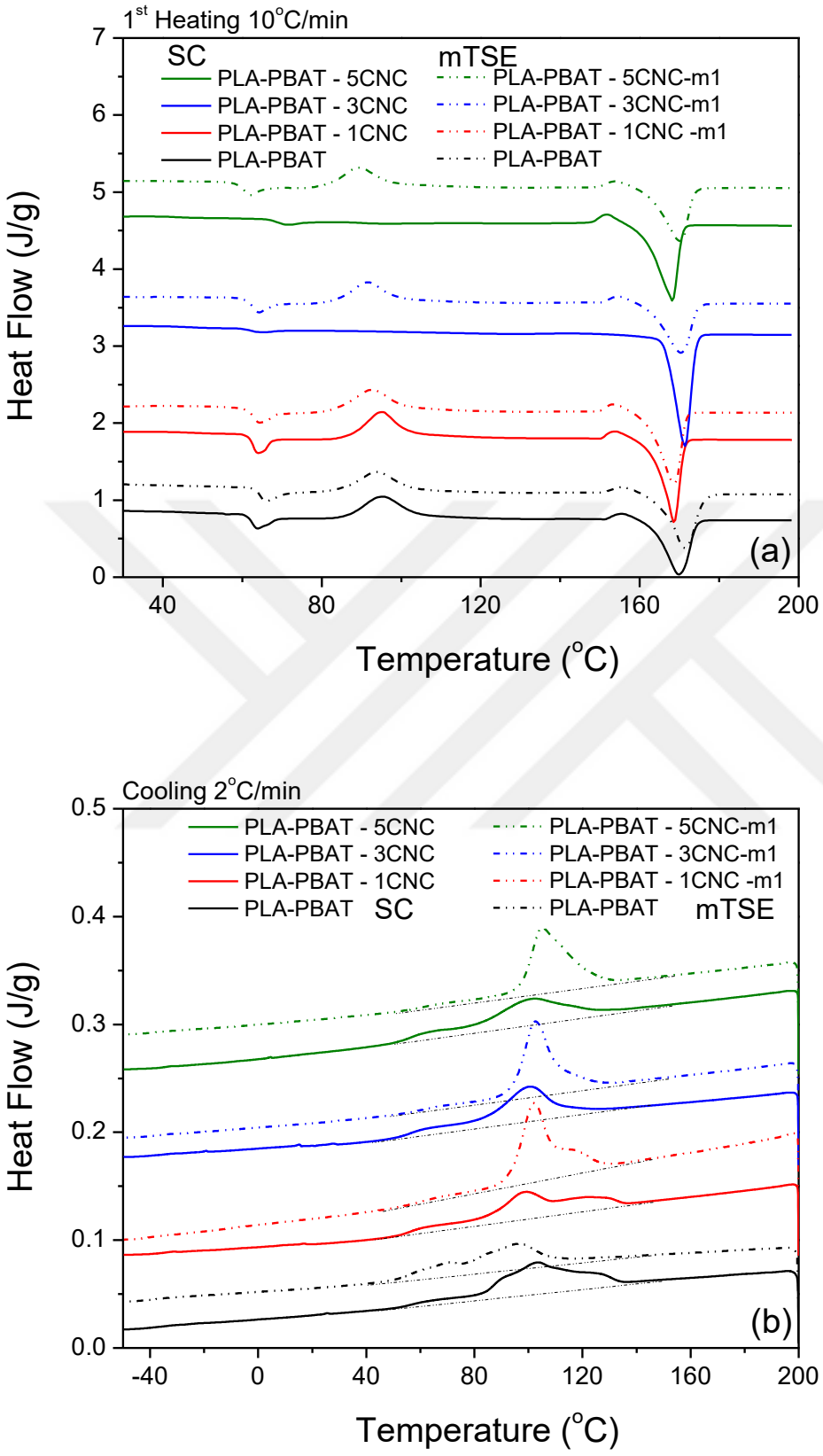

Figure 4.8 : Comparison of DSC curves of samples prepared with SC and mTSE; (a) first heating, (b) cooling and (c) second heating scans.

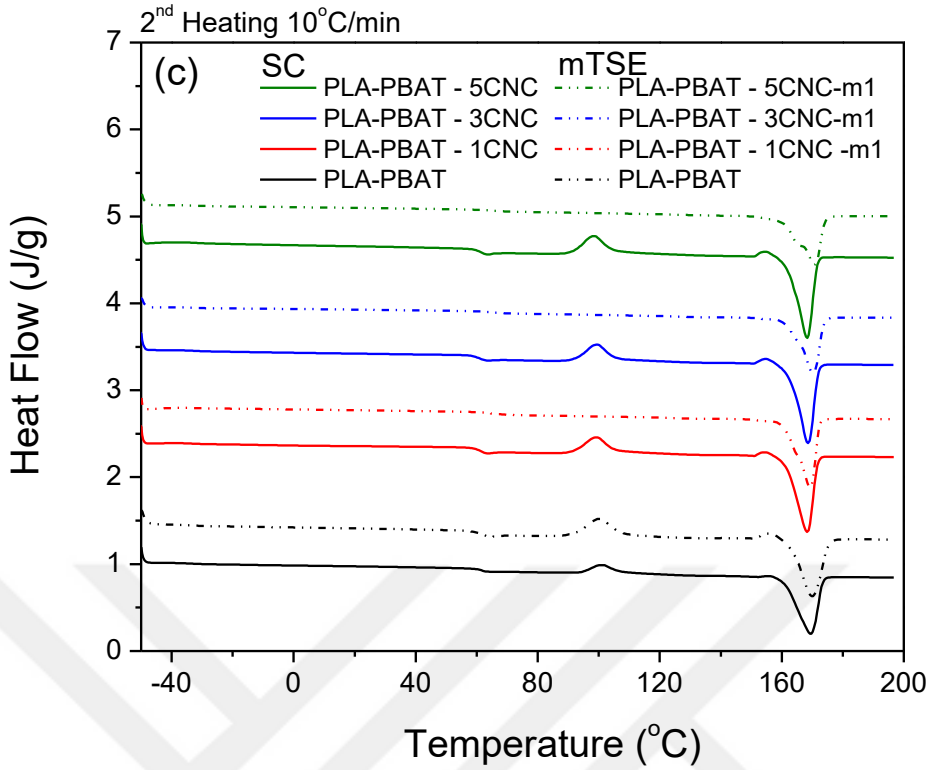

Figure 4.8 (continued) : Comparison of DSC curves of samples prepared with SC and mTSE; (a) first heating, (b) cooling and (c) second heating scans.

Table 4.3 : DSC data of samples prepared through SC and mTSE obtained from first heating, cooling and second heating scans.

	1st Heating				Cooling			2nd Heating			
	T_g	T_{cc}	T_m	X (%)	T_g	T_c	X (%)	T_g	T_{cc}	T_m	X (%)
SC											
PLA/PBAT 75/25	62	95	170	19	55	103	33	61	101	169	43
PLA/PBAT/CNC 74/25/1	62	95	169	19	55	99	25	61	99	168	33
PLA/PBAT/CNC 72/25/3	62	-	171	64	55	100	24	61	100	169	34
PLA/PBAT/CNC 70/25/5	69	-	168	64	55	101	23	61	99	168	37
mTSE											
PLA/PBAT 75/25	64	94	171	23	55	96	17	61	100	170	30
PLA/PBAT/CNC 74/25/1	62	93	169	22	58	102	48	66	-	169	48
PLA/PBAT/CNC 72/25/3	63	92	170	19	58	103	42	66	-	170	42
PLA/PBAT/CNC 70/25/5	60	89	170	21	58	105	44	66	-	171	44

4.3.4. DMA

Figure 4.9 shows comparison of the storage modulus (E′) and tanδ as a function of temperature of the samples prepared through SC and mTSE. Figure 4.10 shows the storage module of samples 45 (below the Tg of PLA) and 85 °C (above the Tg of PLA). Regardless of the preparation routes, the E′ of all samples dropped sharply after 60 °C, i.e. after transition from glassy to rubber region. There was an increase in E′ again after 100 °C, i.e. due to cold crystallization of PLA. The E′ of the blend nanocomposites prepared by mTSE has fallen later than that prepared by SC. This late reduction of the E′ is attributed to the rise in stiffening effect due to its fine dispersion through extruder. Regardless of the processing routes, the addition of 3 and 5 wt. % CNCs have a strong reinforcing effect on the E′ at 85 °C. According to the literature, the reinforcement efficiency of the CNC depends on the degree of dispersion of the CNC and its preferred localization [91]. The low and high reinforcing effect of CNCs could be attributed to their localization in the PBAT and PLA, respectively. It was observed that the tanδ peak shrank and shifted to high temperatures with the addition of CNC. This shows that the system gained stiffness due to CNC.

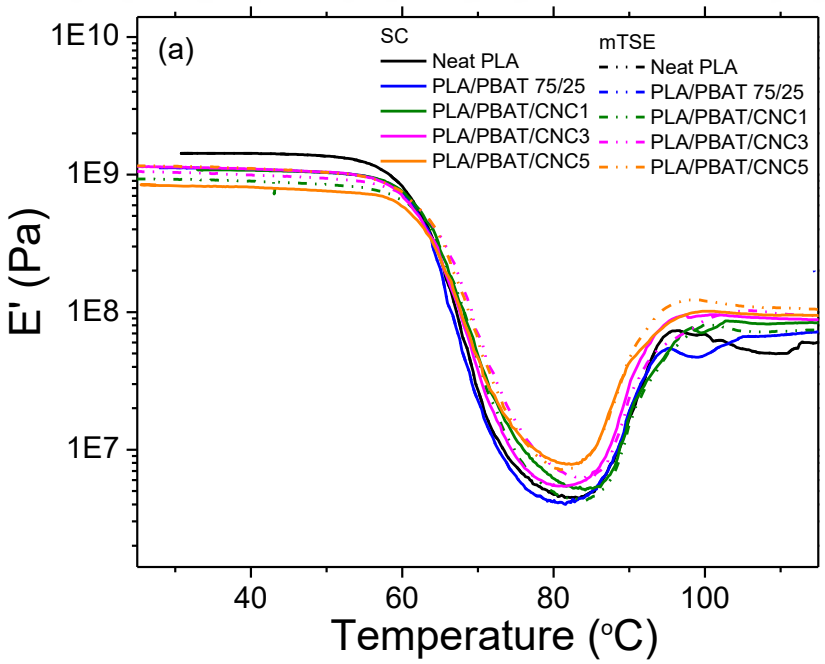

Figure 4.9 : DMA of samples prepared by SC and mTSE; (a) E′ and (b) tanδ curves.

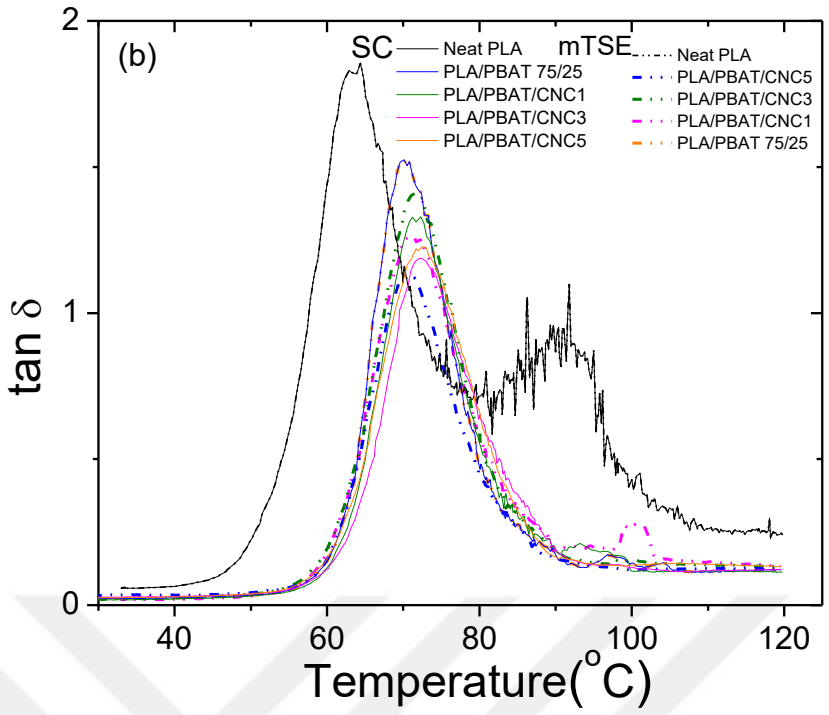

Figure 4.9 (continued) : DMA of samples prepared by SC and mTSE; (a) E′ and (b) tanδ curves.

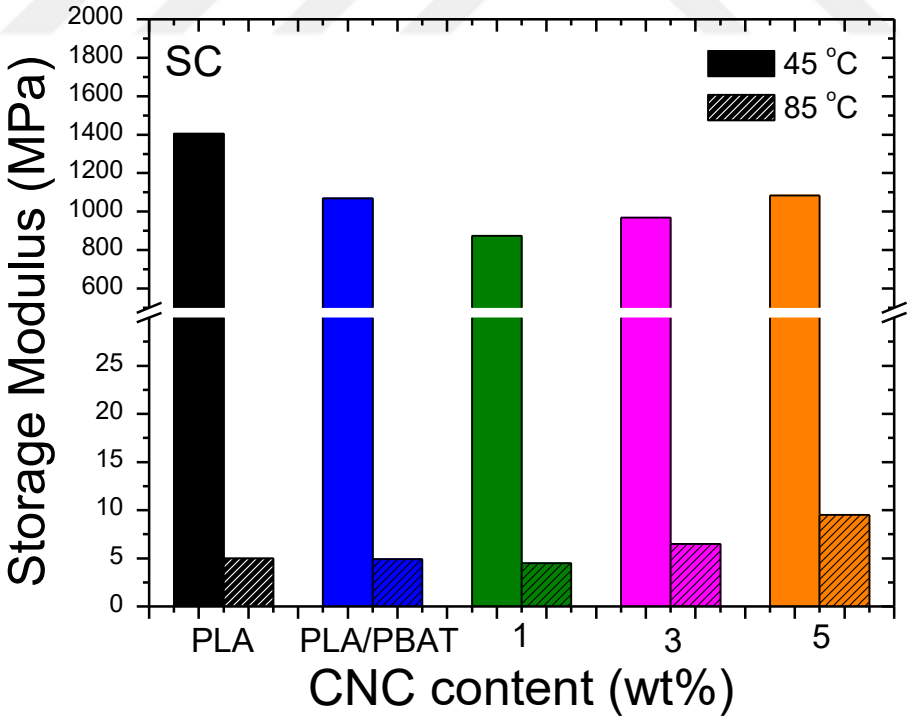

Figure 4.10 : Comparison of the E′ of PLA and PLA/PBAT/CNC blend nanocomposites with different CNC loadings prepared by SC and mTSE.

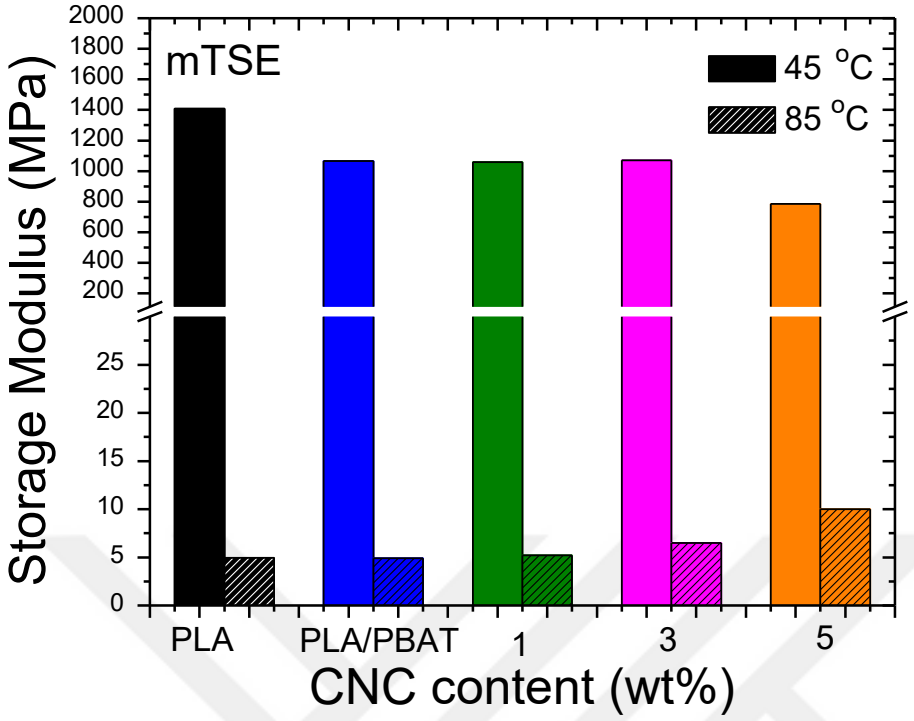

Figure 4.10 (continued) : Comparison of the E′ of PLA and PLA/PBAT/CNC blend nanocomposites with different CNC loadings prepared by SC and mTSE.

4.3.5. Mechanical analysis

Figures 4.11 and 4.12 show the tensile, izod impact and flexural properties of all samples prepared with mTSE, respectively. The addition of the high elongation at break PBAT phase to PLA naturally formed a flexible blend structure [68]. As can be seen from the figures, there was no expected improvement in blend nanocomposites, except for blend nanocomposites containing 5 wt.% CNC, due to non-homogeneous morphology and incompatibility between the components [48]. The addition of 1 and 3 wt.% CNC did not significantly affect the strength and modulus of PLA/PBAT blends. This may be due to the absence of much finer and more homogeneous PBAT droplets as CNC is localized in PBAT. Regarding elongation at break, the blend nanocomposite containing 1 wt.% CNC showed the highest value compared to neat PLA and PLA/PBAT blend. The reason for this increase can be shown that the increases the dispersed phase size by increasing the elasticity of the dispersed phase due to the localization of nanoparticles in the dispersed phase [92, 93]. It was observed that, with the incorporation of 5 wt.% CNC, Young's module and izod impact strength

remarkable increased. According to the literature, if the nanoparticles are localized in the matrix phase, the modulus, strength and impact properties of the sample increase [61, 94].

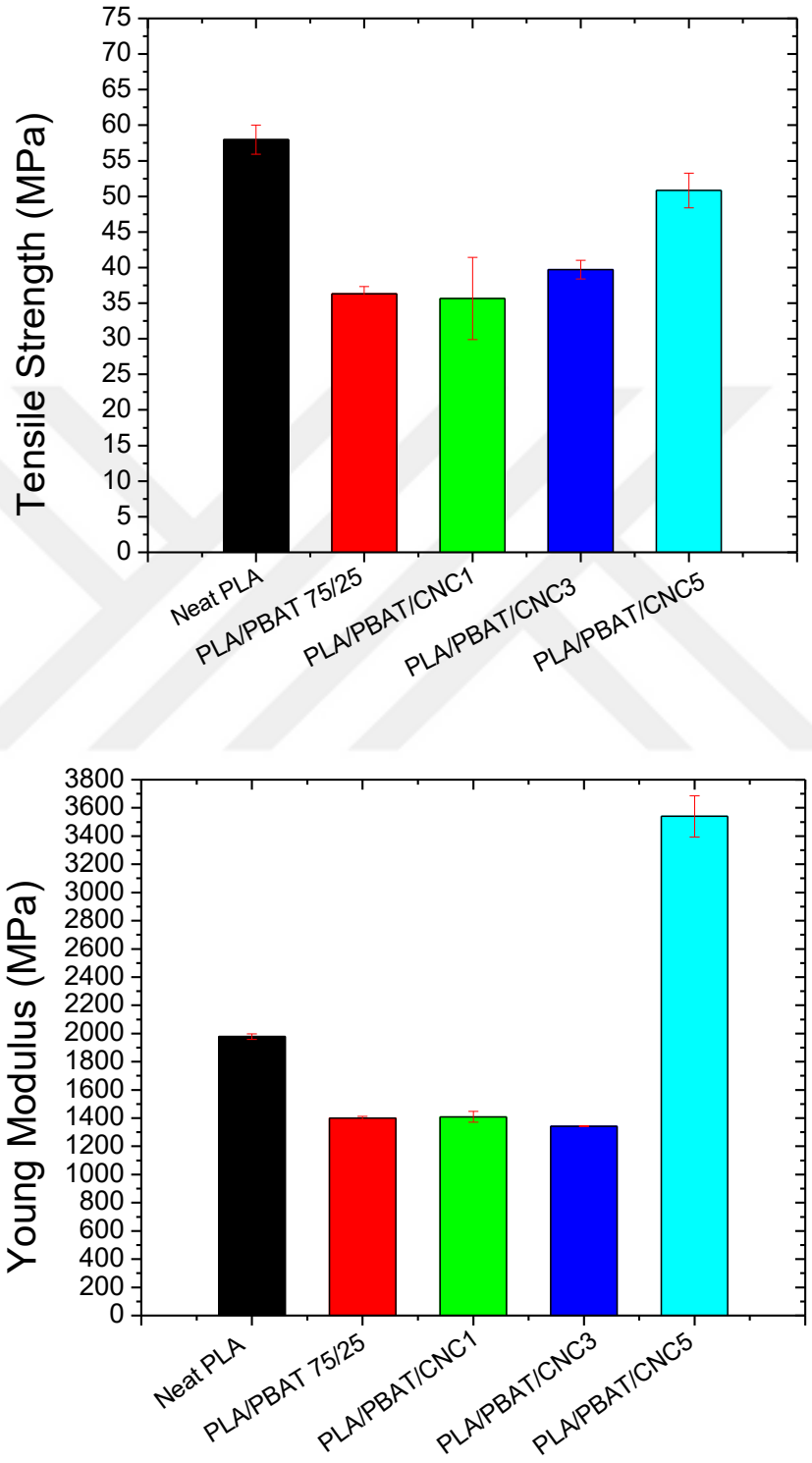

Figure 4.11 : Tensile properties and izod impact strength of samples prepared through mTSE.

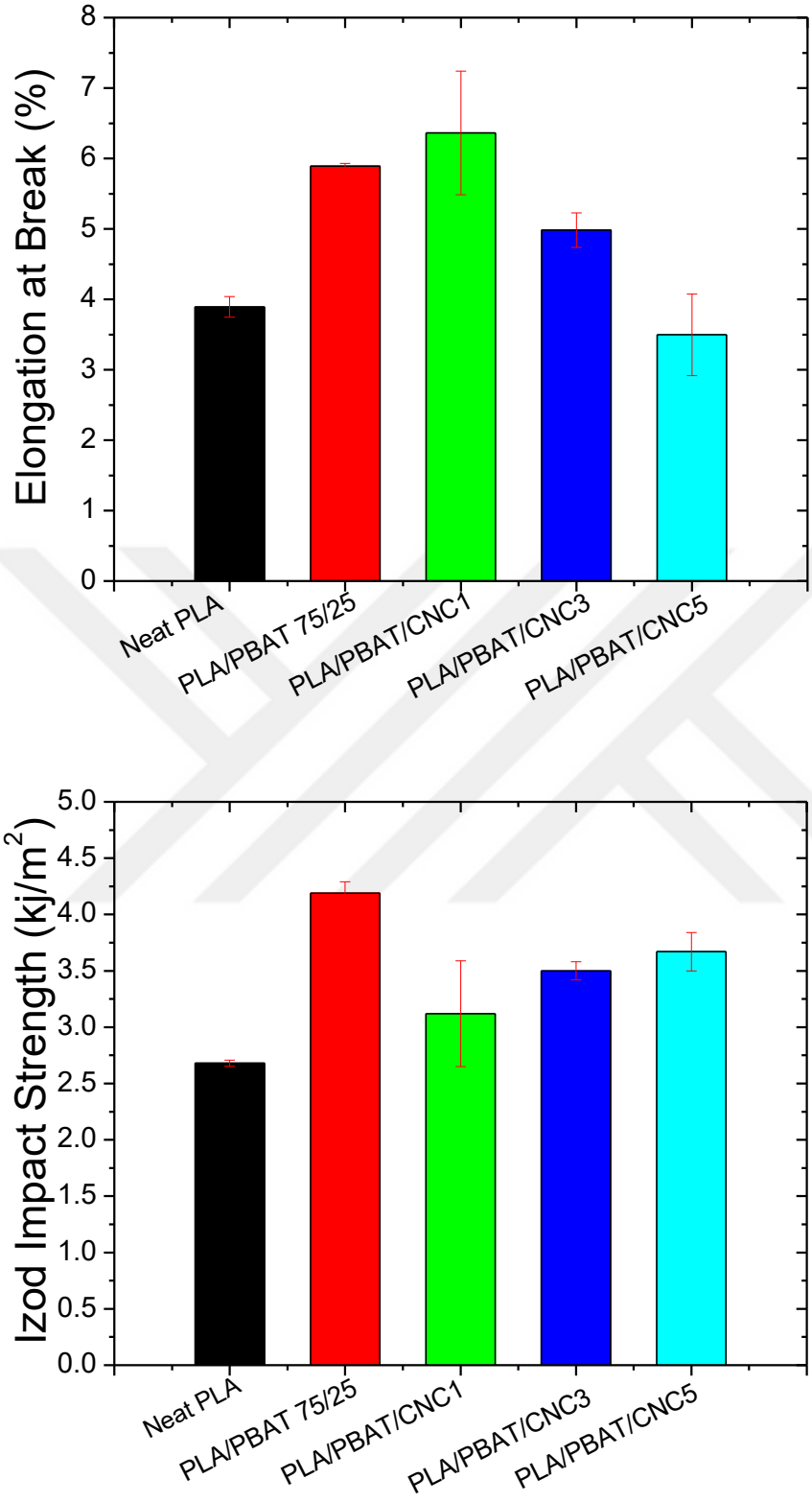

Figure 4.11 (continued) : Tensile properties and izod impact strength of samples prepared through mTSE.

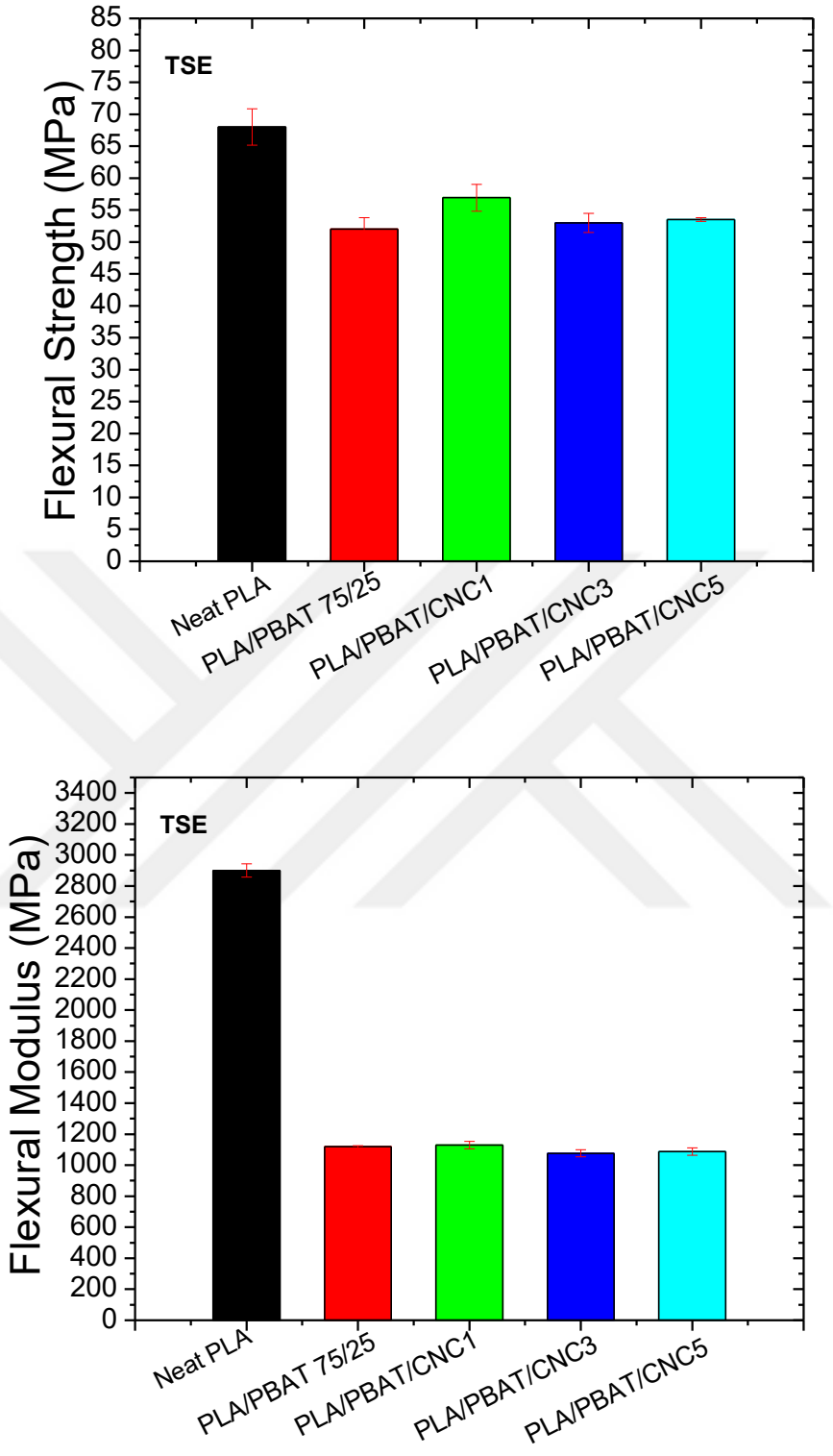

Figure 4.12 : Flexural properties of samples prepared through mTSE.

4.4. PLA/PBAT/CNC WITH DIFFERENT PBAT CONTENT

4.4.1. Morphology analysis

Figure 4.13 shows SEM images of blend and blend nanocomposites with a fixed 3 wt.% CNC and 10, 25 and 50 wt.% of PBAT content prepared through mTSE. It is known that different morphologies are obtained by mixing the polymers in different ratios. The blends with 10 and 25 wt.% PBAT contents and their blend nanocomposites containing 3 wt.% CNC showed a matrix-dispersed phase morphology. In both the blend of nanocomposites, the droplet size of PBAT appears larger than that of neat blends. The blend with 50 wt.% PBAT and its blend nanocomposites containing 3wt. % CNC showed co-continuous morphology.

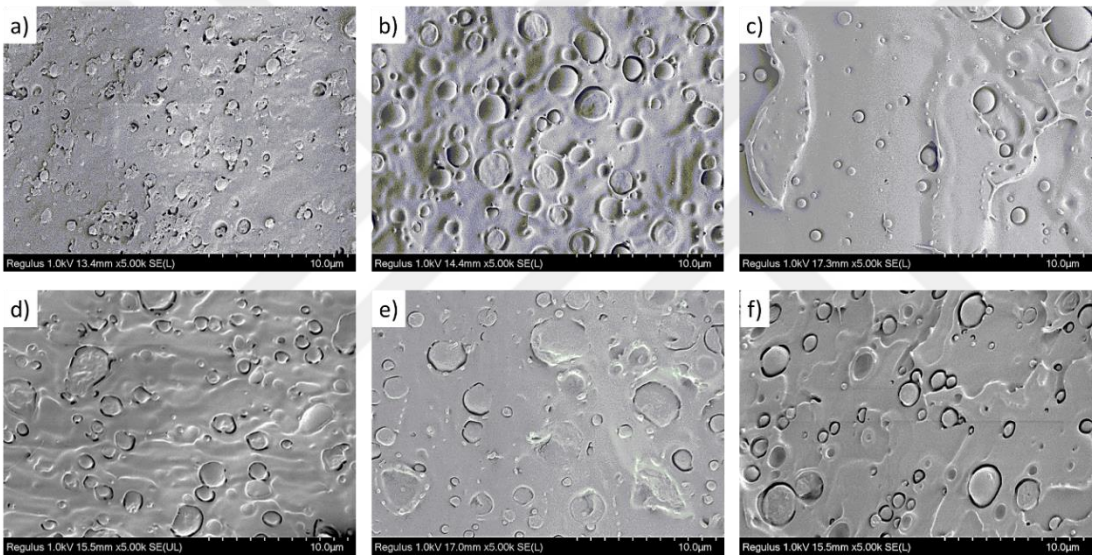

Figure 4.13 : SEM images of blend and blend nanocomposites with different PBAT content and constant 3 wt% CNC; a) PLA/PBAT (90/10), b) PLA/PBAT (75/25), c) PLA/PBAT (50/50), d) PLA/PBAT/CNC (87/10/3), e) PLA/PBAT/CNC (72/25/3) and f) PLA/PBAT/CNC (48.5/48.5/3).

4.4.2. Rheological analysis

Figure 4.14 shows how the rheological properties of blend and blend nanocomposites containing 3 wt.% CNC change with different PBAT ratios. Neat blends were prepared by direct melt mixing method (TSE), while the blend nanocomposites were prepared by the combination of solution casting and melt mixing (mTSE). As shown in Figure 4.14.a, when the content of PBAT increased from 10 to 25 wt.%, the complex viscosity of the blend increased at low frequencies. However, when the PBAT content reaches 50 wt.%, the blend shows a lower viscosity than the blend with 25 wt.%, indicating

the evolution of a continuous morphology that reverses the viscosity trend. The same trend was seen in the storage module results [49]. Although it has been reported in the literature that the viscosity of blends increased due to the use of nanoparticles, the use of 3 wt.% CNC caused a decrease in the viscosity of blend nanocomposites containing 10 and 25 wt.% PBAT. The decrease in the viscosity of these blend nanocomposites may be due to the localization of the CNC in the PBAT phase or the solution remaining in the blend nanocomposites. On the other hand, there was a significant increase in viscosity when the 3 wt.% CNC was included in the blend containing 50 wt.% PBAT. The reason for this increase can be assumed that the CNC can form a solid network structure within the PBAT phase, since the blend nanocomposite has a continuous morphology. In the stress growth test, it was observed that there was no coalescence in the PBAT phase dispersed in the PLA matrix after CNC was added to the blends.

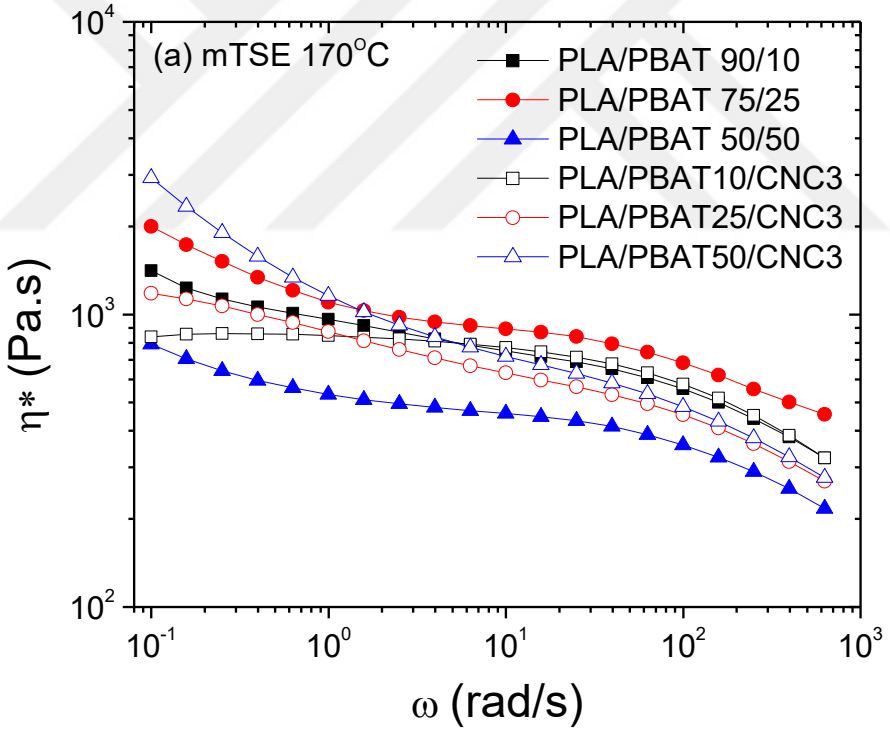

Figure 4.14 : Rheological properties of the blends and blend nanocomposites with various PBAT contents: (a) complex viscosity, η∗, (b) storage modulus, G′, and (c) transient shear viscosity, η^{+}.

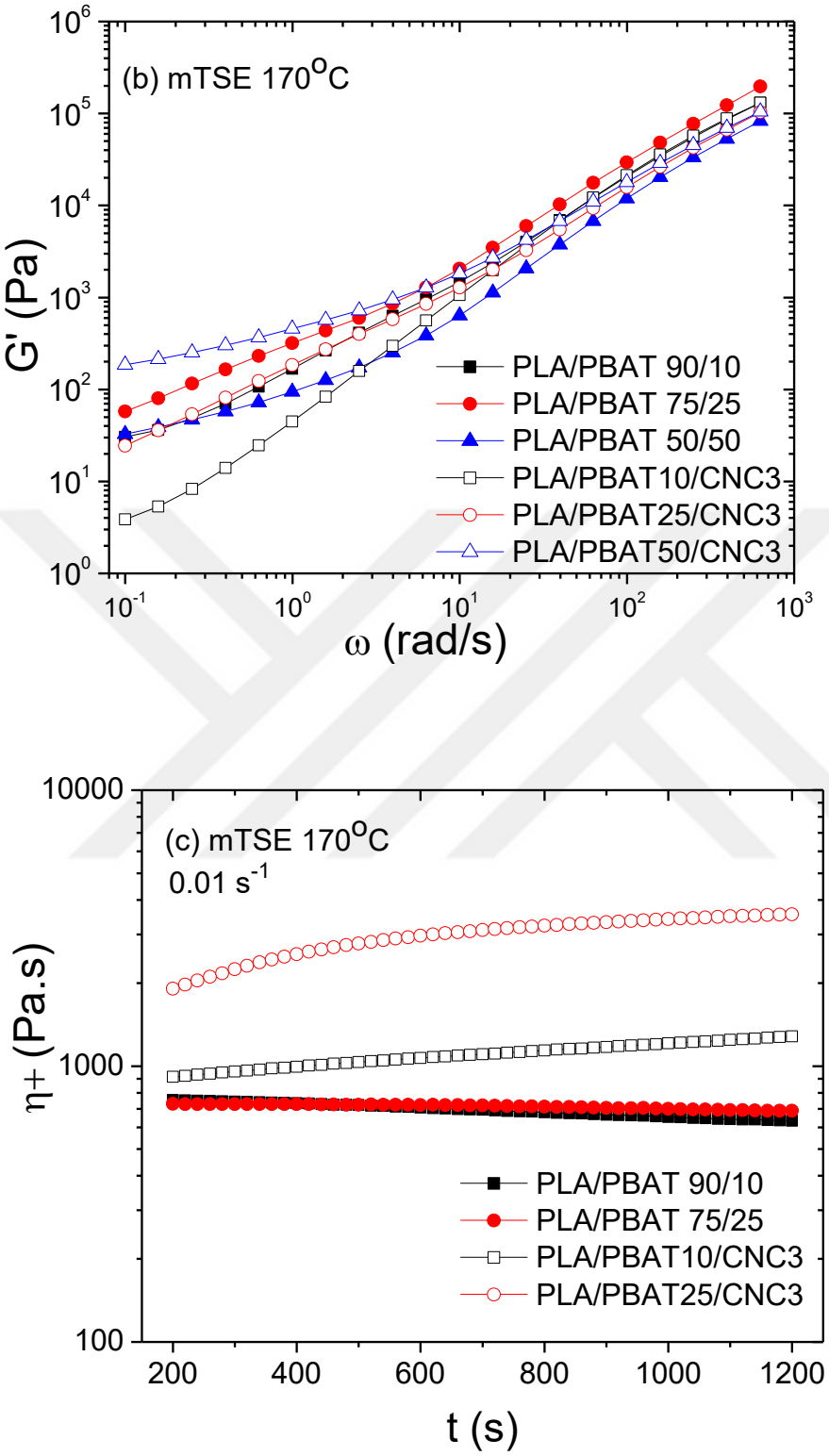

Figure 4.14 (continued) : Rheological properties of the blends and blend nanocomposites with various PBAT contents: (a) complex viscosity, η∗, (b) storage modulus, G′, and (c) transient shear viscosity, η^{+}.

4.4.3. DSC analysis

Figure 4.15 shows DSC plots of PLA/PBAT blend and PLA/PBAT/CNC blend nanocomposites with different PBAT contents prepared with mTSE methods. The glass transition (T_g), cold crystallization (T_{cc}), melt crystallization (T_c), and melting (T_m) temperatures as well as the degree of crystallinity (X_c) of the samples are also reported in Table 4.4. The first heating was not interpreted due to the thermal backgrounds of the samples. In cooling cycle, it was observed that the crystallization temperature of the system decreased from 98 to 88 °C by increasing the PBAT content in the blend from 10 to 50 wt.%. It has been shown in the literature that the PBAT phase is melt at PLA crystallization temperatures, which can prevent PLA nucleation and negatively affect PLA crystallization [95]. When 3 wt.% CNC was added in the blend, it was observed that the exothermic peak seen during the cooling cycle shifted to higher temperatures and showed a narrower peak. The reason for this can be explained as follows; Firstly, part of the CNC is localized in PLA, which causes acceleration of the crystallization of PLA, and secondly, CNCs localized in PBAT increase the viscoelastic properties of PBAT and cause the PBAT phase to play a nucleation region on the PLA. Thus, in the second heating, the crystallization rates of the blends increased with the addition of CNC. Moreover, the absence of the cold crystallization peak of PLA in blend nanocomposites during the second heating supports this result. On the other hand, the blend nanocomposite containing 50 wt.% PBAT showed two melting temperatures, the high and low temperatures reflected the melting temperature of PLA and PBAT, respectively.

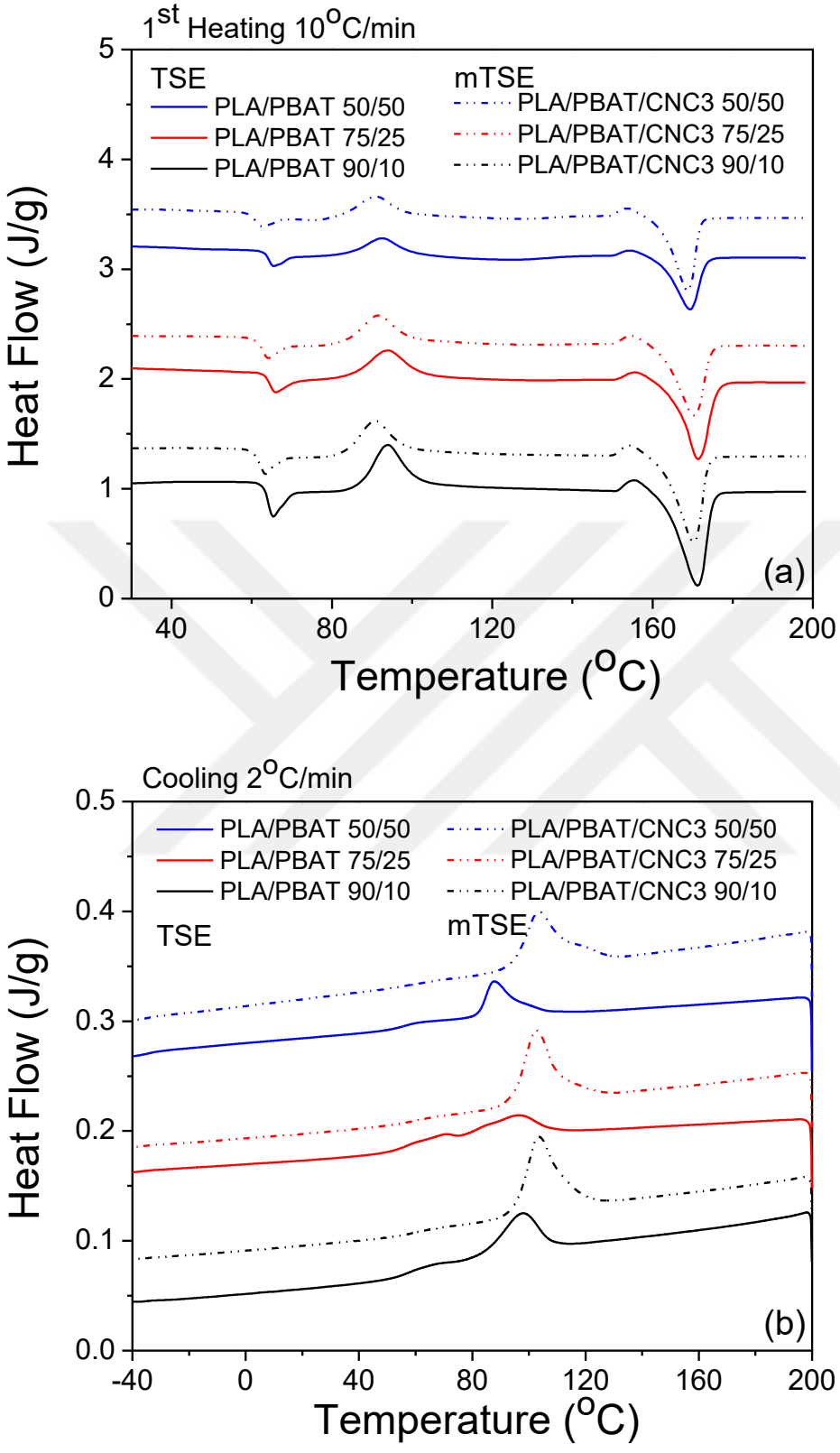

Figure 4.15 : DSC curves of blends and blend nanocomposites with different PBAT loadings: (a) first heating, (b) cooling and (c) second heating scans.

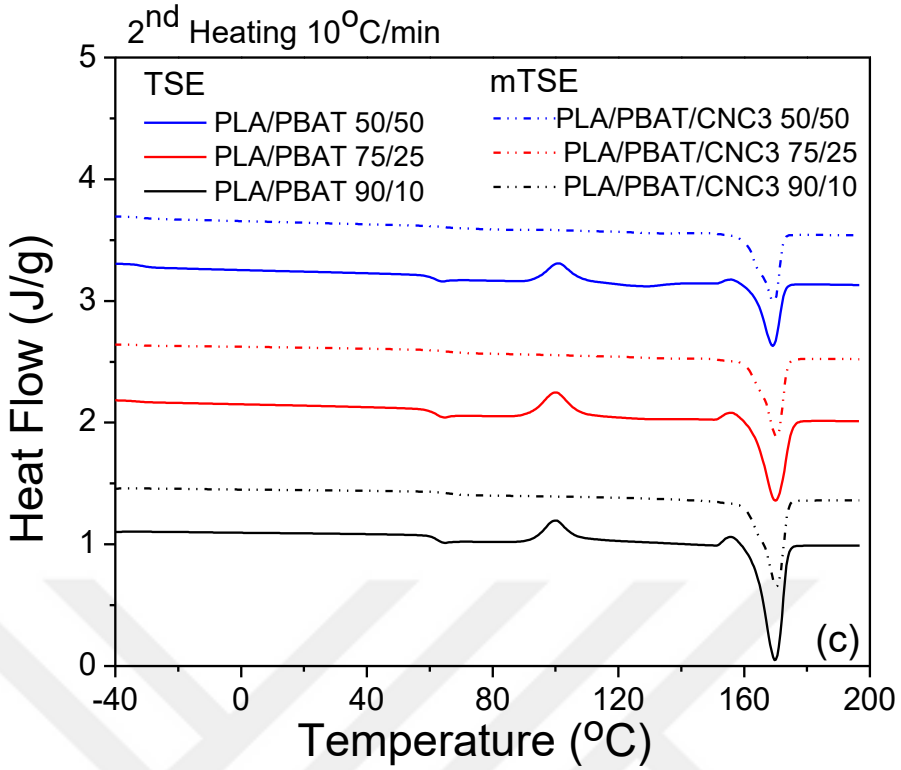

Figure 4.15 (continued) : DSC curves of blends and blend nanocomposites with different PBAT loadings: (a) first heating, (b) cooling and (c) second heating scans.

Table 4.4 : DSC data of blends and blend nanocomposites with different PBAT loadings obtained from first heating, cooling and second heating scans.

	1st Heating					Cooling				2nd Heating				
	T_g	T_{cc}	T_m	$T_{m,PBAT}$	X%	T_g	$T_{g,PBAT}$	T_c	X%	T_g	T_{cc}	T_m	$T_{m,PBAT}$	X%
PLA/PBAT 90/10	64	94	171	-	20	56	-	98	19	62	100	170	-	37
PLA/PBAT 75/25	64	94	171	-	23	55	-	96	17	61	100	170	-	30
PLA/PBAT 50/50	64	93	169	125	26	55	-36	88	26	61	101	169	129	30
PLA/PBAT/CNC 87/10/3	62	91	170	-	16	56	-	103	35	66	-	170	-	41
PLA/PBAT/CNC 72/25/3	63	92	170	-	19	58	-	103	42	66	-	170	-	42
PLA/PBAT/CNC 48.5/48.5/3	61	91	169	127	34	55	-36	103	54	65	-	169	-	52

4.4.4. DMA

Figure 4.16 shows the storage module (E′) and tan delta (tanδ) versus temperature graphs of PLA/PBAT blend and PLA/PBAT/CNC blend nanocomposites with different PBAT ratios prepared by the mTSE method. Figure 4.17 shows the storage module of samples 45 (below the T_g of PLA) and 85 °C (above the T_g of PLA). The E′

curves first show a straight plateau (glassy region), a decrease around 60 °C and an increase due to cold crystallization around 100 °C. In the glass transition region, it was observed that the E′ decreased with increasing PBAT content in PLA/PBAT blends. However, the addition of CNC did not cause a significant increase in the E′ of the blends in this region. On the other hand, in the rubber region, the E′ of the blends increased somewhat with the addition of CNC, and the highest increase was observed in the blend nanocomposite with the highest PBAT ratio. In Figure 4.15.b, as the PBAT ratio increased, it was observed that the damping peak of the blends decreased as it functioned as a stress concentrator. It is also seen that the addition of CNC causes a decrease in the tanδ peak.

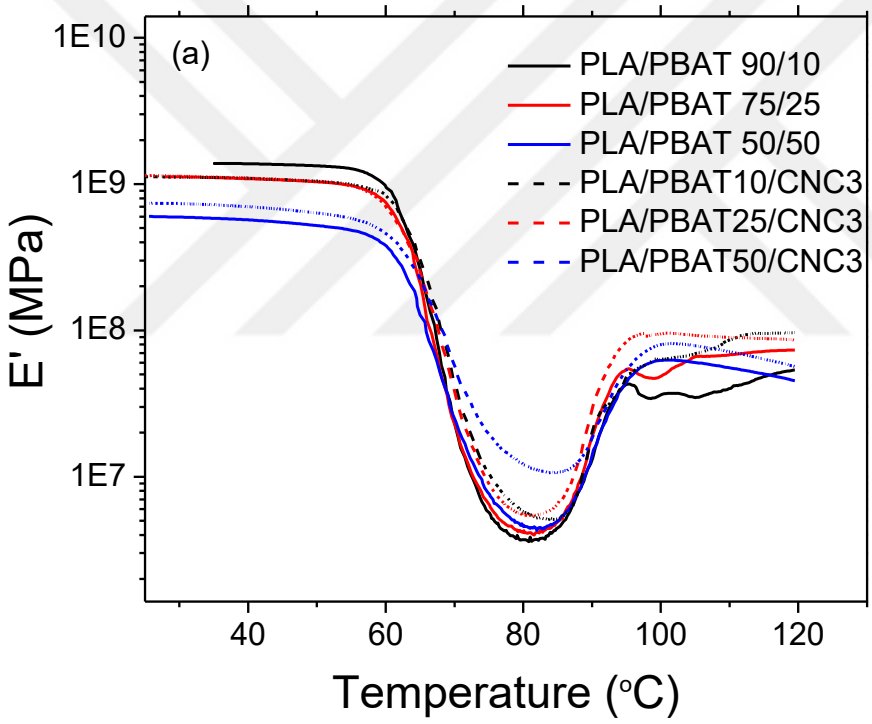

Figure 4.16 : DMA graphs of blends and blend nanocomposites with different PBAT loadings: (a) E′ and (b) tanδ curves.

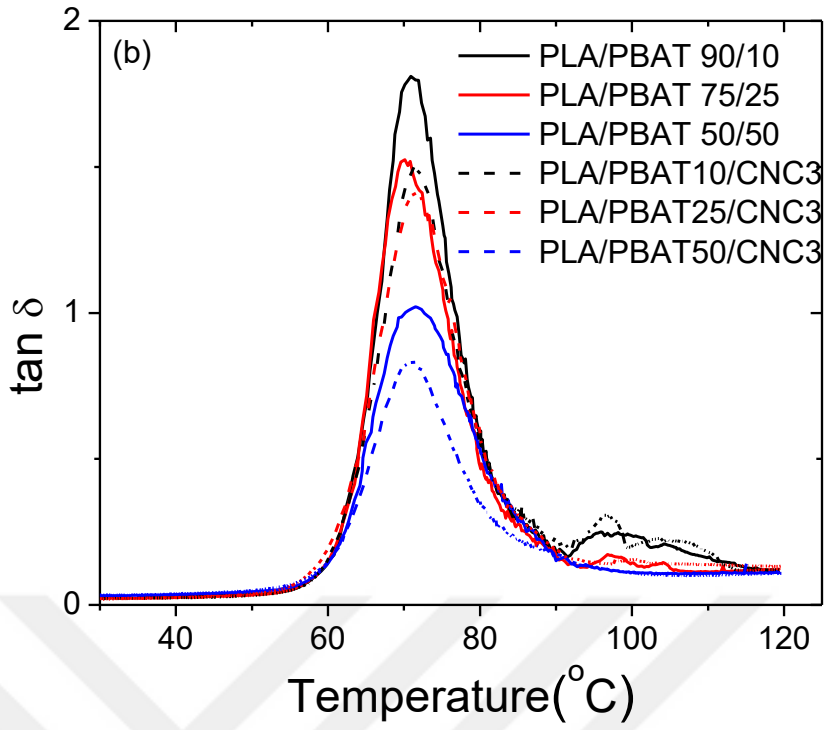

Figure 4.16 (continued) : DMA graphs of blends and blend nanocomposites with different PBAT loadings: (a) E′ and (b) tanδ curves.

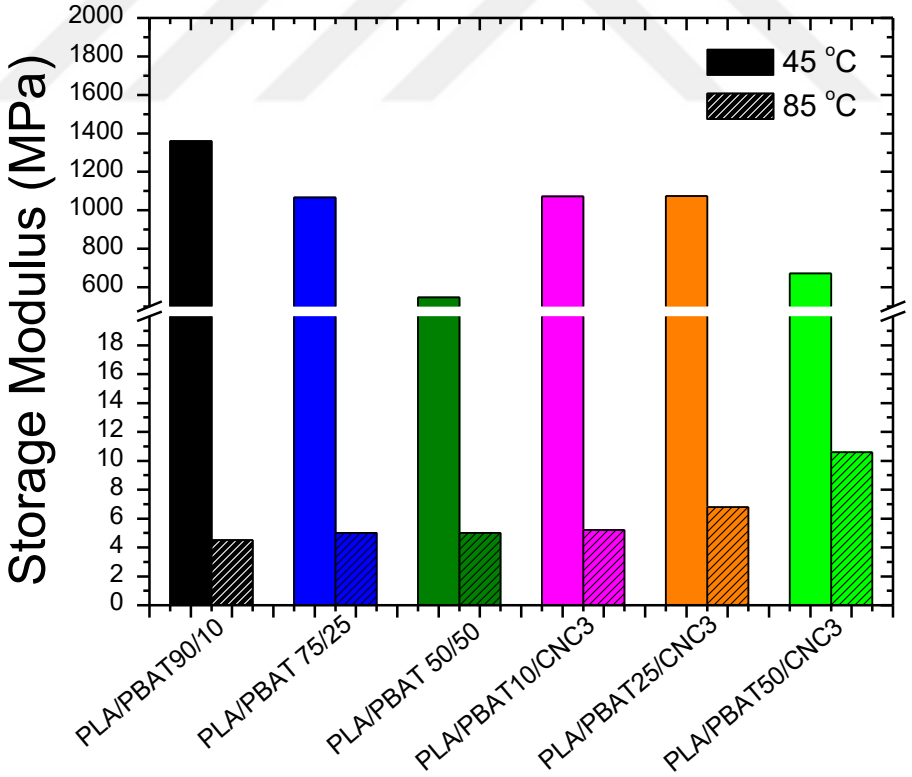

Figure 4.17 : Comparison of the E′ of PLA and PLA/PBAT/CNC blend nanocomposites with different PBAT loadings.

4.4.5. Mechanical analysis

Figure 4.18 and 4.19 show the tensile, izod impact and flexural properties of PLA/PBAT blends and PLA/PBAT/CNC blend nanocomposites with different PBAT loadings. Tensile and flexural strength and modulus of PLA decreased with increasing PBAT content. This reduction may possibly be related to the presence of a soft and elastomeric PBAT phase, which reduces crystallinity in the neat PLA, which was also confirmed in DSC studies in previous chapters. On the other hand, the addition of the flexible PBAT phase to the PLA increased the elasticity and the elongation at break of the blend. Also, with the addition of CNC, there has been little change in the mechanical properties of the blends, which may be associated the absence of an effective dispersion of CNC. In addition, the presence of 10 wt.% PBAT in PLA reduced the brittleness properties of PLA, which is evident from the increase in impact strength. However, a decrease in the tensile strength of PLA was observed with increases in PBAT loading, and this may be due to phase separation caused by incompatibility between polymers. In addition, the addition of 3 wt.% CNC to the PLA/PBAT blend containing 10 wt.% PBAT significantly reduced impact strength due to its rigidity. In other blends containing 3 wt.% CNC, almost no changes in mechanical properties have been observed; this can be attributed to the CNC's lack of dispersion in the blends.

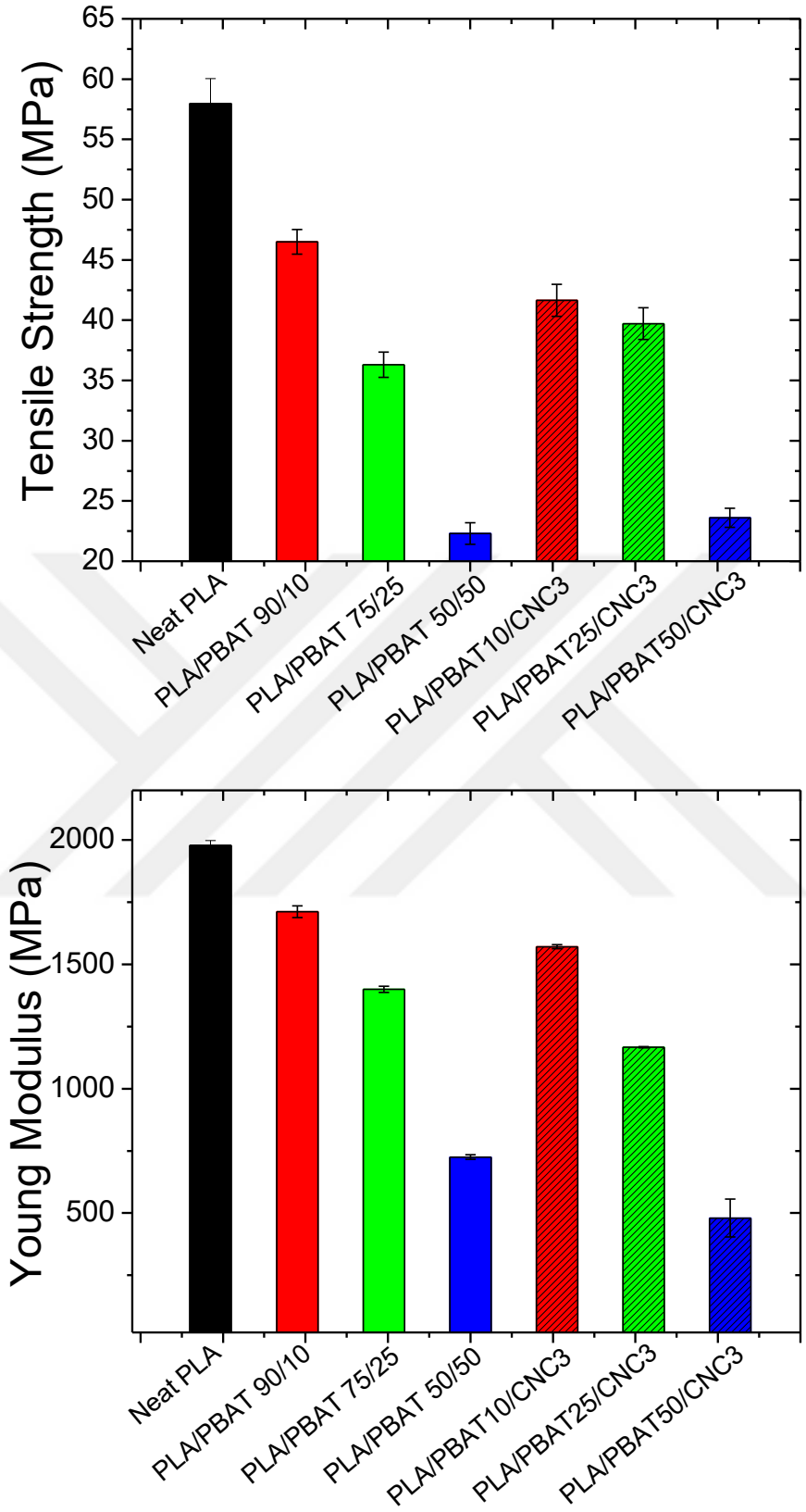

Figure 4.18 : Tensile properties and Izod impact strength of samples with different PBAT loadings.

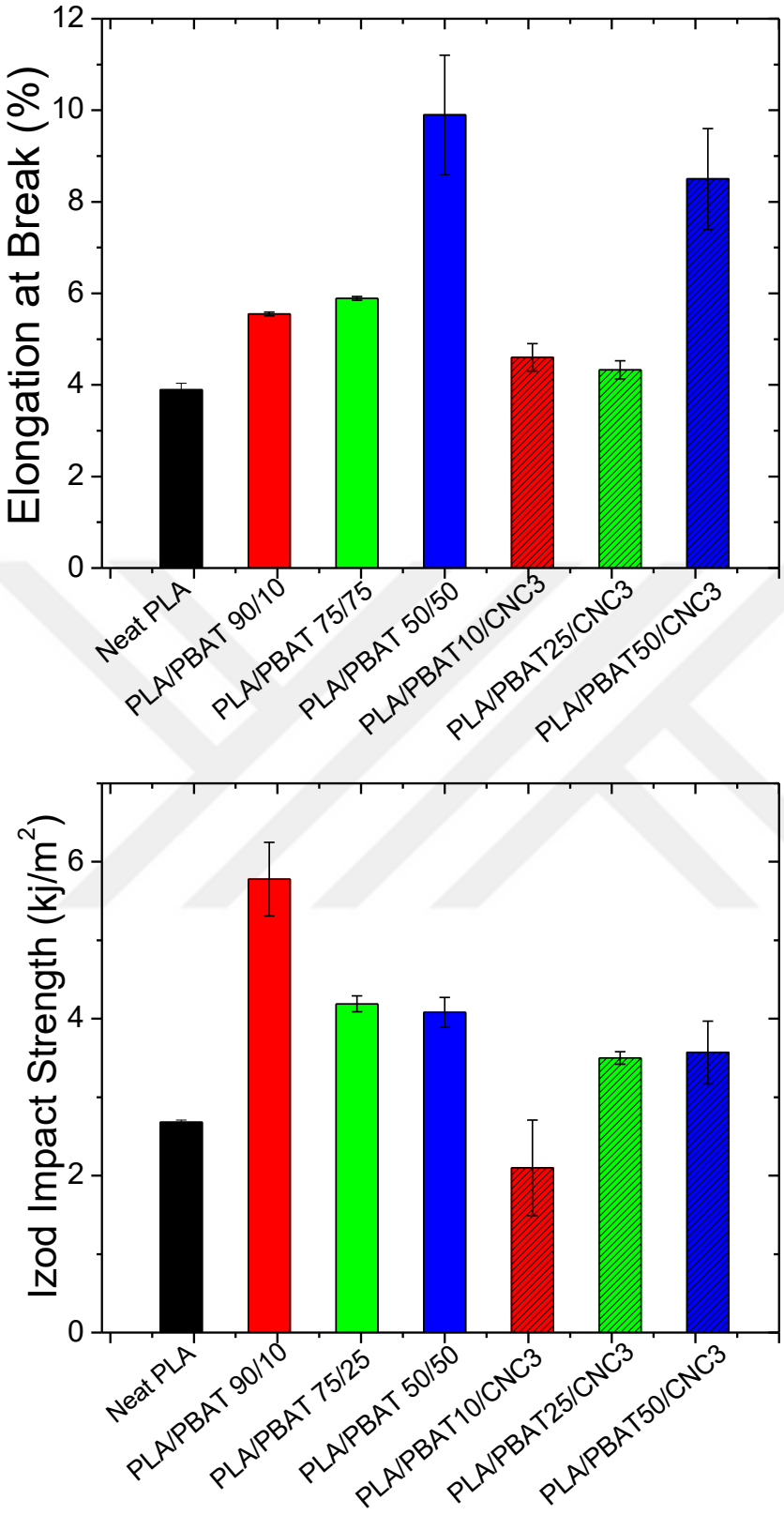

Figure 4.18 (continued) : Tensile properties and Izod impact strength of samples with different PBAT loadings.

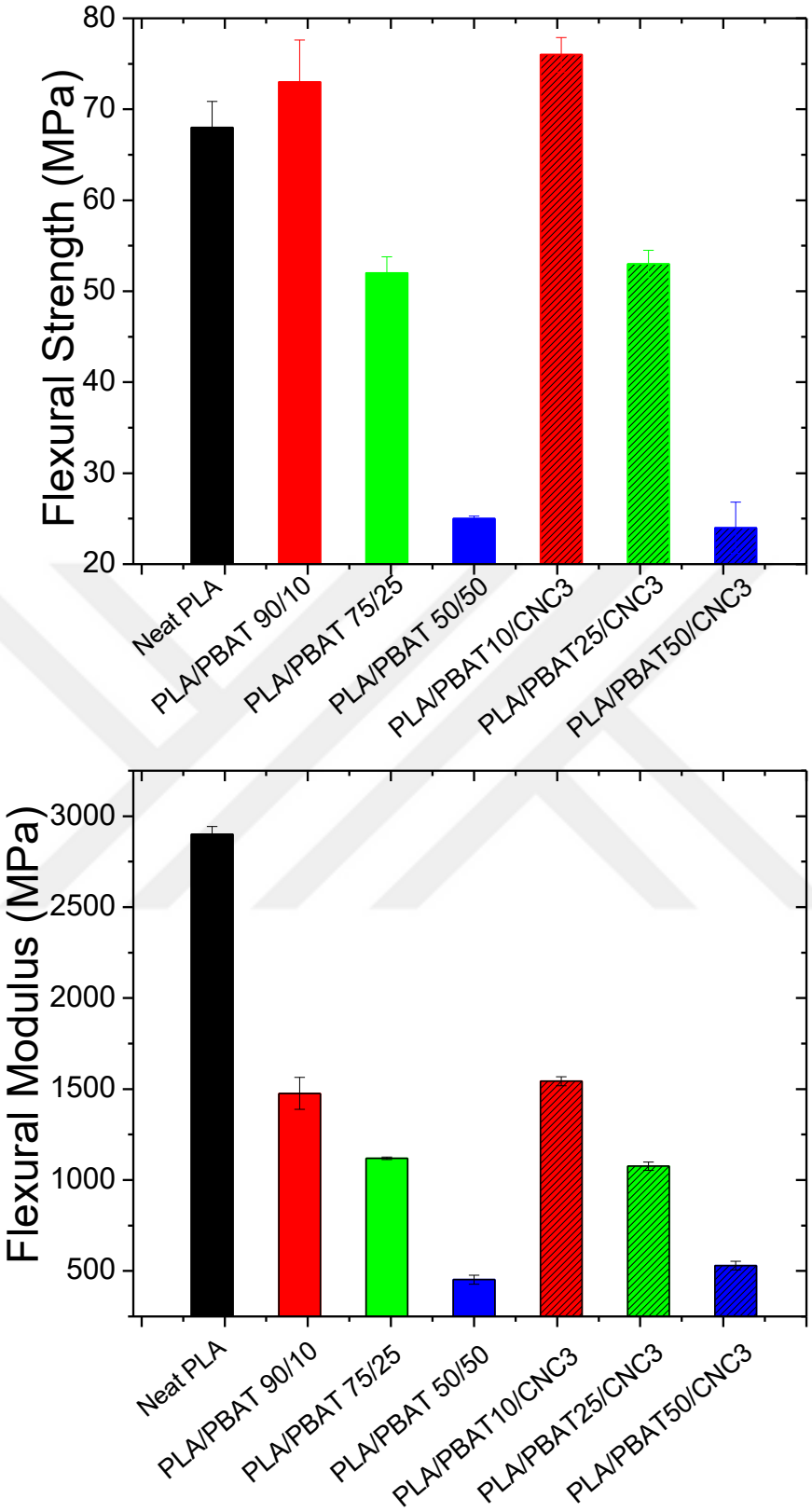

Figure 4.19 : Flexural properties of samples with different PBAT loadings.

4.5. PLA/PBAT/CNC WITH DIFFERENT MIXING STRATEGIES AND PROCESSING METHOD

4.5.1. Morphology analysis

Figure 4.20 shows SEM images of samples with three mixing strategies and processing through mTSE and mIM. Three mixing strategies were used to prepare PLA/PBAT blend nanocomposites containing 3 wt.% CNC, as follows: (m1) masterbatch prepared by direct mixing of all three components by SC method and then diluted using melt mixing with the addition of PLA and PBAT; (m2) PLA/CNC masterbatch prepared through solution casting method and then diluted using melt mixing with the addition of PLA and PBAT; and (m3) PBAT/CNC masterbatch prepared through solution casting method and then diluted using melt mixing with the addition of PLA and PBAT. Neat PLA / PBAT blends containing 25 wt.% PBAT were prepared directly by TSE or IM. In the neat blends, it was observed that the droplet size of PBAT prepared by IM was larger than that prepared by TSE. The reason for this can be attributed to the high shear forces in the extruder, because leads to droplet break-up of the PBAT. In M1 and M2 strategies, it was assumed that the CNC was already in the PLA phase, since the blend nanocomposite prepared by the mTSE method was diluted from the masterbatch containing 7wt.% CNC. The large droplets in these strategies may be due to the re-agglomeration of CNC in the PLA matrix. In the blend nanocomposites prepared with mTSE, the morphology did not show much change with the addition of CNC, except m3 strategy. The blend nanocomposite prepared with the M3 strategy showed continuous morphology. The reason for this may be due to the inability of the CNC to migrate from PBAT to PLA because there is not enough time in TSE, and therefore PBAT may have started to coalescence. As a result, morphology has evolved from a dispersed-matrix to a continuous morphology. According to the literature, the IM has a simple shear flow between the sample and the walls of the room, while a TSE has strong elongation areas in addition to the shear flow. Therefore, the shear rates of the TSE are expected to be significantly higher than the IM [90]. Thus, PBAT is expected to have a much higher viscosity in the IM than in the TSE. In the m2 strategy, because of the high viscosity of PBAT, the CNC could not migrate to the preferred PBAT phase as the thermodynamic equilibrium localization and therefore it was localized in low viscosity PLA. Also, in the m3 strategy, the CNC, which was previously mixed with PBAT, could migrate from PBAT to interface or a low viscosity

PLA over time. Therefore, in strategies prepared with mIM, the droplet size of PBAT was small. As a result, in this processing method, kinetic parameters are considered to be more dominant than the thermodynamic effect in CNC localization.

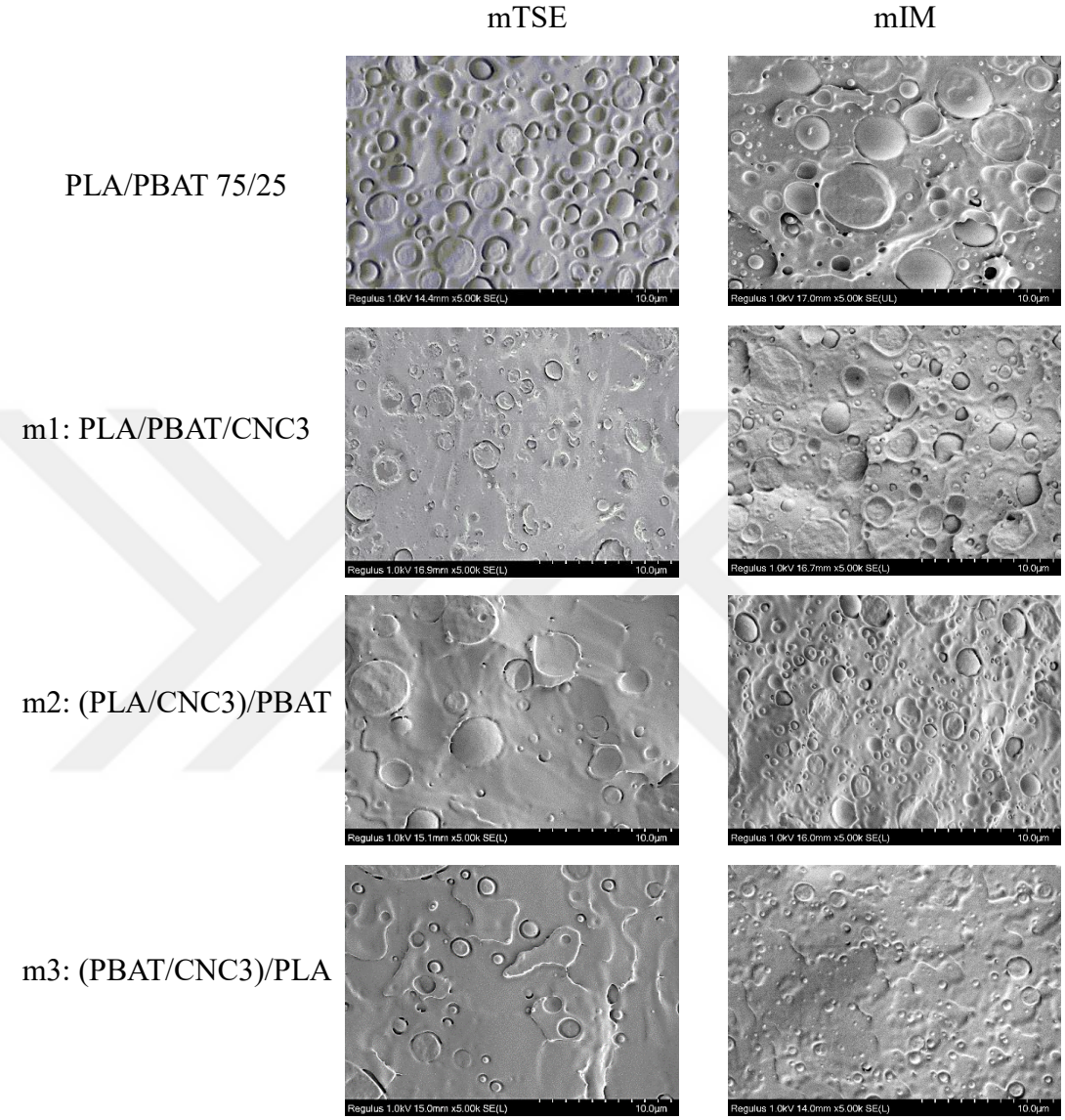

Figure 4.20 : SEM images of samples with different mixing strategies and processing methods.

4.5.2. Rheological analysis

Figure 4.21 shows rheological properties of samples with three mixing strategies and processing through mTSE and mIM. It has been reported that shear flow significantly reduces the interaction among particles and causes significant changes in viscoelastic behavior [96]. The complex viscosity, $\eta*$, and storage modulus, G', of the blend prepared with the IM is lower compared to the blend prepared with the TSE. This is due to the non-uniform morphology as seen from the SEM images, as well as the

droplet size of the PBAT being too large. In addition, it was observed that the η∗ and G′ of blend nanocomposites prepared with mTSE were higher than that of blend nanocomposites prepared with mIM. We did not compare the rheological properties of the blend nanocomposites with blends prepared by directly melt mixing due to the remaining solvent in the blend nanocomposites. In Figure 4.21.c, the increase in transient viscosity observed over time in blend nanocomposites containing 3 wt.% CNC may result from the level of dispersion of the CNC in the blend. In the mTSE, the viscosity of the blend nanocomposite prepared with m3 was higher than other strategies. This is assumed that the sample prepared with the M3 strategy could create a better CNC network in PBAT due to the continuous morphology. On the other hand, the viscosity increases in blend nanocomposite prepared by m2 strategy and mIM processing shows that a strong CNC network is formed in the PLA matrix.

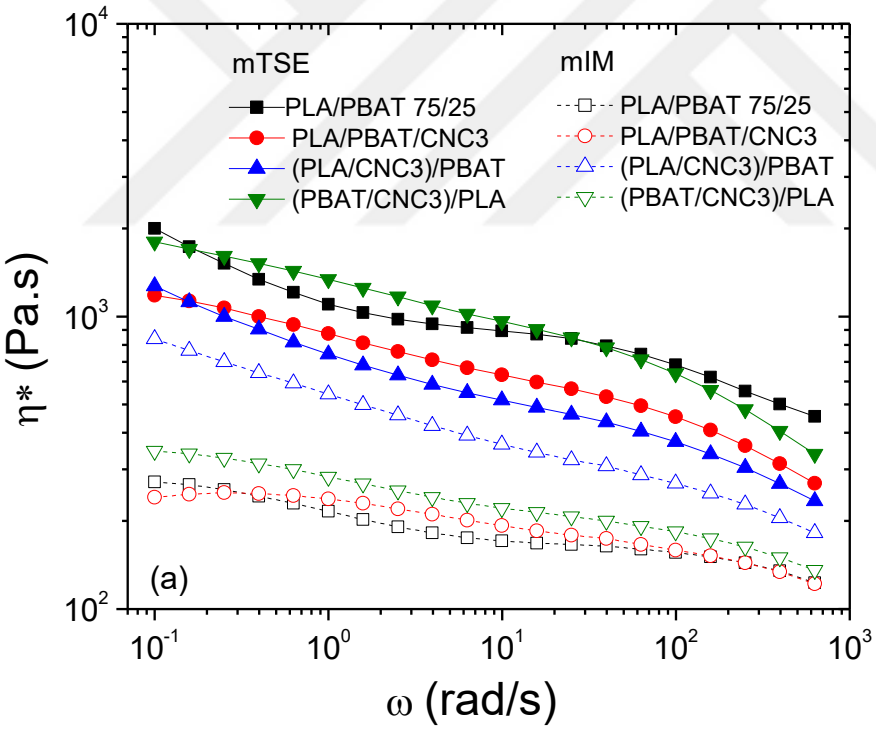

Figure 4.21 : Rheological properties of samples with different mixing strategies and processing methods.

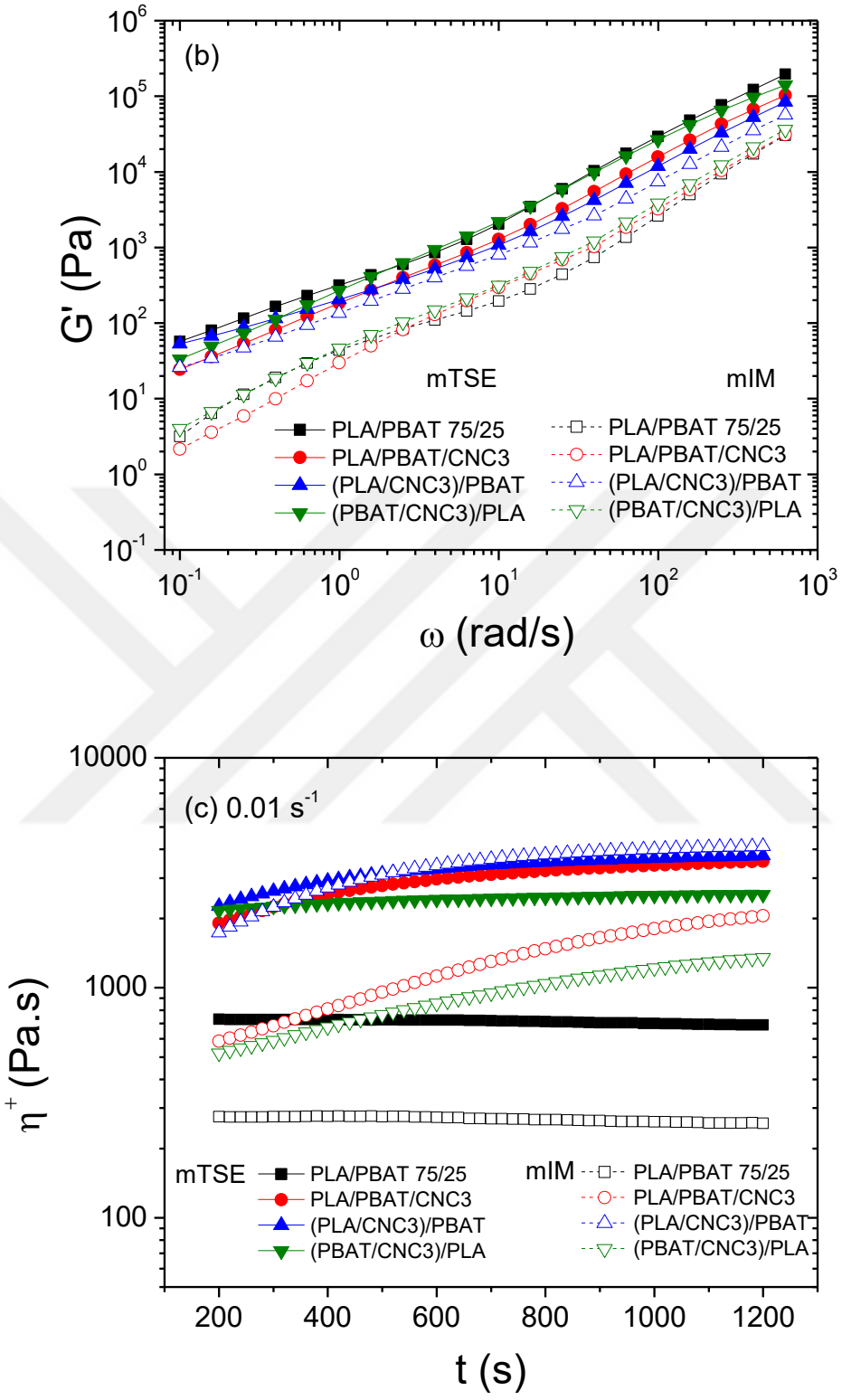

Figure 4.21 (continued): Rheological properties of samples with different mixing strategies and processing methods.

4.5.3. DSC analysis

Figure 4.22 shows DSC plots of neat PLA/PBAT blend and PLA/PBAT/CNC blend nanocomposites with fixed 3 wt.% CNC content prepared with different three mixing strategies and processing through mTSE and mIM. The glass transition (T_g), cold crystallization (T_{cc}), melt crystallization (T_c), and melting (T_m) temperatures as well as the degree of crystallinity (X_c) of the samples are also reported in Table 4.5. Since the samples have different thermal backgrounds, the first heating results were not interpreted. In the cooling cycles, it was observed that the crystallization temperatures of the blend nancomposites increased with addition of 3 wt.% CNC. This indicates that CNC acts as nucleation for PLA and facilitates crystallization kinetics. Again, in the cooling cycle, a shoulder was seen at the exothermic peaks of blend nanocomposites prepared using m1 and m2 strategies with the mIM method. This behavior indicates that the CNC is localized in the PLA or interface, causing the PLA to begin crystallization earlier. The blend nanocomposite prepared with m3 strategy did not show a shoulder, but the peak narrowed. Therefore, we can conclude that PBAT begins to solidify due to CNC localization in the PBAT phase and the crystallization of PLA accelerates around the solidified PBAT. In both methods, when the m2 strategy is used, the increase in the crystallinity rate of the PLA can be attributed to the localization of the CNC in the PLA phase, and this result confirms the rheology and morphology results.

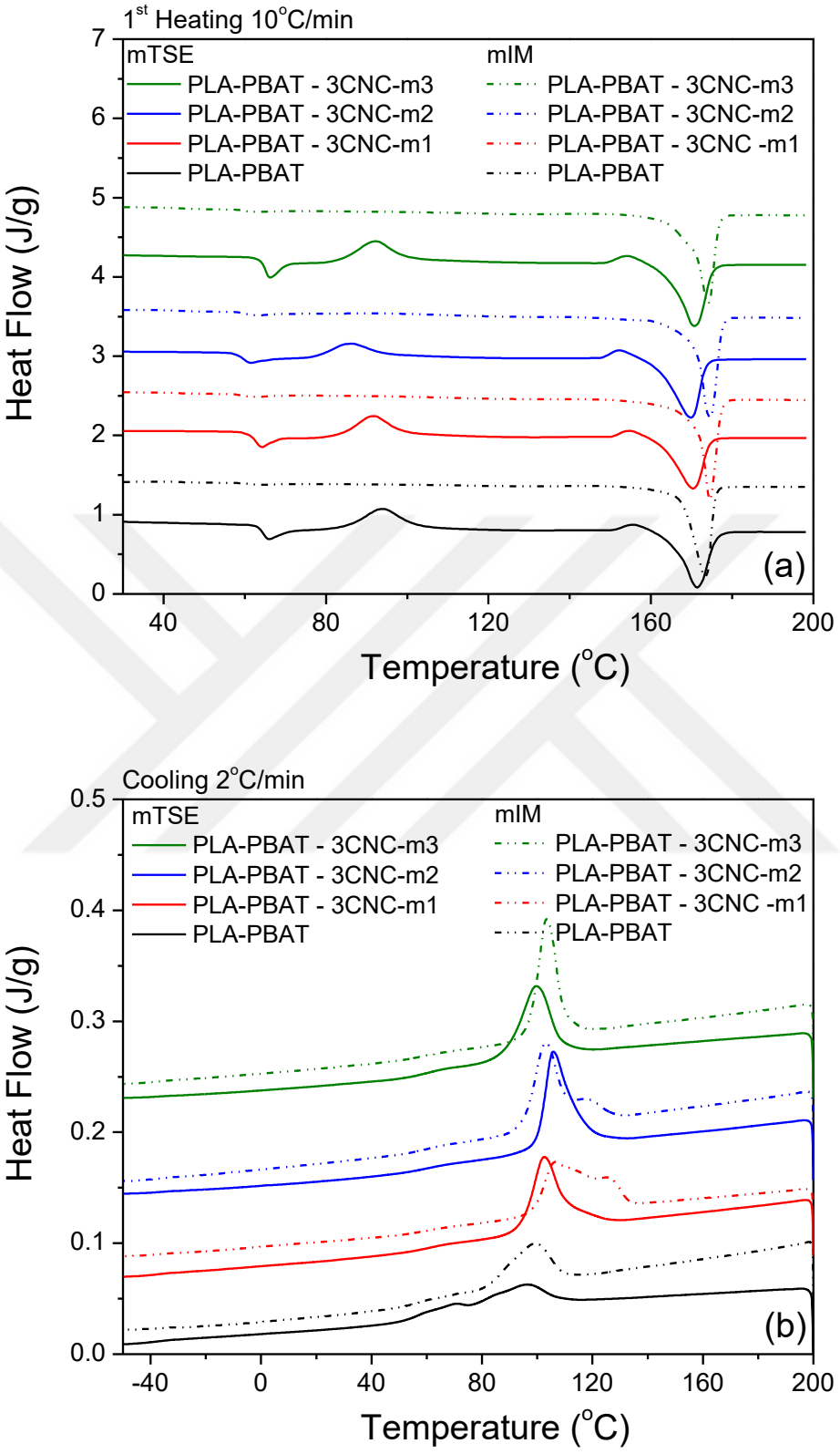

Figure 4.22 : DSC curves of samples prepared with different processing and three mixing strategies; (a) first heating, (b) cooling and (c) second heating scans.

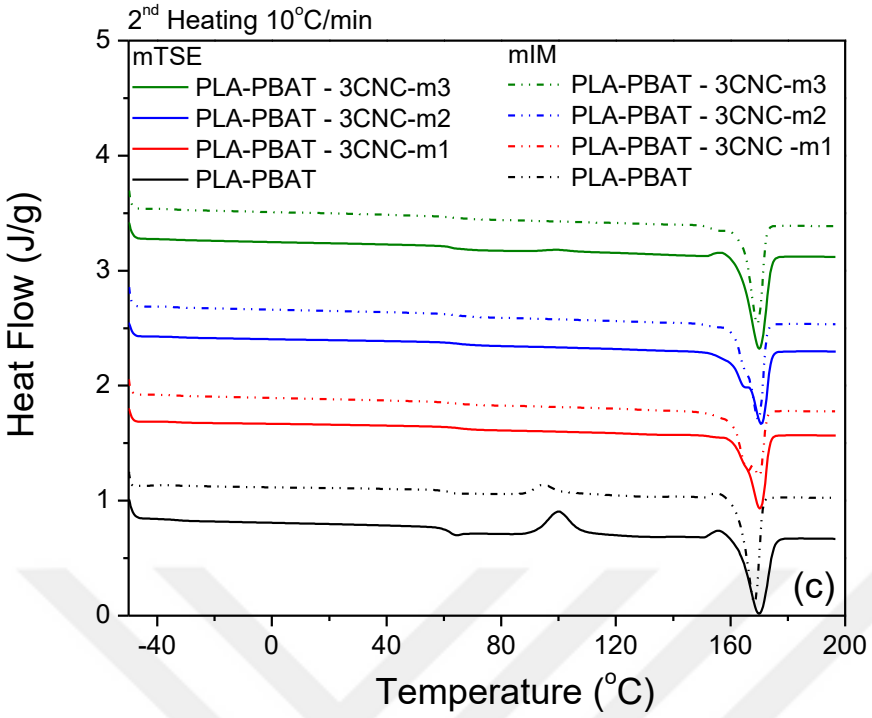

Figure 4.22 (continued) : DSC curves of samples prepared with different processing and three mixing strategies; (a) first heating, (b) cooling and (c) second heating scans.

Table 4.5 : DSC data of samples prepared with different processing and three mixing strategies obtained from first heating, cooling and second heating scans.

	1st Heating				Cooling			2nd Heating			
	T_g	T_{cc}	T_m	X%	T_g	T_c	X%	T_g	T_{cc}	T_m	X%
					mTSE						
75/25	64	94	171	23	55	96	17	61	100	170	30
m1	63	92	170	19	58	103	42	66	-	170	42
m2	59	86	170	36	58	106	46	66	-	171	48
m3	65	92	171	30	59	100	40	63	100	170	51
					mIM						
75/25	61	-	174	57	56	99	27	62	95	168	46
m1	60	-	175	61	56	107	46	66	-	170	48
m2	61	-	174	67	56	103	49	65	-	170	52
m3	60	-	174	61	56	103	43	66	-	169	46

4.5.4. DMA

Figure 4.23 shows the storage module (E′) and tanδ graphs of samples prepared with different processing and three mixing strategies. Figure 4.24 shows the E′ of samples at 45 and 85 °C. All storage module curves first hold the plateau and then begin to decrease rapidly after 60 °C due to glass transition, after 100 °C, there is an increase again due to cold crystallization. When all the situations were compared at 45 °C, the

highest value in the E′ was seen using m1 strategy and mIM. With the addition of CNC in both processes at 85 °C, the E′ has dropped less than the neat blend and this showed the reinforcing effect of the CNC. Again, in any case, there is a decrease in tanδ peak with the addition of CNC.

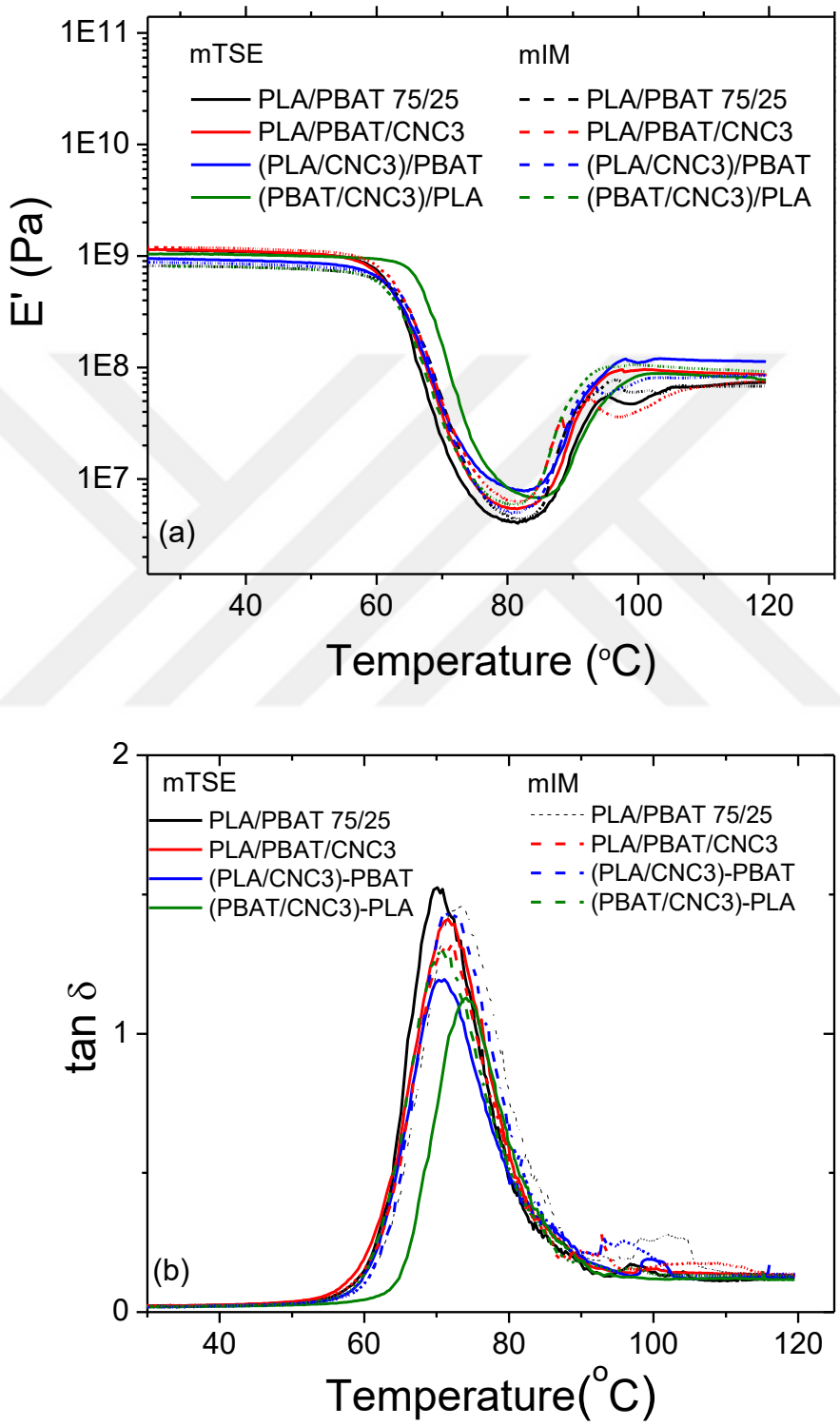

Figure 4.23 : DMA of blends and blend nanocomposites with different processing methods and three mixing strategies; (a) E′ and (b) tanδ curves.

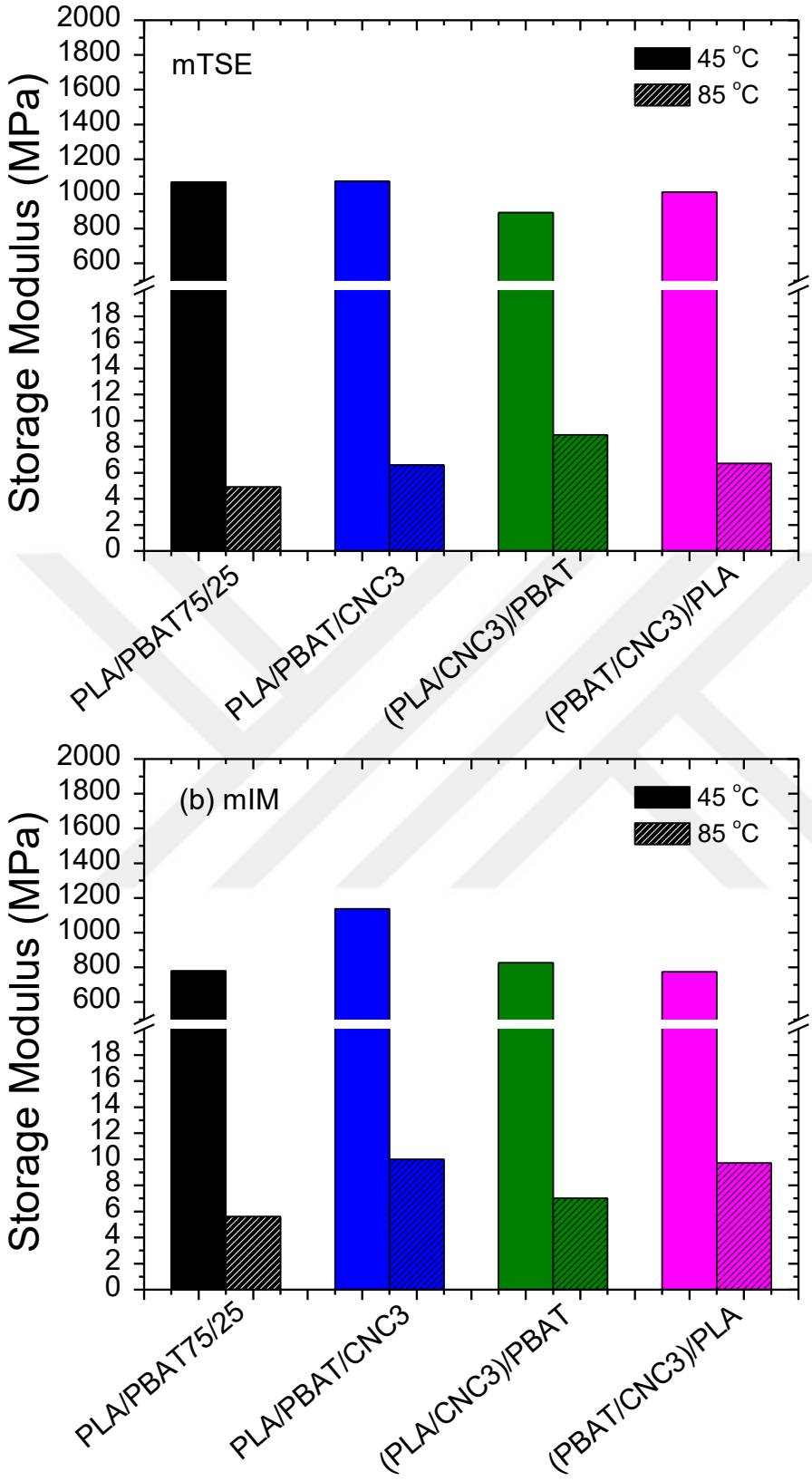

Figure 4.24 : Comparison of the E′ of PLA and PLA/PBAT/CNC blend nanocomposites with different processing methods and three mixing strategies.

4.5.5. Mechanical analysis

Figure 4.25 shows the tensile properties and izod impact strength of blend and blend nanocomposites prepared using three different mixing strategies with mTSE and mIM. In the blends prepared with both processing techniques, a decrease in strength and modulus was observed compared to neat PLA. Although the module drop was the same in both processes, the strength of the blend prepared with mIM was lower than that prepared with mTSE. This may be related to the level of miscibility between the blend components. In SEM images, the PBAT droplet sizes from the blend prepared with mTSE are smaller, which gives a more homogeneous morphology compared to that prepared with mIM. The reason for the smaller droplet size is the more droplet breakup due to more severe shear and elongation deformation in the extruder. The elongation at break and izod impact strength of the PLA/PBAT blend prepared with mTSE increased compared to neat PLA due to the soft structure of PBAT. However, as noted above, since a good dispersion was not achieved in the blend prepared with mIM, a reduction was observed compared to neat PLA. When we examined the strength and modulus of blend nanocomposites containing 3 wt.% CNC prepared with different strategies, it was seen that they were lower than neat PLA except for the modulus of the (PBAT/CNC3)/PLA (m3 strategy) prepared with mIM. Apart from the sample prepared with the M3 strategy and mTSE, a decrease in the elongation at break of the blend nanocomposites was observed due to the stiffness of the CNC. Regardless of the mixing strategies, when we look at the results of izod impact strength, it was observed that the toughness decreases in blend nanocomposites containing 3wt.% CNC prepared with mTSE. However, although the toughness of the blend nanocomposites prepared with the mIM increased compared to the neat blend, the desired increase could not be achieved.

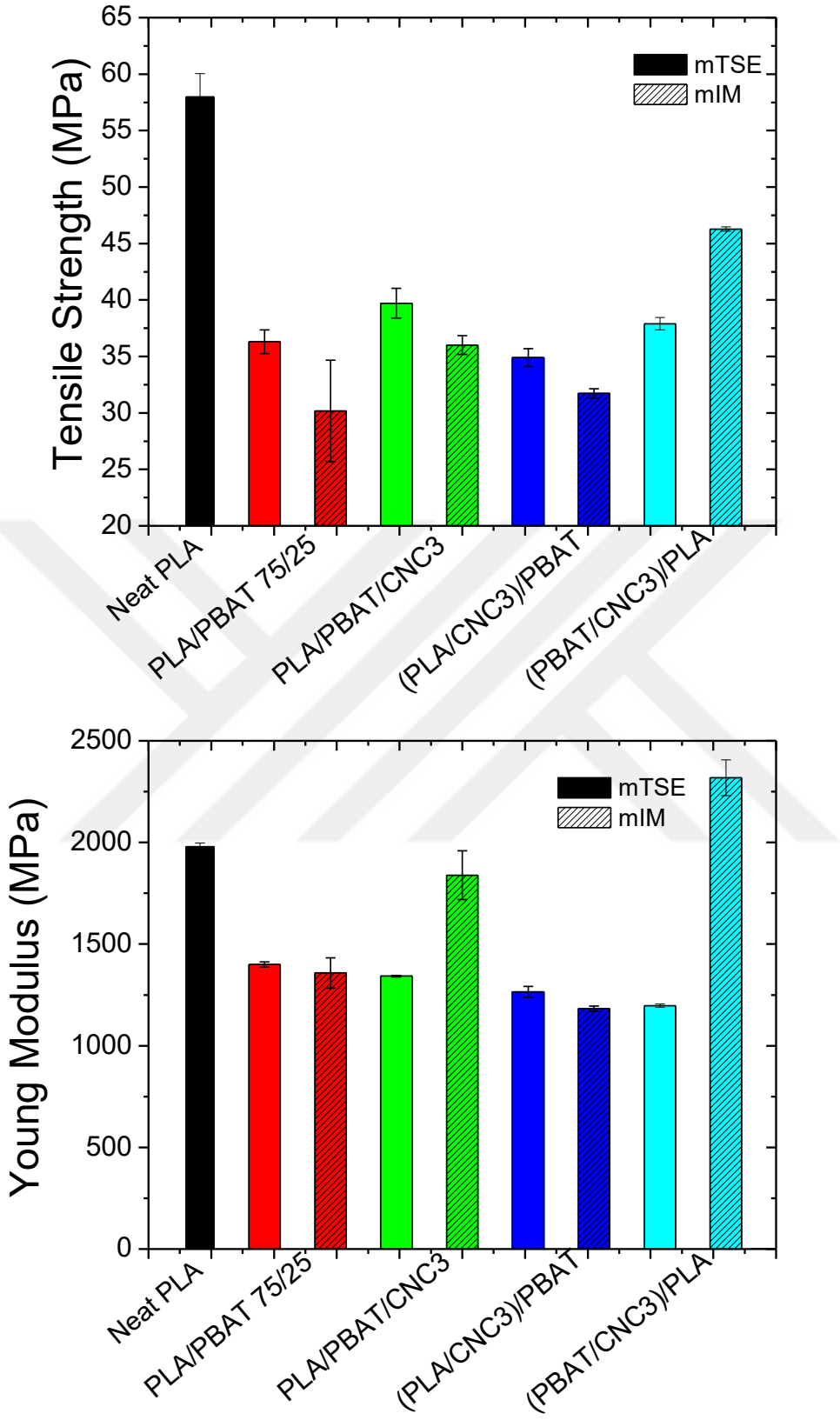

Figure 4.25 : Tensile properties and Izod impact strength of samples with different processing and mixing strategies.

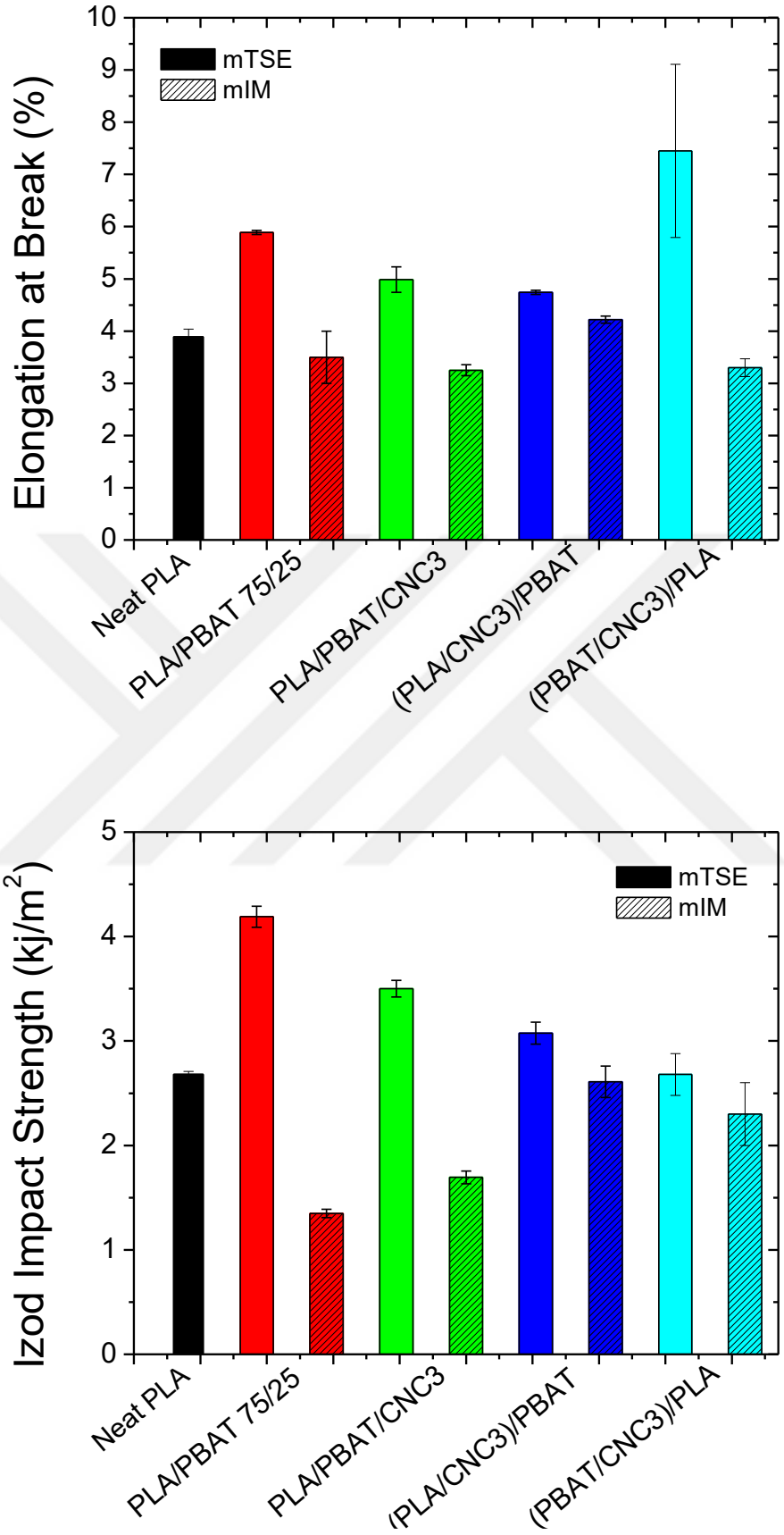

Figure 4.25 (continued) : Tensile properties and Izod impact strength of samples with different processing and mixing strategies.

5. CONCLUSION

In this study, selective localization of CNC in PLA/PBAT blend nanocomposites prepared with different processing methods and mixing strategies were investigated in detail by rheological, morphological, thermal and mechanical analyzes.

In the first part of the study, the thermodynamic effect on the localization of CNC in blend nanocomposites was investigated. The interfacial tension between PLA / PBAT, PLA / CNC and PBAT / CNC were estimated using the harmonic-mean approach, utilizing the surface energies of CNC, PLA and PBAT at 170 °C. It was found from the Young's model that CNC particles had a strong affinity for the PBAT phase.

Due to the hydrogen bonds on the surface of the CNC, it is difficult to the disperse CNC in hydrophobic polymer solutions. Therefore, the second part of the study involves the investigation of the CNC dispersion in the PLA/PBAT blend prepared with solution casting (SC). The dispersion and localization of the CNC in the blend were determined by scanning electron microscopy (SEM) and rheology analysis. SEM analysis demonstrated that the PBAT droplet size in the blend containing 1 wt.% CNC was higher than that in the nest blend. However, when the CNC content increased, a decrease in droplet size was observed. When the PBAT phase begins to crystallize when the solvent is evaporated, the viscosity of the PBAT increases. For this reason, the CNC cannot enter the PBAT phase and the CNC is localized in the interface or in the PLA phase. These observations are consistent with DSC and rheological analysis. The percolation threshold has been observed to occur at 3 wt.% CNC. For this reason, it is assumed that the CNC is localized in the PLA phase. It is offered from these results that the effect of kinetic parameters on the migration and localization of CNC is more dominant than thermodynamic effect.

The third part of the study covers the investigation of blend nanocomposites prepared with the combination of SC and melt mixing using twin screw extruder (TSE). The masterbatch with 7 wt.% CNC prepared by SC is diluted into 1,3 and 5 wt.% CNC through TSE. Rheology analysis shows that the viscosity and the storage module of

the blend nanocomposites at low frequencies are low compared to neat blend. It is assumed that the CNC starts to agglomerate when diluted because it is localized in the PLA phase in the masterbatch.

The fourth part of the study involves the investigation of blend nanocomposites containing a fixed 3 wt.% CNC and different PBAT ratios. There was a significant increase in viscosity when the 3 wt.% CNC was included in the blend containing 50 wt.% PBAT. The reason for this increase can be assumed that the CNC can form a solid network structure within the PBAT phase, since the blend nanocomposite has a continuous morphology.

The last part of the study involves the investigation of blend nanocomposites prepared with different mixing strategies and processing methods. The PLA/PBAT/CNC, PLA/CNC and PBAT/CNC masterbatches containing 7 wt.% CNC prepared by SC is diluted into 3 wt.% CNC through TSE or internal mixer (IM) with the addition neat PLA and PBAT. CNC migrate to PLA phase in each strategy since the internal mixer method took place over a long period of time. However, finer droplets of PBAT were obtained in PLA/PBAT/CNC blend nanocomposites prepared through twin-screw extruder due to higher shear force. In each method, the CNC migrates to PLA stage and is localized because the IM method takes place for a long time. However, finer droplets of PBAT is obtained in PLA/PBAT/CNC blend nanocomposites prepared through TSE due to higher shear force.

It has been observed that viscoelastic properties increase due to the good dispersion of CNC in blend nanocomposites prepared with SC. However, when we look at the mechanical properties, the expected results could not be achieved due to the remaining solution in samples of toughness, ductility and izod impact strength. For this reason, samples should be prepared by direct melt mixing method in order to increase the mechanical properties of PLA. In the samples prepared by direct melt mixing method, due to the hydrophilic structure of the CNC, it is observed that it cannot be dispersed well in the polymer and creates agglomeration. Therefore, CNC must be a surface modification to prevent agglomeration.

REFERENCES

[1] **Kaplan, D.L.** (1998). Introduction to biopolymers from renewable resources, *Biopolymers from renewable resources*, 1-29.

[2] **Yu, L., Dean, K. & Li, L.** (2006). Polymer blends and composites from renewable resources, *Progress in Polymer Science*, 31(6), 576-602.

[3] **Ghanbarzadeh, B. & Almasi, H.** (2013). Biodegradation: Life of Science, Croatia: InTech Publications, 141-186.

[4] **Nofar, M., Maani, A.** (2015). Interfacial and rheological properties of PLA/PBAT and PLA/PBSA blends and their morphological stability under shear flow, *Journal of Rheology*, 59(2), 317-333.

[5] **Dorgan, J.R., Lehermeier, H. & Mang, M.** (2000). Thermal and rheological properties of commercial-grade poly (lactic acid)s, *Journal of Polymers and the Environment*, 8(1), 1-9.

[6] **Jamshidian, M., Tehrany, E.A.** (2010). Poly-Lactic Acid: production, applications, nanocomposites, and release studies, *Comprehensive Reviews in Food Science and Food Safety*, 9(5), 552-571.

[7] **Nofar, M., Sacligil, D.** (2019). Poly (lactic acid) blends: Processing, properties and applications, *International Journal of Biological Macromolecules*, 125, 307-360.

[8] **Nofar, M., Salehiyan, R.** (2020). Ductility improvements of PLA-based binary and ternary blends with controlled morphology using PBAT, PBSA, and nanoclay, *Composites Part B: Engineering*, 182, 107661.

[9] **Signori, F., Coltelli, M.B. & Bronco, S.** (2009). Thermal degradation of poly(lactic acid) (PLA) and poly(butylene adipate-co-terephthalate) (PBAT) and their blends upon melt processing, *Polymer Degradation and Stability*, 94(1), 74-82.

[10] **Habibi, Y., Lucia, L.A. & Rojas, O.J.** (2010). Cellulose nanocrystals: chemistry, self-assembly, and applications. *Chemical Reviews*, 110(6), 3479-3500.

[11] **Khoshkava, V.** (2014). *Polypropylene (PP) nanocomposites incorporating nanocrystalline cellulose (NCC)*, Ph.D. Thesis, Departmen of Chemical Engineering, McGill University, Canada.

[12] **Blanco, A. B, Monte, M.C.** (2018). Nanocellulose for industrial use: cellulose nanofibers (CNF), cellulose nanocrystals (CNC), and bacterial cellulose (BC), *Handbook of Nanomaterials for Industrial Applications*, 74-126.

[13] **Wu, D., Lin, D.** (2011). Selective Localization of Nanofillers: Effect on Morphology and Crystallization of PLA/PCL Blends, *Macromolecular Chemistry and Physics,* 212(6), 613-626.

[14] **Nair, L.S. & Laurencin, C.T.** (2007). Biodegradable polymers as biomaterials, *Progress in Polymer Science,*32(8-9), 762-798.

[15] **Drumright, R.E., Gruber, P.R. & Henton, D.E.** (2000). Polylactic acid technology, *Advanced Materials,* 12(23), 1841-1846.

[16] **Garlotta, D.** (2001). A literature review of poly (lactic acid), *Journal of Polymers and the Environment,* 9(2), 63-84.

[17] **Auras, R., Harte, B. & Selke, S.** (2004). An overview of polylactides as packaging materials. *Macromolecular Bioscince,* 4(9), 835-64.

[18] **Nofar, M., Salehiyan, R. & Ray, S.S.** (2019). Rheology of poly (lactic acid)-based systems, *Polymer Reviews,* 59(3), 465-509.

[19] **Nofar, M. & Park, C.B.** (2014). Polylactide Foams: Fundamentals, Manufacturing, and Applications, *Progress in Polymer* 39,1721-1741.

[20] **Lim, L.T., Auras, R. & Rubino, M.** (2008). Processing technologies for poly (lactic acid), *Progress in Polymer Science,* 33(8),820-852.

[21] **Ahvenainen, R.,** (2003). *Novel food packaging techniques*, USA, CRC Press LLC.

[22] **Mikos, A.G., Lyman, M.D.** (1994). Wetting of poly (L-lactic acid) and poly (DL-lactic-co-glycolic acid) foams for tissue culture, *Biomaterials,* 15(1), 55-58.

[23] **Lasprilla, A.J., Martinez, G.A.R.** (2012). Poly-lactic acid synthesis for application in biomedical devices—A review, *Biotechnology Advances*, 30(1), 321-328.

[24] **Saeidlou, S., Huneault, M., Li, H. & Park C.B.** (2012). Poly(lactic acid) crystallization, *Progress in Polymer Science,*37(12), 1657-1677.

[25] **Suryanegara, L., Nakagaito A.N. & Yano, H.** (2009). The effect of crystallization of PLA on the thermal and mechanical properties of microfibrillated cellulose-reinforced PLA composites, *Composites Science and Technology,* 69(7-8), 1187-1192.

[26] **Rodrigues, B.V.M., Silva, A.S.** (2016). Influence of low contents of superhydrophilic MWCNT on the properties and cell viability of electrospun poly (butylene adipate-co-terephthalate) fibers, *Materials Scince and Engineering: C,* 59, 782-791.

[27] **Ferreira, F.V., Cividanes, L.S., Gouveia, R.F. & Lona, L.M.F.** (2019). An overview on properties and applications of poly (butylene adipate-co-terephthalate)–PBAT based composites, *Polymer Engineering and Science,* 59(s2), E7-E15.

[28] **Müller, R.J., Kleeberg, I. & Deckwer W.D.** (2001). Biodegradation of polyesters containing aromatic constituents, *Journal of Biotechnology,* 86(2), 87-95.

[29] **Bastarrachea, L., Dhawan, S.** (2010). Biodegradable Poly (butylene adipate-co-terephthalate) Films Incorporated with Nisin: Characterization and Effectiveness against Listeria innocua, *Journal of Food Science,* 75(4), E215-E224.

[30] **Li, G., Shankar, S., Rhim, J.W. & Oh B.Y.** (2015), Effects of preparation method on properties of poly (butylene adipate-co-terephthalate) films, *Food Science and Biotechnology,* 24(5), 1679-1685.

[31] **Utracki, L.A. & Favis, B.D.** (1989). *Handbook of Polymer Science and Technology: Polymer alloys and blends,* New York and Basel, Marcel Dekker, Inc., 4, 121-185.

[32] **Macosko, C.W.** (2000). Morphology development and control in immiscible polymer blends, *Macromolecular Symposia,* 149(1), 171-184.

[33] **Nofar, M., Heuzey, M.C.** (2016). Coalescence in PLA-PBAT blends under shear flow: Effects of blend preparation and PLA molecular weight, *Journal of Rheology,* 60(4), 637-648.

[34] **Wu, S.,** (1982). *Polymer interface and adhesion*. New York and Basel, Marcel Dekker, Inc.

[35] **Girifalco, L. & Good, R.J.** (1957). A theory for the estimation of surface and interfacial energies. I. Derivation and application to interfacial tension, *The Journal of Physical Chemistry,* 61(7), 904-909.

[36] **Palierne, J.F** (1990). Linear rheology of viscoelastic emulsions with interfacial tension, *Rheologica Acta,* 29(3), 204-214.

[37] **Lacroix, C., Aressy, M. & Carreau, P.J.** (1997). Linear viscoelastic behavior of molten polymer blends: a comparative study of the Palierne and Lee and Park models, *Rheologica Acta*, 36(4), 416-428.

[38] **Bousmina, M.** (1999). Rheology of polymer blends: linear model for viscoelastic emulsions, *Rheologica Acta,* 38(1), 73-83.

[39] **Taylor, G.I.** (1932). The viscosity of a fluid containing small drops of another fluid, *Proceedings of the Royal Society of London,* 138(834), 41-48.

[40] **Taylor, G.I.** (1934). The formation of emulsions in definable fields of flow, *Proceedings of the Royal Society of London,*146(858): p. 501-523.

[41] **Puyvelde, P.V., Valenkar, S. & Moldenaers, P.** (2001). Rheology and morphology of compatibilized polymer blends, *Current Opinion in Colloid & Interface Science,* 6(5-6), 457-463.

[42] **Tucker III, C.L. & Moldenaers, P.** (2002). Microstructural evolution in polymer blends, *Annual Review of Fluid Mechanics,* 34(1), 177-210.

[43] **Grace, H.P.** (1982). Dispersion Phenomena in High Viscosity Immiscible Fluid Systems and Application of Static Mixers as Dispersion Devices in Such Systems, *Chemical Engineering Communications,* 14(3-6), 225-277.

[44] **Yousfi, M., Dadouche, T.** (2018). Development of nanofibrillar morphologies in poly (l-lactide)/poly (amide) blends: Role of the matrix elasticity and identification of the critical shear rate for the nodular/fibrillar transition, *Royal Society of Chemistry*, 8(39), 22023-22041.

[45] **Wang, L.F., Rhim, J.W. & Hong, S.I.** (2016). Preparation of poly (lactide)/poly (butylene adipate-co-terephthalate) blend films using a solvent casting method and their food packaging application, *LWT-Food Science and Biotechnology,* 68, 454-461.

[46] **Kang, Y., Chen, P.** (2018). Preparation of open-porous stereocomplex PLA/PBAT scaffolds and correlation between their morphology, mechanical behavior, and cell compatibility, *Royal Society of Chemistry*, 8(23), 12933-12943.

[47] **Nofar, M., Tabatabaei, A.** (2017). Mechanical and bead foaming behavior of PLA-PBAT and PLA-PBSA blends with different morphologies, *European Polymer Journal,* 90, 231-244.

[48] **Jiang, L., Wolcott, M.P. & Zhang, J.** (2006). Study of biodegradable polylactide/poly (butylene adipate-co-terephthalate) blends, *Biomacromolecules,* 7(1), 199-207.

[49] **Li, K., Peng, J., Turng, L.S., & Huang, H.X.** (2011). Dynamic rheological behavior and morphology of polylactide/poly (butylenes adipate-co-terephthalate) blends with various composition ratios, *Advances in Polymer Technology,* 30(2), 150-157.

[50] **Jiang, L., Liu, B. & Zhang, J.** (2009). Properties of poly (lactic acid)/poly (butylene adipate-co-terephthalate)/nanoparticle ternary composites, *Industrial & Engineering Chemistry Research,* 48(16), 7594-7602.

[51] **Heshmati, V.** (2017). *Biobased PLA/PA11 Blends and the Incorporation of Cellulose Nanocrystal*, Ph.D. Thesis, Department Of Chemical Engineering, École Polytechnique de Montréal, Canada.

[52] **Zakeri, B**. (2017). *Tailoring the Surface Charge of Cellulose Nanocrystals (CNC) Using a Polycation*, Ph.D. Thesis, Department Of Chemical Engineering, École Polytechnique de Montréal, Canada.

[53] **Moon, R.J., Martini, A.** (2011). Cellulose nanomaterials review: structure, properties and nanocomposites, *Chemical Society Reviews,* 40(7), 3941-94.

[54] **Lin, N., Huang, J.** (2011). Surface acetylation of cellulose nanocrystal and its reinforcing function in poly(lactic acid), *Carbohydrate Polymers,* 83(4), 1834-1842.

[55] **Bagheriasl, D., Carreau, P.J.** (2016). Shear rheology of polylactide (PLA)–cellulose nanocrystal (CNC) nanocomposites, *Cellulose*, 23(3),1885-1897.

[56] **Gupta, A., Simmons, W., Schueneman, G.T. & Mintz, E.A.** (2016). Lignin-coated cellulose nanocrystals as promising nucleating agent for poly(lactic acid), *Journal of Thermal Analysis and Calorimetry*, 126(3), 1243-1251.

[57] **Zhang, C., Salick, M.R.** (2015). Incorporation of poly(ethylene glycol) grafted cellulose nanocrystals in poly(lactic acid) electrospun nanocomposite fibers as potential scaffolds for bone tissue engineering, *Materials Science and Engineering: C*, 49, 463-471.

[58] **Nasti, G., Gentile, G.** (2016). Double percolation of multiwalled carbon nanotubes in polystyrene/polylactic acid blends, *Polymer*, 99, 193-203.

[59] **Maani, A., Blais, B., Heuzey, M.C. & Carreau, P.J.** (2012). Rheological and morphological properties of reactively compatibilized thermoplastic olefin (TPO) blends, *Journal of Rheology*, 56(3), 625-647.

[60] **Sumita, M., Sakata, K.** (1991). Dispersion of fillers and the electrical conductivity of polymer blends filled with carbon black, *Polymer Bulletin*, 25(2), 265-271.

[61] **Fenouillot, F., Cassagnau, P. & Majesté, J.C.** (2009). Uneven distribution of nanoparticles in immiscible fluids: Morphology development in polymer blends, *Polymer*, 50(6), 1333-1350.

[62] **Adrar, S., Habi, A., Ajji, A. & Grohens, Y.** (2018). Synergistic effects in epoxy functionalized graphene and modified organo-montmorillonite PLA/PBAT blends, *Applied Clay Science*, 157, 65-75.

[63] **Feng, J., Chan, C.M. & Li, J.X.** (2003). A method to control the dispersion of carbon black in an immiscible polymer blend, *Polymer Engineering & Science*, 43(5), 1058-1063.

[64] **Dil, E.J. & Favis, B.D.** (2015). Localization of micro-and nano-silica particles in heterophase poly (lactic acid)/poly (butylene adipate-co-terephthalate) blends, *Polymer*, 76, 295-306.

[65] **Wu, D., Lin, D.** (2011). Selective localization of nanofillers: effect on morphology and crystallization of PLA/PCL blends, *Macromolecular Chemistry and Physics*, 212(6), 613-626.

[66] **Ko, S., Hong, M.K.** (2009). Morphological and rheological characterization of multi-walled carbon nanotube/PLA/PBAT blend nanocomposites, *Polymer Bulletin*, 63(1), 125-134.

[67] **Urquijo, J., Aranburu, N.** (2017). CNT-induced morphology and its effect on properties in PLA/PBAT-based nanocomposites, *European Polymer Journal*, 93, 545-555.

[68] **Kumar, M., Mohanty, S., Nayak, S.K. & Parvaiz M.R.** (2010). Effect of glycidyl methacrylate (GMA) on the thermal, mechanical and morphological property of biodegradable PLA/PBAT blend and its nanocomposites, *Bioresource Technology*, 101(21), 8406-15.

[69] **Mohapatra, A.K., Mohanty, S. & Nayak, S.K.** (2014). Study of thermo-mechanical and morphological behaviour of biodegradable PLA/PBAT/layered silicate blend nanocomposites, *Journal of Polymers and the Environment*, 22(3), 398-408.

[70] **Dil, E.J., Virgilio, N. & Favis, B.D.** (2016). The effect of the interfacial assembly of nano-silica in poly (lactic acid)/poly (butylene adipate-co-terephthalate) blends on morphology, rheology and mechanical properties, *European Polymer Journal*, 85, 635-646.

[71] **Pinto, A.M., Cabral, J.** (2013). Effect of incorporation of graphene oxide and graphene nanoplatelets on mechanical and gas permeability properties of poly (lactic acid) films, *Polymer International*, 62(1), 33-40.

[72] **Girdthep, S., Komrapit, N.** (2015). Effect of plate-like particles on properties of poly (lactic acid)/poly (butylene adipate-co-terephthalate) blend: A comparative study between modified montmorillonite and graphene nanoplatelets, *Composites Science and Technology*, 119, 115-123.

[73] **Ye, A., Wang, S.** (2019). Poly (ethylene oxide)-promoted dispersion of graphene nanoplatelets and its effect on the properties of poly (lactic acid)/poly (butylene adipate-co-terephthalate) based nanocomposites, *Materials Letters*, 253, 34-37.

[74] **Motloung, M.P., Ojijo, V., Bandyopadhyay, J. & Ray, S.S.** (2019). Morphological characteristics and thermal, rheological, and mechanical properties of cellulose nanocrystals-containing biodegradable poly (lactic acid)/poly (ε-caprolactone) blend composites, *Journal of Applied Polymer Science*, 137(19), 48665.

[75] **Heshmati, V., Kamal, M.R. & Favis, B.D.** (2018). Cellulose nanocrystal in poly (lactic acid)/polyamide11 blends: Preparation, morphology and co-continuity, *European Polymer Journal*, 98, 11-20.

[76] **Heshmati, V., Kamal, M.R. & Favis, B.D.** (2018). Tuning the localization of finely dispersed cellulose nanocrystal in poly (lactic acid)/bio-polyamide11 blends, *Journal of Polymer Science Part B: Polymer Physics*, 56(7), 576-587.

[77] **Arrieta, M.P., Fortunati, E.** (2014). PLA-PHB/cellulose based films: Mechanical, barrier and disintegration properties, *Polymer Degradation and Stability*, 07, 139-149.

[78] **Arrieta, M.P., Fortunati, E.** (2014). Multifunctional PLA–PHB/cellulose nanocrystal films: Processing, structural and thermal properties, *Carbohydrate Polymers*, 107, 16-24.

[79] **Arrieta, M.P., Lopez, J.** (2016). Biodegradable electrospun bionanocomposite fibers based on plasticized PLA–PHB blends reinforced with cellulose nanocrystals, *Industrial Crops and Products*, 93, 290-301.

[80] **Arrieta, M.P., Fortunati, E.** (2015). Bionanocomposite films based on plasticized PLA–PHB/cellulose nanocrystal blends, *Carbohydrate Polymers*, 121, 265-275.

[81] **Bitinis, N., Verdejoa, R.** (2013). Poly(lactic acid)/natural rubber/cellulose nanocrystal bionanocomposites part I. Processing and morphology. *Carbohydrate Polymers*, 96(2), 611-20.

[82] **Bitinis, N., Fortunati, E.** (2013). Poly(lactic acid)/natural rubber/cellulose nanocrystal bionanocomposites. Part II: properties evaluation. *Carbohydrate Polymers*, 96(2), 621-7.

[83] **Ma, P., Jiang, L., Yu, M., Dong, W. & Chen, M.** (2016). Green antibacterial nanocomposites from poly (lactide)/poly (butylene adipate-co-terephthalate)/nanocrystal cellulose–silver nanohybrids, *ACS Sustainable Chemistry & Engineering*, 4(12), 6417-6426.

[84] **Fischer, E. W., Sterzel, H.J. & Wegner, G.** (1973). Investigation of the structure of solution grown crystals of lactide copolymers by means of chemical reactions, *Kolloid-Zeitschrift und Zeitschrift für Polymere,* 251(11), 980-990.

[85] **Nofar, M., Heuzey M.-C., Carreau, P.J. & Kamal, M.R.** (2016). Effects of nanoclay and its localization on the morphology stabilization of PLA/PBAT blends under shear flow, *Polymer*, 98, 353-364.

[86] **Khoshkava, V. & Kamal, M.R.** (2013). Effect of surface energy on dispersion and mechanical properties of polymer/nanocrystalline cellulose nanocomposites, *Biomacromolecules*, 14(9), 3155-3163.

[87] **Wu, D., Zhang, Y., Zhang, M. & Yu, M.** (2009). Selective localization of multiwalled carbon nanotubes in poly (ε-caprolactone)/polylactide blend, *Biomacromolecules*, 10(2), 417-424.

[88] **Shi, X., Qin, J.** (2018). Introduction of stereocomplex crystallites of PLA for the solid and microcellular poly(lactide)/poly(butylene adipate-co-terephthalate) blends, *RSC Advances*, 8(22), 11850-11861.

[89] **Jonoobi, M., Harun, J., Mathew, AP. & Oksman, K.** (2010). Mechanical properties of cellulose nanofiber (CNF) reinforced polylactic acid (PLA) prepared by twin screw extrusion, *Composites Science and Technology*, 70(12), 1742-1747.

[90] **Taghizadeh, A. & Favis B.D.** (2013). Carbon nanotubes in blends of polycaprolactone/thermoplastic starch, *Carbohydrate polymers*, 98(1), 189-198.

[91] **Shakouri, Z. & Nazockdast, H.** (2018). Microstructural development and mechanical performance of PLA/TPU blends containing geometrically different cellulose nanocrystals, *Cellulose*, 25(12), 7167-7188.

[92] **Kontopoulou, M., Liu, Y., Austin, J.R. & Parent, J.S.** (2007). The dynamics of montmorillonite clay dispersion and morphology development in immiscible ethylene–propylene rubber/polypropylene blends, *Polymer,* 48(15), 4520-4528.

[93] **Hong, J.S., Namkung, H., Ahn, K.H., Lee, S.J. & Kim, C.** (2006). The role of organically modified layered silicate in the breakup and coalescence of droplets in PBT/PE blends, *Polymer,* 47(11), 3967-3975.

[94] **Lee, H. Fasulo, P.D., Rodgers, W.R. & Paul, D.R.** (2005). TPO based nanocomposites. Part 1. Morphology and mechanical properties, *Polymer,* 46(25), 11673-11689.

[95] **Yeh, J.T., Tsou, C.H.** (2010). Compatible and crystallization properties of poly (lactic acid)/poly (butylene adipate-co-terephthalate) blends, *Journal of Applied Polymer Science,* 116(2), 680-687.

[96] **Abbasi, S., Carreau, P.J. & Derdouri, A.** (2010). Flow induced orientation of multiwalled carbon nanotubes in polycarbonate nanocomposites: Rheology, conductivity and mechanical properties, *Polymer,* 51(4), 922-935.

CURRICULUM VITAE

Name Surname **:** Deniz Sema SARUL

Place and Date of Birth **:** Istanbul/16.06.1993

E-Mail **:** semasarul@gmail.com

EDUCATION

- **M.Sc.** (2018-2020): Polymer Science & Technology Department, Istanbul Technical University, Istanbul, Turkey – TUBITAK 1001 Bursary (Project No: 117M238)
- **B.Sc.** (2012-2017): Chemical Engineering Department, Engineering Faculty, Kocaeli University, Kocaeli, Turkey

PUBLICATIONS, PRESENTATIONS AND PATENTS ON THE THESIS:

Journal Articles:

- Vatansever, E., Arslan D., Sarul, D.S., Kahraman, Y., Durmus, A., Nofar, M. (2020). Effects of molecular weight and crystallizability of polylactide on the cellulose nanocrystal dispersion quality in their nanocomposites, *International Journal of Biological Macromolecules*, 154, 276-290.
- Arslan D., Vatansever, E., Sarul, D.S., Kahraman, Y., Gurbuz, G., Durmus, A., Nofar, M. (2020). Effect of preparation method on the properties of polylactide/cellulose nanocrystal nanocomposites, *Polymer Composite,* 1-11.
- Vatansever, E., Arslan D., Sarul, D.S., Kahraman, Y., Gurbuz, G., Durmus, A., Nofar, M. Development of CNC reinforced PBAT nanocomposites with reduced percolation threshold: A comparative study on the preparation method, *Journal of Polymers and the Environment, submitted*.

Conference Papers:

- Vatansever, E., Arslan D., Sarul, D.S., Nofar, M. Cellulose Nanocrystal Incorporated Nanocomposites, 35th Polymer Processing Society Conference 2019, Izmir, Turkey, May. 2019, presented.